

# **CNWRA** A center of excellence in earth sciences and engineering

A Division of Southwest Research Institute™  
6220 Culebra Road • San Antonio, Texas, U.S.A. 78228-5166  
(210) 522-5160 • Fax (210) 522-5155

October 29, 2002  
Contract No. NRC-02-02-012  
Account No. 20.06002.01.091

U.S. Nuclear Regulatory Commission  
ATTN: Mr. Jeffrey Pohle  
Division of Waste Management  
TWFN, Mail Stop 7-D13  
Washington, DC 20555

**SUBJECT:** Thermal Effects on Flow KTI Intermediate Milestone 06002.01.091.340: Geostatistical Analysis of Pneumatic, Hydraulic, and Thermal Properties of Unsaturated Fractured Tuffs—Letter Report

Dear Mr. Pohle:

Enclosed please find the report titled "Geostatistical Analysis of Pneumatic, Hydraulic, and Thermal Properties of Unsaturated Fractured Rocks at the Apache Leap Research Site, A Yucca Mountain Analog." This report fulfills the requirements for the subject milestone, which is due October 31, 2002.

This report summarizes and evaluates available unsaturated zone hydrologic and thermal property data measured or estimated at the Apache Leap Research Site and at Yucca Mountain. Where possible, a comparison is made with data from Yucca Mountain to give some indication of the reasonableness of using Apache Leap as an analog site. This report also develops and evaluates geostatistical information from the Apache Leap Research Site that could be used to generate stochastic properties for numerical modeling. Previous modeling efforts, which used hypothetical geostatistical information, suggested that incorporation of heterogeneity could have a significant effect on estimates of flow patterns, which could translate to effects on estimates of seepage into drifts. The geostatistical information will be used to assess the importance of including intralayer heterogeneity in ambient or thermohydrological unsaturated zone flow models applied at Yucca Mountain. This work will support the review of DOE and NRC technical agreements TEF.2.08 and TEF.2.10, which address the topic of parameter uncertainty.

If you have any questions, please contact Randall Fedors at 210-522-6818 or me at 210-522-5151.

Sincerely yours,



Asadul H. Chowdhury, Manager  
Mining, Geotechnical, and Facility Engineering

AHC/ph  
Enclosure

cc:	J. Linehan (letter only)	J. Schlueter	B. Leslie	W. Patrick	<u>Letter only:</u>
	B. Meehan	K. Stablein	C. Trottier	B. Sagar	CNWRA Directors
	D. DeMarco	D. Brooks	J. Bradbury	T. Nagy (SwRI Contracts)	CNWRA Element Mgrs.
	E. Whitt	T. McCartin	M. Nataraja	P. Maldonado	
	W. Reamer	P. Justus	B. Jagannath	R. Fedors	
	L. Campbell	J. Greeves		C. Dinwiddie	



Washington Office • Twinbrook Metro Plaza #210  
12300 Twinbrook Parkway • Rockville, Maryland 20852-1606

**GEOSTATISTICAL ANALYSIS OF PNEUMATIC,  
HYDRAULIC, AND THERMAL PROPERTIES OF  
UNSATURATED FRACTURED ROCKS AT THE  
APACHE LEAP RESEARCH SITE, A YUCCA  
MOUNTAIN ANALOG**

*Prepared for*

**U.S. Nuclear Regulatory Commission  
Contract NRC-02-02-012**

*Prepared by*

**Cynthia L. Dinwiddie  
Randall W. Fedors  
Walter A. Illman**

**Center for Nuclear Waste Regulatory Analyses  
San Antonio, Texas**

**October 2002**

## ABSTRACT

Heterogeneity of key parameters for mass and heat flow through fractured tuffs is the primary topic of this report. Large-scale models used by the U.S. Department of Energy (DOE) assume that homogeneous layers adequately represent the unsaturated system at Yucca Mountain, Nevada. DOE thermohydrologic and small-scale seepage models incorporate parameter variability, but there is little information from Yucca Mountain to constrain statistical descriptions of heterogeneity. Measured data from an analog site are available for estimating the required geostatistical data. The Apache Leap Research Site is located in fractured tuff with climatic and topographic conditions similar to that of the region around Yucca Mountain, Nevada. Thus, the site has the potential to be a good small-scale analog of the Yucca Mountain. This report summarizes geostatistical information from the Apache Leap Research Site. Where possible, a comparison is made with data from Yucca Mountain to give some indication of the reasonableness of using Apache Leap as an analog site.

Previous modeling efforts (Illman and Hughson, 2001; Fedors, et al., 2002), which used hypothetical geostatistic information, suggest that incorporation of heterogeneity will have a significant effect on estimates of flow patterns that would translate to effects on estimates of seepage into drifts. The work presented in this report is intended to be preparatory for additional modeling efforts that will be used to assess the importance of including intralayer heterogeneity unsaturated zone flow models applied at Yucca Mountain using measured and estimated geostatistical data from the Apache Leap Research Site.

### References:

Fedors, R.W., J.R. Winterle, W.A. Illman, C.L. Dinwiddie, and D.L. Hughson. "Unsaturated Zone Flow at Yucca Mountain, Nevada: Effects of Fracture Heterogeneity and Flow in the Nonwelded Paintbrush Tuff Unit." San Antonio, Texas: CNWRA. 2002.

Illman, W. A., and D. L. Hughson. "Monte Carlo Analyses of Unsaturated Flow in Thick Vadose Zones of Layered, Fractured Rocks." American Geophysical Union Fall 2001 Meeting, San Francisco, California, December 10-14, 2001. *EOS Transactions Supplement*. American Geophysical Union. Vol. 82, No. 47. 2001.

# CONTENTS

Section	Page
ABSTRACT .....	iii
FIGURES .....	vii
TABLES .....	ix
ACKNOWLEDGMENTS .....	xi
<b>1 INTRODUCTION .....</b>	<b>1-1</b>
1.1 Background and Objectives .....	1-1
1.2 Programmatic Relevance .....	1-4
1.3 Report Organization .....	1-4
<b>2 THE APACHE LEAP RESEARCH SITE .....</b>	<b>2-1</b>
2.1 Site Description and Summary of Data Collection .....	2-1
2.2 Data Description .....	2-6
2.2.1 Field Estimates of Fracture Air Permeability .....	2-6
2.2.2 Field Estimates of Fracture Liquid Permeability .....	2-7
2.2.3 Laboratory Estimates of Matrix Air Permeability .....	2-8
2.2.4 Laboratory Estimates of Matrix Liquid Permeability .....	2-8
2.2.5 Fracture Frequency .....	2-8
2.2.6 Effective Fracture Porosity .....	2-10
2.2.7 Effective Matrix Porosity .....	2-10
2.2.8 Matrix van Genuchten Alpha .....	2-11
2.2.9 Matrix Klinkenberg Coefficient .....	2-11
2.2.10 Matrix Volumetric Water Content .....	2-12
2.2.11 Dry Thermal Conductivity .....	2-12
2.2.12 Saturated Thermal Conductivity .....	2-13
2.2.13 Dry Rock Specific Heat .....	2-13
2.3 Exploratory Data Analysis .....	2-13
2.4 Comparison with Permeability Estimates from Other Tests .....	2-20
2.5 Summary .....	2-26
<b>3 THE YUCCA MOUNTAIN SITE .....</b>	<b>3-1</b>
3.1 Site Description and Summary of Data Collection .....	3-1
3.1.1 Field Estimates of Fracture Air Permeability .....	3-1
3.1.2 Laboratory Estimates of Matrix Liquid Permeability .....	3-2
3.1.3 Fracture Frequency .....	3-2
3.1.4 Effective Fracture Porosity .....	3-5
3.1.5 Effective Matrix Porosity .....	3-6
3.1.6 Fracture van Genuchten Alpha .....	3-6
3.1.7 Matrix van Genuchten Alpha .....	3-6
3.1.8 Field Estimates of Fracture Volumetric Water Content .....	3-7
3.1.9 Laboratory Estimates of Matrix Gravimetric and Volumetric Water Content .....	3-7
3.1.10 Dry Thermal Conductivity .....	3-7
3.1.11 Saturated Thermal Conductivity .....	3-7

## CONTENTS (continued)

Section	Page
3.1.12	Dry Rock Specific Heat . . . . . 3-8
3.2	Comparison of Apache Leap Research Site and Yucca Mountain Data . . . . . 3-8
3.2.1	Comparison of Properties . . . . . 3-8
3.2.1.1	Fracture Permeability . . . . . 3-8
3.2.1.2	Matrix Permeability . . . . . 3-9
3.2.1.3	Fracture Frequency . . . . . 3-9
3.2.1.4	Effective Fracture and Matrix Porosity . . . . . 3-10
3.2.1.5	Fracture and Matrix van Genuchten Alpha . . . . . 3-11
3.2.1.6	Fracture and Matrix Klinkenberg Coefficient . . . . . 3-11
3.2.1.7	Fracture and Matrix Water Content . . . . . 3-11
3.2.1.8	Dry and Saturated Thermal Conductivity . . . . . 3-12
3.2.1.9	Dry Rock Specific Heat . . . . . 3-12
3.2.2	Comparison of Scales . . . . . 3-12
3.2.3	Parameter Correlations . . . . . 3-13
3.3	Summary . . . . . 3-15
4	GEOSPATIAL ANALYSIS OF APACHE LEAP RESEARCH SITE DATA . . . . . 4-1
4.1	Experimental Variograms . . . . . 4-1
4.2	Model Fitting . . . . . 4-1
4.3	Comparison with Other Apache Leap Research Site Geostatistical Analyses . . . . . 4-13
4.3.1	Geostatistical Analysis of Bassett, et al. (1994, Chapter 4) and Rasmussen, et al. (1996, pp. 52-91) . . . . . 4-13
4.3.2	Geostatistical Analysis by Bassett, et al. (1997) . . . . . 4-13
4.3.3	Geostatistical Analyses of Illman, et al. (1998) and Chen, et al. (2000) . . . . . 4-14
5	DISCUSSION . . . . . 5-1
6	SUMMARY . . . . . 6-1
7	REFERENCES . . . . . 7-1
APPENDIX	

## FIGURES

Figure	Page
2-1	Location Map of the Apache Leap Research Site Test Area (Star) . . . . . 2-2
2-2	Plan View of Boreholes, Plastic Cover, and Field Laboratory at the Apache Leap Research Site . . . . . 2-3
2-3	Three-Dimensional Perspective of Boreholes at the Apache Leap Research Site . . . 2-4
2-4	Histograms of (a) Dry Thermal Conductivity, (b) Saturated Thermal Conductivity, (c) Dry Rock Specific Heat, (d) van Genuchten $\alpha$ . . . . . 2-15
2-5	Histograms of (a) Dry Thermal Conductivity, (b) Saturated Thermal Conductivity, (c) Dry Rock Specific Heat, (d) LOG <sub>10</sub> van Genuchten $\alpha$ . . . . . 2-16
2-6	Air Permeability Versus Fracture Density . . . . . 2-20
2-7	Water Permeability Plotted Against Air Permeability for Field and Laboratory Data at Apache Leap . . . . . 2-22
2-8	Klinkenberg Coefficient Plotted Against Liquid Permeability for Laboratory Data: Apache Leap Research Site . . . . . 2-22
2-9	Liquid Permeability Plotted Against Air Permeability for Field and Klinkenberg Corrected Laboratory Data: Apache Leap Research Site . . . . . 2-23
2-10	Plot of the Field Permeability Versus the Difference Between Field and Laboratory Derived Values of Permeability for Both Air and Water . . . . . 2-23
4-1	Fitted Experimental Variogram for Field Estimates of LOG <sub>10</sub> Air Permeability with Lag of 1.12 m . . . . . 4-4
4-2	Fitted Experimental Variogram for Field Estimates of LOG <sub>10</sub> Air Permeability with Lag of 2.0 m . . . . . 4-4
4-3	Fitted Experimental Variogram for Field Estimates of LOG <sub>10</sub> Air Permeability with Lag of 3.0 m . . . . . 4-5
4-4	Fitted Experimental Variogram for Field Estimates of LOG <sub>10</sub> Air Permeability with Lag of 4.0 m . . . . . 4-5
4-5	Fitted Experimental Variogram for Field Estimates of LOG <sub>10</sub> Air Permeability with Lag of 5.0 m . . . . . 4-6
4-6	Fitted Experimental Variogram for Field Estimates of LOG <sub>10</sub> Liquid Permeability with Lag of 6.0 m . . . . . 4-6
4-7	Fitted Experimental Variogram for Laboratory Estimates of LOG <sub>10</sub> Air Permeability with Lag of 3.0 m . . . . . 4-7
4-8	Fitted Experimental Variogram for Laboratory Estimates of LOG <sub>10</sub> Liquid Permeability with Lag of 3.0 m . . . . . 4-7
4-9	Fitted Experimental Variogram of Fracture Density with Lag of 3.0 m . . . . . 4-9
4-10	Fitted Experimental Variogram of LOG <sub>10</sub> Porosity with Lag of 3.0 m . . . . . 4-9
4-11	Fitted Experimental Variogram of LOG <sub>10</sub> van Genuchten $\alpha$ Coefficient with Lag of 3.0 m . . . . . 4-10
4-12	Fitted Experimental Variogram of LOG <sub>10</sub> Klinkenberg Coefficient with Lag of 3.0 m . . . . . 4-10
4-13	Fitted Experimental Variogram of Water Content with Lag of 3.0 m . . . . . 4-11
4-14	Fitted Experimental Variogram of Dry Thermal Conductivity with Lag of 3.0 m . . . . 4-11

## FIGURES (continued)

Figure		Page
4-15	Fitted Experimental Variogram of Saturated Thermal Conductivity with Lag of 3.0 m .....	4-12
4-16	Fitted Experimental Variogram of Dry Rock Specific Heat with Lag of 3.0 m .....	4-12

## TABLES

Table	Page
2-1	Sample Statistics of Fracture Permeability and Fracture Porosity Values Obtained from Type-Curve Interpretations of Cross-Hole Data . . . . . 2-8
2-2	Mean Fracture Frequency Values for Boreholes at the Apache Leap Research Site . . . . . 2-10
2-3	LOG <sub>10</sub> Air-Filled Fracture Porosity As Interpreted for Cross-Hole Test PP4 . . . . . 2-11
2-4	Summary Statistics of the Original Data Set . . . . . 2-14
2-5	Summary Statistics of LOG <sub>10</sub> -Transformed Data Values. . . . . 2-17
2-6	Correlation Matrix of Analyzed Variables. . . . . 2-19
2-7	Summary Statistics of Single-Hole Air Permeability Data. . . . . 2-25
3-1	Comparison of Apache Leap Research Site and Yucca Mountain Field-Estimated Air Permeabilities and Their Relationship to Fracture Density . . . . . 3-3
3-2	Comparison of Properties Estimated at Apache Leap Research Site and Yucca Mountain. . . . . 3-4
3-3	Frequency of Fractures in Boreholes at Yucca Mountain for the Paintbrush Nonwelded Tuff . . . . . 3-5
3-4	Comparison of Fracture Air Permeability, Variance, and Measurement Scales . . . 3-14
4-1	Summary of Variogram Parameters . . . . . 4-2
4-2	Summary of Combined Rasmussen, et al. and Guzman, et al. LOG <sub>10</sub> -Transformed Air Permeability Data . . . . . 4-14

## ACKNOWLEDGMENTS

This report was prepared to document work performed by the Center for Nuclear Waste Regulatory Analyses (CNWRA) for the U.S. Nuclear Regulatory Commission (NRC) under Contract No. NRC-02-02-012. The activities reported here were performed on behalf of the NRC Office of Nuclear Material Safety and Safeguards, Division of Waste Management. The report is an independent product of the CNWRA and does not necessarily reflect the views or regulatory position of the NRC.

The authors would like to thank P. Houston for her dedication to report preparation, D. Farrell and D. Sims for their insightful technical reviews, B. Sagar for his programmatic review, and C. Cudd, C. Gray, B. Long, and J. Pryor for their editorial reviews, all of which greatly improved the final report.

## QUALITY OF DATA, ANALYSES, AND CODE DEVELOPMENT

**DATA:** CNWRA-generated original data contained in this report meet quality assurance requirements described in the CNWRA Quality Assurance Manual. Sources of other data should be consulted for determining the level of quality for those data.

**ANALYSES AND CODES:** The ISATIS Version 3.1.3 geostatistical package was used for analyses contained in this report. This computer code is controlled under the CNWRA Software Configuration Procedures.

# 1 INTRODUCTION

## 1.1 Background and Objectives

The U.S. Department of Energy (DOE) has recently recommended Yucca Mountain, Nye County, Nevada, as the site for the nation's first geologic repository for high-level nuclear waste. The current waste isolation strategy implements a multiple concept with the waste placed in corrosion-resistant waste packages prior to their emplacement in drifts that will be located within unsaturated, variably fractured volcanic tuffs. A key criterion for the licensing of the proposed repository is whether the engineered and natural barrier systems will provide effective long-term isolation of the waste from the accessible biosphere. The long-term safety of the proposed repository is being evaluated using performance assessments, which include features, events, and processes that are important to repository performance. The unsaturated zone thermohydrology portion of this assessment requires representative host rock unsaturated flow, solute transport, and thermal parameters as input, including statistical moments, distributional characteristics, and covariance structures.

To obtain spatial information on thermohydrologic parameters and connectivity of permeable flow pathways in fractured volcanic tuffs, extensive field studies have been conducted by DOE researchers through means of hydraulic and pneumatic injection tests at Yucca Mountain. Field tests include a large number of single- and cross-hole pneumatic injection and gaseous tracer tests under isothermal conditions, borehole infiltration tests, and pneumatic tests during the single-heater experiments and the ongoing drift-scale heating experiments. Air permeability values determined through air injection tests conducted under isothermal conditions are assumed to represent the permeability of the fracture network in the host rock. Results of the field tests have shown considerable spatial variation of hydraulic and pneumatic properties. In particular, air permeability values determined from air injection tests conducted in the Exploratory Studies Facility varied over at least five orders of magnitude within a single hydrostratigraphic unit (CRWMS M&O, 2000a).

There is considerable uncertainty in the rate of percolation flux through Yucca Mountain and its effect on repository performance. To study the movement of moisture near and within the repository area, DOE researchers have modeled percolation flux through Yucca Mountain using a three-dimensional site-scale numerical model with homogeneous layers (CRWMS M&O, 2000b; see also Wu, et al., 1999 and Bandurraga and Bodvarsson, 1999). On a smaller scale, the drift-scale model for seepage employs a more refined grid and incorporates heterogeneity within layers (CRWMS M&O, 2000b). The thermohydrologic model used to generate input for the abstraction of water percolating near the drifts in the DOE Total System Performance Assessment code assumed homogeneous layers, but a sensitivity analysis of the effect of intralayer heterogeneity was recently documented (CRWMS M&O, 2001). Intralayer heterogeneity of fracture permeability is a required component in continuum models for representing the process of fingers or rivulets of liquid water that breach the dryout zone and arrive at the drift during the thermally perturbed period of the repository life cycle. Heat load and thermal conductivity are the most sensitive parameters for predicting the magnitude and duration of the thermal pulse. Heat load will be constrained by design. Recent efforts by DOE using the thermohydrologic model (CRWMS M&O, 2001) are beginning to evaluate the effect of intralayer heterogeneity of thermal conductivity on temperature and relative humidity conditions in the drifts.

Representation of the fractured tuff porous media has evolved from equivalent continuum models to dual-porosity models and, most recently, to dual-permeability models. Matrix and fractures are treated as separate but interacting continua in the latter two models. In the dual-permeability representation, fluids move from cell to cell in both continua. In the dual-porosity representation, fluids move only in the fracture continuum, and matrix cells act as storage. The TOUGH2 (Pruess, 1991) and NUFT (Nitao, 1998) codes currently implement dual-permeability representations of the fractured tuff for DOE thermohydrological and unsaturated zone models (CRWMS M&O, 2001, 2000b). These codes are designed to handle multiphase flow and heat transfer involving liquid water, water vapor, and air in a heterogeneous fractured medium. Various empirical relations are used to describe two-phase flow properties, most notably the van Genuchten (1980) function relating the relative permeability and saturation functions.

The dual-permeability Yucca Mountain unsaturated zone site-scale model (CRWMS M&O, 2000b) was intended to support assessment of the system performance. The site-scale numerical model has been calibrated using temperature, water potential, and saturation data collected in the field, and has been shown to reproduce the overall heat distribution, moisture profiles, and pneumatic pressure variations in different lithologic units. Permeability values employed in the numerical model were calibrated by inverse modeling of core and field data. Each layer in the three-dimensional site-scale model was assigned a uniform value of permeability. Heterogeneity between subhorizontal layers is included, but each hydrostratigraphic layer is considered homogeneous with the exception of zeolitic zonation in the Calico Hills units lying below the repository horizon. The thermohydrologic model used by the DOE (CRWMS M&O, 2001) uses parameters derived from the unsaturated zone site-scale model. A three-dimensional grid was developed to evaluate the sensitivity of heterogeneity of fracture permeability to dripping on a waste package (CRWMS M&O, 2001). Extreme cases of fracture heterogeneity were needed before dripping increased above the seepage threshold, though preferential pathways above the drifts did develop. The seepage threshold conceptualization in the thermohydrologic model may underpredict the amount of water entering drifts (Fedors, et al., 2002a), thus constraining any conclusions. More relevant to the topic of this report, the sole basis for the generation of heterogeneous properties was a variogram from a small {18 m<sup>3</sup> [640 ft<sup>3</sup>]} and dominantly horizontal volume of fractured rock above the ceiling of Niche 3650. The small measurement volume in the middle nonlithophysal unit is not likely representative of heterogeneity across the repository. Furthermore, that the variogram has a finite sill is likely an artifact of including measurements made in the zone of excavation-induced fracturing (Fedors, et al., 2002a).

A two-dimensional model of unsaturated groundwater flow was constructed (Illman and Hughson, 2001; Fedors, et al., 2002b) using the computer program MULTIFLO (Lichtner, et al., 2000) to investigate the effect of heterogeneous fracture permeability distributions on deep percolation processes at Yucca Mountain. In these simulations, the fractured rock was represented using a dual-permeability model, in which the matrix and fracture constitute two distinct continua represented by two overlapping, interacting numerical grids. The exchange of fluids between the two continua is governed by Darcy's law, and the area of the matrix-fracture interface is open to flow. The coefficient for the interaction term between the two continua was constrained to a constant value. The fracture network was treated as a distinct stochastic continuum, and the matrix as a separate homogeneous continuum. For their numerical study, arbitrary LOG<sub>10</sub>-transformed permeability statistics (in particular, variance and correlation structure) were used for fracture permeability heterogeneity because geostatistical analyses of

Yucca Mountain data sets were unavailable. In many lithologic units, the available experimental data are insufficient for determining the spatial statistics of fracture permeability. Numerical analysis of unsaturated flow through layered fractured tuffs, which considered the spatial variability of the fracture permeability within the layers, revealed the development of preferential pathways and flow focusing, which lead to locally high flux rates that could significantly change estimates of seepage into drifts. With a uniform flux at the top boundary, and without explicitly building-in high-permeability flow pathways nor discrete features to represent fractures, water flow rates in localized pathways were found to be very high (more than ten times the input flow rate). This work suggested the importance of spatial variability in the permeability parameter to deep percolation, as well as the potential for preferential flow to breach the dryout zone during the thermal period.

Several important questions about the conceptual model of flow and transport at Yucca Mountain arise when the large range of fracture permeabilities and its effect on the numerical modeling of deep percolation processes are considered. What other flow and transport parameters are highly heterogeneous? To what degree are they variable? And what are the effects of this variability on processes such as deep percolation, coupled liquid and gas flow, radionuclide transport, and thermal effects on flow? Most importantly, what are the consequences to model results and repository performance when the spatial variability in parameters is not considered?

To help answer some of these questions, a geostatistical analysis of data collected by Rasmussen, et al. (1990) from unsaturated fractured tuffs at the Apache Leap Research Site, a potential hydrogeologic analog to Yucca Mountain, is presented in this report. The field and laboratory research program based at the Apache Leap Research Site was funded by the U.S. Nuclear Regulatory Commission (NRC) to provide data sets related to the interstitial, hydraulic, pneumatic, and thermal properties of unsaturated fractured rock. The main purpose of this program was to provide the NRC with laboratory and field data that can be employed to test flow and transport modeling concepts in unsaturated fractured tuffs. The first objective of this report is to summarize the statistical data on hydrological and thermal properties for the Apache Leap Research Site and the Yucca Mountain site in order to assess the quality of Apache Leap Research Site as an analog for the unsaturated zone at Yucca Mountain. The second objective is to summarize the results from geostatistical analyses of pneumatic, hydraulic, and thermal properties of unsaturated fractured tuffs, which were collected by Rasmussen, et al. (1990) at the Apache Leap Research Site. Analyzed parameters include (i) field estimates of air permeability, (ii) field estimates of liquid permeability, (iii) laboratory estimates of air permeability, (iv) laboratory estimates of liquid permeability, (v) fracture frequency, (vi) effective matrix and fracture porosity, (vii) alpha-value of the van Genuchten moisture characteristic function, (viii) matrix Klinkenberg coefficient, (ix) water content, (x) dry thermal conductivity, (xi) saturated thermal conductivity, and (xii) dry rock specific heat. The analyses were conducted using the software package ISATIS, a general-purpose statistical package that includes a wide range of geostatistical estimation and simulation algorithms (Geovariances, 1997).

This report provides information on the parameter variability of unsaturated fractured tuffs at the Apache Leap Research Site, which are potentially analogous to tuffs found at Yucca Mountain. A three-dimensional stochastic field of permeability and other parameters can be obtained through the application of existing geostatistical simulation techniques. The information in this

report can be used to support performance assessments and confirmatory modeling of flow and transport processes at Yucca Mountain.

## **1.2 Programmatic Relevance**

This work is driven by the hypothesis that it is important to consider intralayer heterogeneity of matrix and fracture properties for focusing of flow, seepage into drifts, and transport of radionuclides to the water table. Conceptually, heterogeneity in matrix and fracture properties may lead to flow focusing of percolating water. Omitting flow focusing is expected to lead to nonconservative measures of dose, but to what extent is unclear. Previous numerical modeling (Illman and Hughson, 2001; Fedors, et al., 2002b) demonstrated that the inclusion of fracture permeability heterogeneity affects distribution of percolation flux at the repository horizon. Because there were no geostatistical analyses of Yucca Mountain data, geostatistical parameters were necessarily assumed for use in the generation of heterogeneous fields. If the thermohydrological properties can be shown to be similar at the two sites, the Apache Leap Research Site offers geostatistical data for a fractured tuff site that could be used to constrain the geostatistical parameters used at Yucca Mountain. Assuming that the data from the Apache Leap Research Site will be used as an analog to Yucca Mountain in future modeling, and if such modeling again demonstrates a significant effect on the repository performance, then it may be necessary to collect additional data at Yucca Mountain. The DOE Systematic Testing Program in the Enhanced Characterization of the Repository Block draft currently being performed should provide useful data on heterogeneity that, when made available, can be evaluated for adequacy based dual-permeability, stochastic models.

Parameter uncertainty in the ambient and thermohydrological models should be propagated through linked process models into the abstraction for total system performance assessment to help aid in the understanding of both the expected performance and possible performance of the proposed repository. Thermal Effects on Flow technical agreements TEF2.10 and TEF2.08 call directly for parameter uncertainty to be incorporated (or else a basis presented for uncertainty not being incorporated in both process and abstracted models).

The work presented in this report is intended to be preparatory for modeling efforts that will be used to assess the importance of including intralayer heterogeneity in the isothermal and nonisothermal unsaturated zone flow models applied at Yucca Mountain.

## **1.3 Report Organization**

Chapter 2 provides a detailed site description of the Apache Leap Research Site. A suite of hydrological and thermal property data previously collected at the Apache Leap Research Site by Rasmussen, et al. (1990) are described systematically through an exploratory data analysis to provide a foundation for assessing their quality as analog data for the unsaturated zone at Yucca Mountain. The exploratory data analysis includes the computation of summary statistics (e.g., the minimum and maximum values, the mean, the variance, and the standard deviation). Histograms of the data set are plotted, and the shape of the distribution is described with the coefficient of variation, the skewness, and the kurtosis. Univariate and multivariate analyses of the data are presented, as well as the correlation matrix between the thermohydrologic variables. More recent data collection at this site and its interpretation are also presented. Finally, a summary of other statistical analyses of Apache Leap Research Site data, primarily

permeability data, is provided in support of the conclusions drawn from the Rasmussen, et al. (1990) data.

Chapter 3 provides a Yucca Mountain, Nevada, site description and describes the tests and methods utilized by the DOE to collect thermohydrologic property data. The data are presented for comparison with those collected from the Apache Leap Research Site, a proposed Yucca Mountain analog, and the issues of scale and parameter correlations also are examined. Chapter 4 provides a discussion of experimental variogram calculation and structural analyses for the Rasmussen, et al. (1990) Apache Leap Research Site data. Preliminary fitted variogram models are shown for each analyzed variable. Chapter 5 discusses the geostatistical analyses and what they imply for numerical modeling of fluid flow and solute transport in the unsaturated zone of Yucca Mountain. Chapter 6 provides a summary, including technical issues that require further investigation. Chapter 7 lists the references cited in this report.

## 2 THE APACHE LEAP RESEARCH SITE

### 2.1 Site Description and Summary of Data Collection

Near the western edge of the Pinal Mountains and 3 km [1.9 mi] east of the town of Superior, Arizona, lies the Apache Leap, a 600-m [1,970-ft] west-facing escarpment exposing a volcanic ash-flow tuff sheet (Rasmussen, et al., 1990; Illman, et al., 1998). Researchers from the University of Arizona, while under contract with the U.S. Nuclear Regulatory Commission (NRC), have studied a small volume of this tuff in great detail. The Apache Leap Research Site is located at an elevation of 1,256 m [4,120 ft] above sea level (LeCain, 1995; Figure 2-1); its geology consists of fractured tuff, and climatic and topographic conditions are similar to those in the vicinity of Yucca Mountain, Nevada (Illman, et al., 1998). Thus, the site has the potential to be a good small-scale analog of Yucca Mountain. Additionally, the site has allowed for a unique opportunity to independently study flow, transport, and travel time issues in unsaturated fractured tuff.

While the tuff is more than 300 m [984 ft] thick at the Apache Leap Research Site, the average thickness of the dacite ash-flow sheet was originally 600 m [1,968 ft] but has subsequently weathered to an average 150 m [492 ft]; the areal extent of the formation is 1,000 km<sup>2</sup> [390 mi<sup>2</sup>] (Peterson, 1961; Rasmussen, et al., 1990). The volcanic ash-flow tuff resulted from deposition of a turbulent, high-temperature cloud of gas and pyroclastic materials {particle diameters are <0.40 mm [<0.02 in]} 19 million years ago (Illman, et al., 1998). Phenocrysts, pumice fragments, and foreign rocks are entrained within the volcanic ash deposits, which grade from nonwelded at the top of the formation to partly welded in its midsection to densely welded near its base (Rasmussen, et al., 1990; LeCain, 1995).

The regional climate is temperate and dry, and the mean annual precipitation at the site is approximately 64 cm [25 in] (Rasmussen, et al., 1990; LeCain, 1995). Precipitation generally occurs during two periods: (i) mid-July to late September, and (ii) mid-November to late March (Rasmussen, et al., 1990; Illman, et al., 1998). During summer periods that are characterized by high temperatures and elevated evapotranspiration demand, precipitation is linked to high-intensity, short-duration monsoonal thunderstorms (Rasmussen, et al., 1990; Illman, et al., 1998). During cooler winter periods that are characterized by much lower evapotranspiration demand, storms are of longer duration but lower intensity (Rasmussen, et al., 1990; Illman, et al., 1998). The regional water table lies at a variable depth of 600–1,500 m [1,970–4,920 ft] below the land surface (steep local gradients are apparently due to mine dewatering operations; Rasmussen, et al., 1990; Illman, et al., 1998). The rock above the water table is unsaturated but for a thin perched water zone that exists at a depth of approximately 150 m [490 ft] below the land surface (Illman, et al., 1998).

The Apache Leap Research Site test domain spans a surface area of approximately 55 × 35 m [180 × 115 ft] and a volume of rock on the order of 60,000 m<sup>3</sup> [2.1 million ft<sup>3</sup>] (Illman, et al., 1998). Twenty-two clustered boreholes, either inclined (45° below horizontal) or vertically oriented, were completed to a maximum vertical depth of 30 m [98 ft] within a layer of unsaturated, partially welded tuff (Illman, et al., 1998). The statistical analyses in this report use data from nine of the boreholes (i.e., X-, Y-, and Z-series), representing a volume on the order of 20,000 m<sup>3</sup> [700,000 ft<sup>3</sup>]. Boreholes having the designations X, Y, and Z were drilled during the initial stages of the project, prior to those designated V, W, and G. Though comments are

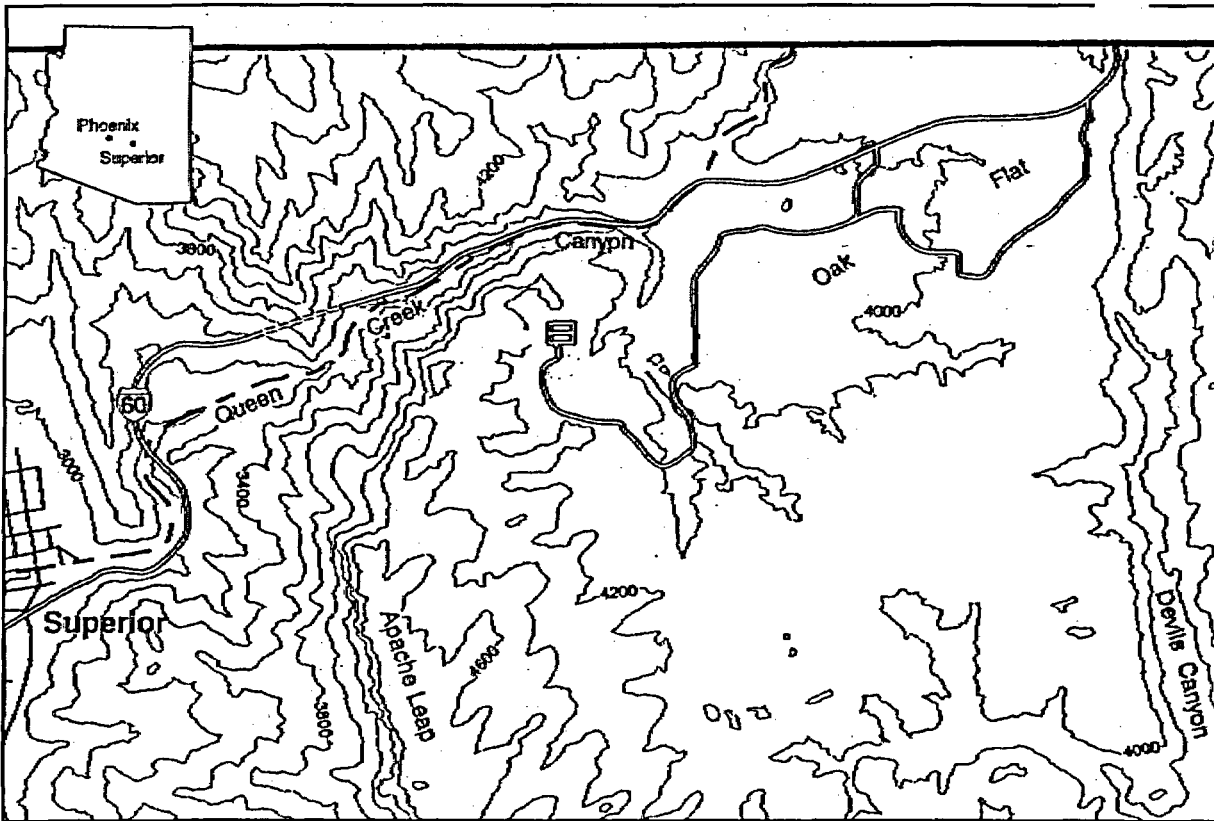


**Figure 2-1. Location Map of the Apache Leap Research Site Test Area (Star). Elevation Contours Are in Feet [1.0 ft = 0.30 m] Above Mean Sea Level (After Illman and Neuman, 2001).**

included in this report on measured properties from the other boreholes, the X-, Y-, and Z-series boreholes are the focus of the geostatistical analyses because a complete suite of hydrological and thermal properties were measured. The Apache Leap Research Site is illustrated in plan view in Figure 2-2. Surveyed wellhead locations (Figure 2-2) and borehole geometries (Figure 2-3) are referenced to a local Cartesian coordinate system ( $x, y, z$ ) oriented  $8^\circ$  west of north, vertical  $z$ -axis positive downward (Illman, et al., 1998). Locations reported in the appendix tables are referenced to this local coordinate system. All boreholes were drilled with conventional rotary equipment using water as the cooling and chip-circulating fluid, and the upper 1.8 m [6.0 ft] of each borehole were cased (Illman, et al., 1998). An orientation mark was inscribed every 1.52 or 3.05 m [5.0 or 10.0 ft] along the borehole (Rasmussen, et al., 1990). A total of 270 m [886 ft] of oriented core were retrieved from the boreholes, and they are stored at the University of Arizona Core Storage Facility (Illman, et al., 1998).

Shortly after borehole completion, a surface area of 1,500 m<sup>2</sup> [16,000 ft<sup>2</sup>] encompassing all boreholes (except for the W2, W2A, and W3 boreholes and all G boreholes) plus an additional 10 lateral meters [33 ft] was covered with a plastic tarp to minimize infiltration and evaporation

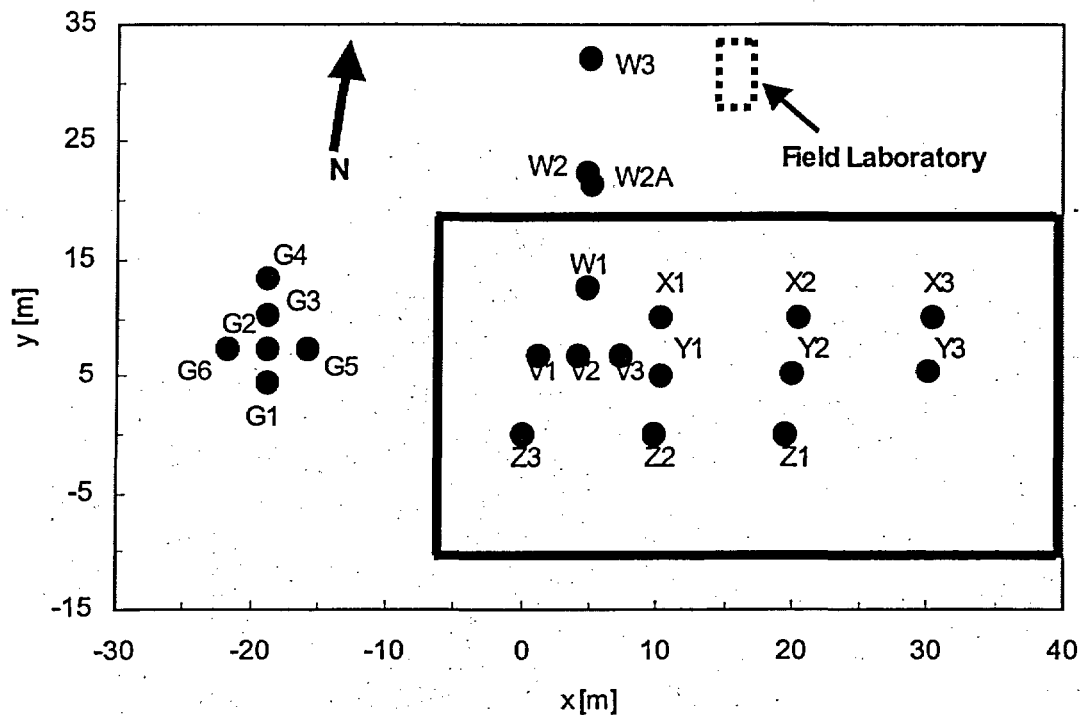


**Figure 2-2. Plan View of Boreholes, Plastic Cover, and Field Laboratory at the Apache Leap Research Site (Adapted from Illman and Neuman, 2001). Data From X-, Y-, and Z-Series Boreholes Were Subject to Geostatistical Analyses in This Report. [1.0 m = 3.28 ft]**

(Rasmussen, et al., 1990; Illman, et al., 1998). The vertical G boreholes are approximately 20 m [66 ft] deep and lie to the west of the plastic tarp (Figure 2-2; Illman, et al., 1998). With the exception of the G boreholes, borehole television images are available (Illman, et al., 1998).

Early work related to the covered site is described by Rasmussen and Evans (1992, 1989, 1987), Tidwell, et al. (1988), Yeh, et al. (1988), Weber and Evans (1988), Chuang, et al. (1990), Rasmussen, et al. (1990, 1993, 1996), Evans and Rasmussen (1991), Haldeman, et al. (1991), and Bassett, et al. (1994). Matrix properties of core segments extracted from 3-m [10-ft] borehole intervals at 105 locations within nine of the boreholes (X-, Y-, and Z- series) were

measured in a lab (Illman, et al., 1998). Measurements included interstitial properties such as bulk density, effective porosity, skeletal density, pore surface area, and pore size distribution; hydraulic properties such as saturated and unsaturated hydraulic conductivity and moisture-retention characteristics, and the alpha-value of the van Genuchten moisture characteristic function; pneumatic properties such as oven-dry and unsaturated air-phase permeability, and the matrix Klinkenberg coefficient (Illman, et al., 1998). Additionally, fracture properties, including permeability and hydraulic conductivity, were measured through single-hole pneumatic and hydraulic tests. These tests were conducted in the same 3-m [10-ft] borehole

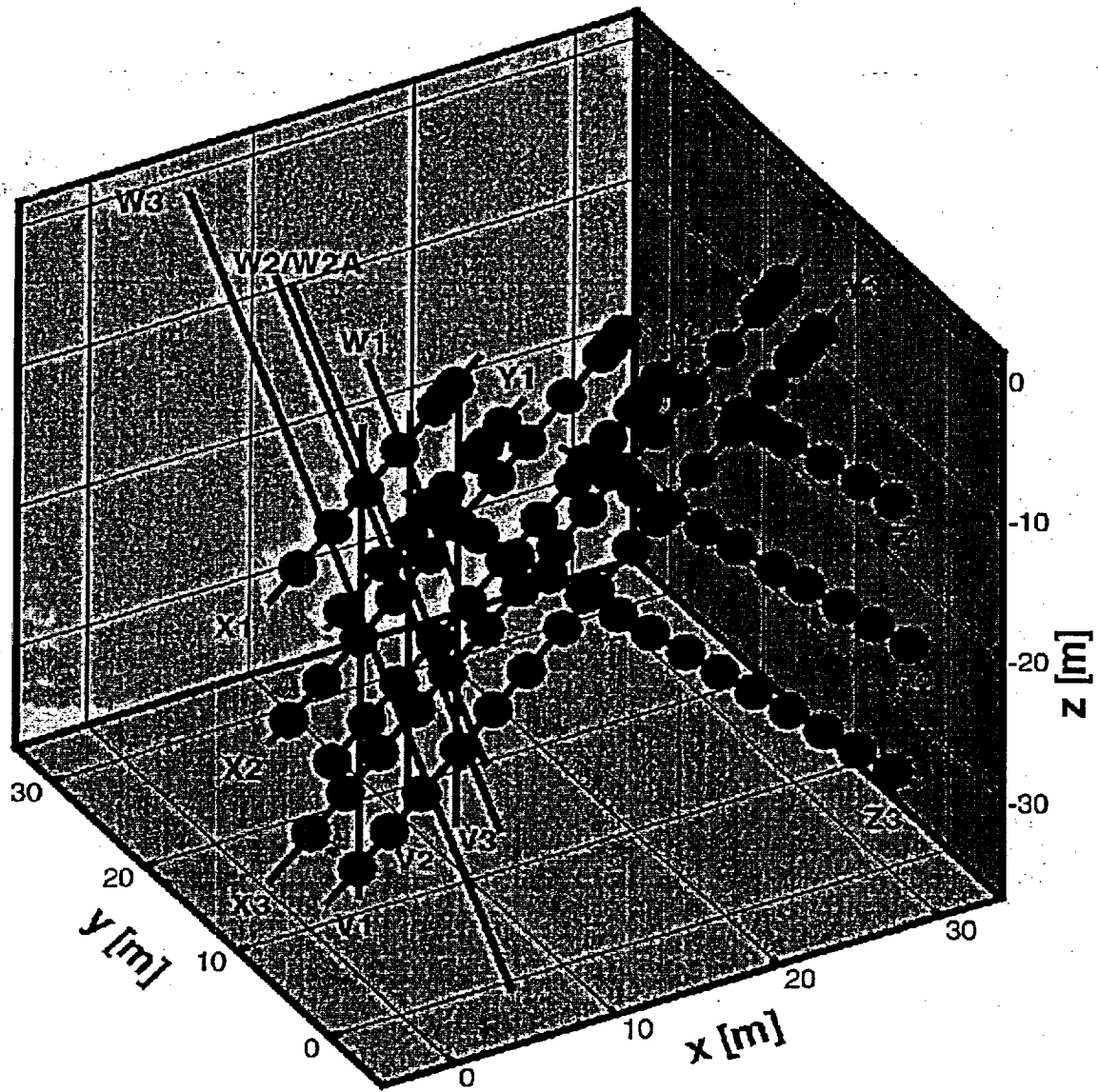


Figure 2-3. Three-Dimensional Perspective of Boreholes at the Apache Leap Research Site with Solid Circles Representing Sample Locations of Data Used in the Geostatistical Analyses [1.0 m = 3.28 ft]

intervals from which core samples had been taken. Further details about the site, its characteristics, and the tests conducted are summarized in Rasmussen, et al. (1990).

More recently, numerous single-hole (Bassett, et al., 1994, Chapter 4; Guzman, et al., 1996) and cross-hole (Illman, et al., 1998) pneumatic injection tests have been conducted at the site. Of more than 270 single-hole tests, 183 were conducted in boreholes V2, W2A, X2, Y2, Y3, and Z2 by setting the packers 1.0 m [3.3 ft] apart (Guzman, et al., 1996). These air permeability data were analyzed geostatistically by Bassett, et al. (1997).

Forty-four cross-hole tests were conducted by Illman (1999; see also Illman, et al., 1998, and Illman and Neuman, 2001) in 16 boreholes belonging to series V, W, X, Y, and Z. The purpose of these tests was to (i) directly characterize the air permeability and air-filled porosity of the rock on a site-wide scale, (ii) determine the spatial extent and connectivity of fractures and/or high-permeability flow channels across the site, and (iii) compare the results with corresponding information that one might deduce from smaller scale (laboratory and single-hole) tests. Air was injected into several 1.0- to 2.0-m [3.3- to 6.6-ft] sections of various boreholes sequentially, and the corresponding air pressure response was measured simultaneously in 38 different intervals situated in neighboring boreholes. Illman and Neuman (2001) provided a detailed description of one of these tests, labeled PP4, which was interpreted by means of type-curve analysis. They analyzed recorded pressures in each monitoring interval separately from those in other intervals, while treating the fractured rock as a uniform, isotropic porous continuum. Each record yielded an equivalent directional air permeability and air-filled porosity for fractures that connect the corresponding monitoring and injection intervals, representing rock volumes with length scales at least as large as the distances between these intervals (meters to tens of meters). Both parameters were found to vary considerably from one monitoring interval to another, reflecting the nonuniform nature of pneumatic rock properties at the Apache Leap Research Site.

Single- and cross-hole pneumatic injection tests have shown that (i) the pneumatic pressure behavior of fractured tuff at the site is amenable to analysis by treating the rock as a continuum on scales ranging from meters to tens of meters, and (ii) this continuum is representative primarily of interconnected fractures (Chen, et al., 2000). Both the single-hole and cross-hole test results have proven to be virtually free of skin effect (Illman and Neuman, 2000, 2001), implying that they represent rock conditions unperturbed by the presence of boreholes.

Vesselinov, et al. (2001a,b) used a three-dimensional numerical inverse model to interpret several cross-hole pneumatic injection tests at the Apache Leap Research Site. Their model solves the airflow equations in their original nonlinear form and accounts directly for the ability of all packed-off borehole intervals to store and conduct air through the system. These authors analyzed pneumatic cross-hole test data in two ways: (i) by considering pressure records from individual borehole monitoring intervals one at a time, while treating the rock as being spatially uniform; and (ii) by considering pressure records from multiple tests and borehole monitoring intervals simultaneously, while treating the rock as a random fractal characterized by a power variogram. The first approach yielded a series of equivalent  $\text{LOG}_{10}$ -transformed air permeability values and  $\text{LOG}_{10}$ -transformed air-filled porosity values for fractures that connect the corresponding monitoring and injection intervals, representing rock volumes with length scales at least as large as the distances between these intervals (meters to tens of meters). The second approach yielded a high-resolution estimate of how air permeability and air-filled porosity, which are defined on grid blocks having a length scale of 1.0 m [3.3 ft], vary spatially throughout the tested rock volume. This approach essentially amounts to three-dimensional pneumatic

tomography (or stochastic imaging) of the rock, a concept originally proposed in the context of hydraulic cross-hole tests by Neuman (1987).

## **2.2 Data Description**

Data employed for the geostatistical analyses presented herein were collected from three sets of inclined boreholes (the X-, Y-, and Z-series) during the initial stage of the field program (Rasmussen, et al., 1990). In this report, CNWRA staff focus on this earlier data set because interstitial, hydrologic, and thermal properties were collected during the early phase of study at Apache Leap Research Site. Sample locations of data used in the geostatistical analyses are shown in Figure 2-3. Each set of three boreholes is separated by 5 m [16 ft], and boreholes within each set are separated by 10 m [33 ft]. Boreholes with a 45° incline were used because of the presence of both horizontal and near-vertical fractures at the site. The boreholes are east-west trending and dip in both directions.

Field estimates of air permeability were made using air injection tests performed at 3-m [10-ft] packed-off spacings (Rasmussen, et al., 1990). As matrix porosity values are generally larger than the porosity of fractures, and pore sizes within the matrix are generally smaller than fracture openings on the average, most of the water resides in the matrix, and its water content is much higher than that of the fractures under isothermal conditions. Air permeability values determined through air injection tests conducted under isothermal conditions were thus assumed by University of Arizona personnel to represent the permeability of the fracture network.

Approximately 270 m [886 ft] of 6.4-cm [2.5-in] diameter oriented core were obtained from the nine X-, Y-, and Z-series inclined boreholes during the drilling phase. Laboratory measurements were made on core-plug samples of the tuff matrix obtained from the oriented core using 5-cm [2-in] long subsections cut from the core at approximately 3-m [10-ft] intervals at 105 locations free of visible fractures. Fracture frequency was reported by Rasmussen, et al. (1990) as the number of fractures intersecting each 3-m [10-ft] borehole interval (identical intervals with packer tests) from oriented cores. Uncorrected fracture frequency values are used to examine the correlation with permeability values and to examine general geostatistical characteristics of the Apache Leap Research Site data. While the uncorrected fracture frequency data are likely sufficient for the correlation study with permeability and for preliminary geostatistical analyses, the fracture frequency data can and will be corrected for orientation bias within this report to represent the distribution of fractures within the test volume and to facilitate comparison with Yucca Mountain (orientation bias refers to the sampling bias created by the borehole orientation in a three-dimensional fracture network).

The following is a brief description of analyzed variables. More detailed descriptions of the experimental design, methodology, and data can be found in Rasmussen, et al. (1990), and quantification of parameter uncertainties are discussed on pages 42–46 of the aforementioned document.

### **2.2.1 Field Estimates of Fracture Air Permeability**

Single-hole pneumatic injection tests were conducted in 87 intervals of 3-m [10-ft] length within nine boreholes (X-, Y-, and Z-series boreholes) by Rasmussen, et al. (1990, 1993, 1996). The support of the parameter is defined nominally by the length of the injection interval, which is 3 m

[10 ft] in this case. According to Rasmussen, et al. (1993), the tests were conducted by injecting air at a constant injection rate between two inflated straddle packers while monitoring pressure within the injection interval. Pressure was said to have reached stable values within minutes in most test intervals. Measured fundamental field variables (i.e., pressure and injection rate) were used to compute air permeability via a formula developed by Dachler (1936), which has since been adapted for airflow. Estimates of field-measured air permeability are listed in Appendix Table 1.

More recently, single-hole pneumatic injection tests at a finer resolution (Bassett, et al., 1994, Chapter 4; Rasmussen, et al., 1996, pp. 52–91) and cross-hole pneumatic injection tests (Illman, et al., 1998; Illman and Neuman, 2001) were conducted. Single-hole tests were conducted in 183 borehole segments by setting the packers 1.0 m [3.3 ft] apart (Guzman, et al., 1996). Additional tests were conducted in segments of lengths 0.5, 2.0, and 3.0 m [1.6, 6.6, and 9.9 ft] in borehole Y2, and 2.0 m [6.6 ft] in borehole X2, bringing the total number of tests to more than 270. Forty-four cross-hole pneumatic injection tests of three types (constant-injection rate, step-injection rates, instantaneous-injection rate) were also conducted at the Apache Leap Research Site, spanning the entire volume of fractured rock previously subjected to single-hole testing, and beyond. The objectives of these tests were to (i) directly characterize the pneumatic properties of the rock on a site-wide scale, (ii) determine the spatial extent and connectivity of fractures and/or high-permeability flow channels across the site, and (iii) to compare the results with corresponding information that one might deduce from smaller scale (laboratory and single-hole) tests.

Sample statistics for fracture air permeability measurements obtained from type-curve interpretation of cross-hole test data, and from steady-state interpretation of 1.0-m [3.3-ft] and 3.0-m [9.9-ft] scale single-hole tests are summarized in Table 2-1. Note that the coefficient of variation for air-filled fracture porosity, which was reported in Illman and Neuman (2001; coefficient of variation equal to 3.0), is incorrect. A more recent calculation, given their reported mean and variance, yields a coefficient of variation equal to 1.16 (the coefficient of variation is calculated as the ratio of the standard deviation to the arithmetic mean).

## 2.2.2 Field Estimates of Fracture Liquid Permeability

Tidwell, et al. (1988) performed single-hole hydraulic injection tests in 87 intervals of 3-m [10-ft] length within nine boreholes (X-, Y-, and Z-series boreholes) at the Apache Leap Research Site, from which core samples had been taken. The hydraulic tests were conducted by maintaining a constant water level near the top of a borehole until a constant injection rate was established. The injection rate was converted into equivalent hydraulic conductivity using three different formulae for steady state flow. The geostatistical analysis performed in this work is based on hydraulic conductivity estimates calculated from one of these three formulae (i.e., the Glover formula) (Tidwell, et al., 1988). These calculated hydraulic conductivities ranged over five orders of magnitude; they are log-normally distributed and strongly skewed toward higher values. Following conversion to liquid permeability, these field estimates are listed in Appendix Table 1. Note that the arithmetic mean value of fracture liquid permeability, which was reported in Rasmussen, et al. (1990), is incorrect by one order of magnitude. A more recent calculation yields  $2.97 \times 10^{-14} \text{ m}^2$  [ $3.01 \times 10^{-2} \text{ D}$ ] [the spreadsheet upon which Appendix Table 1 is based is available upon request, and is found within Center for Nuclear Waste Regulatory Analyses (CNWRA) Scientific Notebook No. 510].

**Table 2-1. Sample Statistics of Fracture Permeability and Fracture Porosity Values Obtained from Type-Curve Interpretations of Cross-Hole Data and from Steady-State Interpretations of Single-Hole Data\***

	Cross-Hole Values		Single-Hole Values
Sample Statistic	LOG <sub>10</sub> (k, m <sup>2</sup> ) [D]	Fracture Porosity (m <sup>3</sup> /m <sup>3</sup> )	LOG <sub>10</sub> (k, m <sup>2</sup> ) [D]
Minimum	-14.3 [5.1 × 10 <sup>-3</sup> ]	2.9 × 10 <sup>-5</sup>	-17.1 [8.0 × 10 <sup>-6</sup> ]
Maximum	-12.3 [5.1 × 10 <sup>-1</sup> ]	7.2 × 10 <sup>-2</sup>	-11.6 [2.5 × 10 <sup>0</sup> ]
Mean	-13.5 [3 × 10 <sup>-2</sup> ]	1.7 × 10 <sup>-2</sup>	-15.2 [6.4 × 10 <sup>-4</sup> ]
Variance	0.36	3.9 × 10 <sup>-4</sup>	8.7 × 10 <sup>-1</sup>
Coefficient of Variation	-4.3 × 10 <sup>-2</sup>	1.16	-6.1 × 10 <sup>-2</sup>

\*Illman, W.A. and S.P. Neuman. "Type-Curve Interpretation of a Cross-Hole Pneumatic Injection Test in Unsaturated Fractured Tuff." *Water Resources Research*. Vol. 37, No. 3. pp. 583-603. 2001.

### 2.2.3 Laboratory Estimates of Matrix Air Permeability

Air permeability of oven-dried core samples was determined using a Hassler-sleeve permeameter described in Rasmussen, et al. (1990). A cylindrical core sample was placed inside the permeameter with a known pressure gradient applied longitudinally across the core segment, inducing one-dimensional flow. The airflow discharge was measured using a calibrated flowmeter. Air permeability was estimated using Darcy's law modified for airflow under ideal gas conditions. Laboratory estimates of air permeability are listed in Appendix Table 1.

### 2.2.4 Laboratory Estimates of Matrix Liquid Permeability

Liquid permeability of core samples was determined using a permeameter described in Rasmussen, et al. (1990). A core sample was placed inside the permeameter with water introduced under pressure at the upper surface of the core segment. Flow through the lower surface was measured using a flowmeter. The rock core was saturated using a sterile, 0.001 M CaSO<sub>4</sub> solution prior to performing the measurement. Laboratory estimates of liquid permeability were calculated with Darcy's law, and are listed in Appendix Table 1.

### 2.2.5 Fracture Frequency

Fracture location, strike orientation, and dip angle for fractures crossing borehole core can be found in Rasmussen, et al. (1990). The boreholes were drilled at a 45° angle to intercept both subvertical and horizontal fractures. Mathematical, graphical, and mechanical methods were used for correcting the apparent dips of fractures in the continuous core taken from inclined boreholes (Weber, 1986). Fracture density can be expressed in terms of either one-, two-, or three-dimensional measures. At the Apache Leap Research Site, only a one-dimensional measure is available from the borehole core logs. As discussed later in this section, without

additional information, it is not known whether borehole data under or over predicts three-dimensional fracture density. Uncorrected fracture frequency is defined here as the number of fractures that intersect a borehole, per unit length. Corrected fracture frequency accounts for orientation bias of the one-dimensional scanline (borehole) in a three-dimensional fracture network. Fracture frequency (uncorrected for orientation bias) data reported by Rasmussen, et al. (1990) are listed in Appendix Table 1.

Fracture populations in the east-west boreholes suggest a prominent north- to northwesterly-striking and westerly-dipping fracture set. Surface exposures indicate that an east-west fracture set is also prominent (Rasmussen, et al., 1990) but is poorly represented in the borehole data. The lack of representation of the east-west fracture set likely reflects the orientation bias caused by the east- and west-trending boreholes.

While the uncorrected fracture frequency data are likely sufficient for the correlation study with permeability at Apache Leap Research Site, the fracture data must be corrected for orientation bias to allow for a comparison of the fractured tuff at the Apache Leap Research Site with that at the Yucca Mountain site. Orientation bias created by boreholes cutting a three-dimensional fracture network can be corrected using the Terzaghi (1965) correction. Orientation bias is also referred to as direction bias. Fractures with fracture planes that are subparallel to the borehole would be grossly under-represented by simply counting the observed fractures in the core, such as the easterly-trending fracture set for the X-, Y-, and Z-series easterly-trending boreholes. There is no orientation bias for fractures with fracture planes perpendicular to the borehole trace. The corrected fracture frequency of each fracture is given by a Terzaghi factor,

$$T_f = \frac{1}{\cos(\theta)} \quad (2-1)$$

where  $\theta$  is the acute angle between the borehole and the normal to the fracture. Following the approach of Waiting, et al. (2001) for  $\theta > 75^\circ$ , a value of four was assigned as the Terzaghi factor to avoid asymptotic increases in fracture frequency as angles of  $90^\circ$  are approached. The calculated Terzaghi factors are listed in Appendix Table 4, along with the original fracture orientation data from Rasmussen, et al. (1990). Uncorrected mean fracture frequency and corrected mean fracture frequency for each of the nine boreholes were calculated and are presented in Table 2-2 for later comparison with data from Yucca Mountain boreholes.

Variations in the fracture network are evident in data from each borehole where the uncorrected fracture frequency varies from 0 to  $7 \text{ m}^{-1}$  [0 to  $2 \text{ ft}^{-1}$ ], and the uncorrected fracture frequency varies from 0 to  $21 \text{ m}^{-1}$  [0 to  $6.4 \text{ ft}^{-1}$ ] for any 1.0-m [3.3-ft] section. For the 3-m [10-ft] core sections, the maximum fracture frequency is  $4.3 \text{ m}^{-1}$  [ $1.3 \text{ ft}^{-1}$ ]. There is also variation between the boreholes. Even when orientation bias is accounted for, there is a factor of two difference in corrected fracture frequency between the Z-series and the X- and Y-series boreholes. This difference could be explained by the observation that the easterly-dipping Z-series boreholes should intersect more of the westerly-dipping fractures than the westerly-dipping X- and Y-series boreholes.

Two other inherent problems with borehole fracture data are mentioned here, but no correction is possible with the available data. One problem is elimination of core-induced fractures from

<b>Borehole</b>	<b>Uncorrected Fracture Frequency, Fractures/m [Fractures/ft]</b>	<b>Corrected Fracture Frequency Fractures/m [Fractures/ft]</b>
X1	0.59 [0.18]	1.37 [0.42]
X2	0.63 [0.19]	1.71 [0.52]
X3	0.66 [0.20]	1.80 [0.55]
Y1	0.49 [0.15]	1.02 [0.31]
Y2	0.43 [0.13]	0.98 [0.30]
Y3	0.50 [0.15]	1.07 [0.32]
Z1	1.35 [0.41]	2.58 [0.79]
Z2	1.66 [0.50]	3.59 [1.09]
Z3	1.09 [0.33]	2.56 [0.78]

the fracture list. The second problem is the lack of information on fracture lengths, which is indirectly used to infer connectivity. To remain consistent with the available Apache Leap Research Site data, only Yucca Mountain borehole data will be used in this report to make the comparison between the two sites (see Chapter 3); additionally, this restriction should reduce the effect of coring-induced fractures and the lack of information on fracture lengths.

### **2.2.6 Effective Fracture Porosity**

The effective fracture porosity is the volume of interconnected fractures per unit volume of rock. Forty-four cross-hole tests were conducted (Illman, et al., 1998; Illman and Neuman, 2001; Vesselinov, et al., 2001b) in 16 boreholes belonging to series V, W, X, Y, and Z. One result of these tests was the direct characterization of effective fracture porosity at the Apache Leap

Research Site. Sample statistics for fracture air-filled porosity measurements obtained from type-curve interpretation of cross-hole test data are summarized in Table 2-1.

Chen, et al. (2000) found that nonuniform inverse methods of interpreting cross-hole tests at the Apache Leap Research Site provide the best means of arriving at air-filled porosity values (Table 2-3). That is, treating the fracture density of the rock volume as uniform when it is nonuniform, leads to higher mean estimates than one would obtain by treating the rock as nonuniform. Statistics for effective fracture porosity data obtained from inverse modeling (Vesselinov, et al., 2001a,b; Hyun, et al., 2002) are discussed in Chapter 3 for comparison with Yucca Mountain data.

### **2.2.7 Effective Matrix Porosity**

The effective porosity of the rock matrix is the volume of interconnected voids per unit volume of rock. Matrix porosity was measured in the laboratory using core exclusive of fractures, making those values representative of tuff matrix. According to Rasmussen, et al. (1990), the effective

Interpretation Type	Minimum [m <sup>3</sup> /m <sup>3</sup> ]	Maximum [m <sup>3</sup> /m <sup>3</sup> ]	Mean [m <sup>3</sup> /m <sup>3</sup> ]	Variance	Coefficient of Variation
Type Curve Analysis	-4.47 [3.4 × 10 <sup>-5</sup> ]	-1.08 [8.3 × 10 <sup>-1</sup> ]	-2.11 [7.8 × 10 <sup>-3</sup> ]	0.65	-0.38
Nonuniform Inverse Analysis	—	—	-3.14 [7.2 × 10 <sup>-4</sup> ]	2.16	-0.47

\*Chen, G., W.A. Illman, D.L. Thompson, V.V. Vesselinov, and S.P. Neuman. "Geostatistical, Type Curve and Inverse Analyses of Pneumatic Injection Tests in Unsaturated Fractured Tuffs at the Apache Leap Research Site Near Superior, Arizona, pp. 73-98." *Dynamics of Fluids in Fractured Rocks*. B. Faybishenko, et al., eds. *Geophysical Monograph 122*. Washington, DC: American Geophysical Union. 2000.

porosity was determined from the difference in mass between a saturated sample and an oven-dried sample (see also Geddis, 1994). Effective matrix porosity data are listed in Appendix Table 2.

### 2.2.8 Matrix van Genuchten Alpha

The alpha value of the van Genuchten moisture characteristic function (henceforward termed van Genuchten alpha) was estimated through least-squares fitting of the moisture characteristic curve of core samples. For comparison with data from other sites, it is important to note that Rasmussen, et al. (1990) estimated values of van Genuchten alpha by assuming constant values of other empirical values for all samples, and with the assumption that residual saturation was zero. van Genuchten alpha data are listed in Appendix Table 2.

### 2.2.9 Matrix Klinkenberg Coefficient

A fundamental assumption of laminar flow theory is that fluids have a velocity equal to zero at solid surfaces; however, when the fluid is a gas, and a low-pressure gas in particular, negligible contact may occur between the gas molecules and the pore walls of a porous medium if the mean free path of the molecules is on the same order as the average pore diameter. In this event, the gas will flow with a higher velocity than that predicted by Darcy's law. The mean free path of a gas molecule is dependent on a number of factors, including temperature, pressure, and composition of the gas; for example, the mean free path of any gas molecule is shorter at high pressure than it is at low pressure. Klinkenberg (1941) observed that the apparent permeability of a porous medium to a gas is inversely proportional to the mean pore pressure, such that apparent gas permeability is not necessarily intrinsic to the porous medium.

The Klinkenberg relationship expresses the apparent gas permeability ( $k_g$ ) in terms of the gas permeability at infinite pore pressure ( $k_\infty$ ), at which it behaves like a liquid, and as a function of the mean pore pressure ( $P_m$ ) as follows:

$$k_g = k_\infty \left( 1 + \frac{b}{P_m} \right), \quad (2-2)$$

where  $b$  is the Klinkenberg coefficient, or the gas slippage factor. Thus, if the Klinkenberg coefficient is negligible, the apparent gas permeability is equal to the intrinsic permeability of the medium. The Klinkenberg coefficient is frequently treated as a constant, while it, in fact, is composed of both porous medium and fluid properties (pore size; gas temperature, viscosity, and molecular weight). Through empirical data analysis, the Klinkenberg coefficient,  $b$ , is frequently expressed as a function of intrinsic permeability in the following manner:

$$b = Ck_{\infty}^{-n} \quad (2-3)$$

where  $C$  and  $n$  are curve fitting parameters. Thus, the gas-slippage phenomenon is more prominent in low permeability material and at low mean pore pressures. Rasmussen, et al. (1990) estimated the matrix Klinkenberg coefficient point-by-point with Eq. (2-2), given knowledge of the mean pore pressure during the air permeability tests [ $P_m = 108$  kPa, with an average atmospheric pressure of 87 kPa (Illman and Neuman, 2001; Vesselinov, et al., 2001b)], the computed air permeability for an oven-dried core,  $k_g$ , and the computed liquid permeability for a completely saturated core,  $k_{\infty}$ . It was explicitly assumed that the difference between the computed air and liquid permeability was caused by the Klinkenberg effect, and it should be noted that the laboratory air permeability values as listed in Appendix Table 1 have not been corrected with the computed Klinkenberg coefficients. Klinkenberg coefficient data are listed in Appendix Table 2. Klinkenberg corrections are discussed further in Section 2.4.

### 2.2.10 Matrix Volumetric Water Content

Over a period of 505 days, Rasmussen, et al. (1990) determined volumetric water content using neutron probes at 105 locations in nine boreholes (X-, Y-, and Z-series boreholes) at the Apache Leap Research Site. They found little variation in neutron readings during the period of measurement. It is assumed that the neutron probe measurements and the corresponding water content values reflect those of the matrix, not those of the fractures. Water content data are listed in Appendix Table 2.

### 2.2.11 Dry Thermal Conductivity

The characterization of thermal properties of unsaturated fractured tuffs is important to the Thermal Effect on Flow key technical issue. Thermal properties dependent on water content were estimated using large oven-dried core segments. Two holes were drilled into the core, and a heating unit was placed in one of the holes. A heat signal generated in the central drill hole was monitored in the outer drill hole with a thermistor probe. The magnitude of this heat signal was used to estimate the thermal conductivity by means of a radial flow equation given in Rasmussen, et al. (1990). Dry thermal conductivity data are listed in Appendix Table 3.

## 2.2.12 Saturated Thermal Conductivity

Saturated thermal conductivity was estimated using the procedure described in Section 2.2.11 but with a fully saturated core sample. Saturated thermal conductivity data are listed in Appendix Table 3.

## 2.2.13 Dry Rock Specific Heat

The dry rock specific heat is analogous to the thermal capacity of the rock; these data are listed in Appendix Table 3. It was obtained from the radial flow equation given in Rasmussen, et al. (1990).

## 2.3 Exploratory Data Analysis

Descriptive statistics of the variables were computed using ISATIS and are reported in Table 2-4. Statistics are calculated on samples where all variables are defined. Three categories of statistical values are computed using ISATIS. Statistics given in Table 2-4 include the number of samples, minimum and the maximum values, arithmetic mean, standard deviation, and the variance, skewness, and kurtosis.

Histograms of the 12 variables are presented in Figure 2-4. Constant class widths are used in computing the histograms. Some noteworthy features are: (i) both field and laboratory estimates of air and liquid permeability are highly skewed to the right; (ii) porosity, fracture frequency, van Genuchten alpha, and the matrix Klinkenberg coefficient are skewed to the right, though to a lesser degree; and (iii) saturated thermal conductivity, dry thermal conductivity, water content, and dry rock specific heat exhibit distributions are approximately normal.

Skewness is a measure of distribution symmetry, while kurtosis is a measure of the peakedness or flatness of the distribution (skewness less than 3.0 indicates distributions with important tails). A zero value of skewness is an indication that the distribution is symmetric. Positive skewness indicates that the distribution exhibits a tail to the right of the maximum and is frequently an indication of a lognormal distribution. For variables with skewness greater than unity, asymmetry outweighs variability such that the variable is not normally distributed; thus, it was decided to obtain the  $\text{LOG}_{10}$  transformation of the field and laboratory estimates of air and liquid permeability, effective porosity, van Genuchten alpha, and the matrix Klinkenberg coefficient. The appropriate transformation in the case of fracture frequency,  $f$ , for which the sample data include zeros, is  $\text{LOG}_{10}(f + 1)$ . Summary statistics of the transformed variables are given in Table 2-5, and the histograms are illustrated in Figure 2-5. The  $\text{LOG}_{10}$ -transformed permeability values appear to have a normal distribution, in general, but both the laboratory and field estimates of air permeability are still positively skewed.

In general, statistical analysis of data collected at the site showed large variability in field and laboratory estimates of permeability. In particular, the field estimates of air permeability (i.e., the permeability of fractures to air) ranged between  $4.58 \times 10^{-17}$  and  $1.34 \times 10^{-12} \text{ m}^2$  [ $4.64 \times 10^{-5}$  and 1.36 Darcies], with a geometric mean of  $7.94 \times 10^{-16} \text{ m}^2$  [ $8.05 \times 10^{-4}$  Darcies]. The field estimates of liquid permeability (i.e., the permeability of fractures to water) ranged between  $2.76 \times 10^{-17}$  and  $1.95 \times 10^{-12} \text{ m}^2$  [ $2.80 \times 10^{-5}$  and 1.98 Darcies], with a geometric mean of  $7.24 \times 10^{-16} \text{ m}^2$  [ $7.34 \times 10^{-4}$  Darcies]. The geometric mean value of fracture air permeability is

Table 2-4. Summary Statistics of the Original Data Set\*

Variables	Number of Data Values	Minimum	Maximum	Arithmetic Mean	Standard Deviation	Variance	Skewness	Kurtosis
Field Air Permeability	86	$4.58 \times 10^{-17} \text{ m}^2$ [ $4.64 \times 10^{-5} \text{ D}$ ]	$1.34 \times 10^{-12} \text{ m}^2$ [1.36 D]	$2.70 \times 10^{-14} \text{ m}^2$ [ $2.74 \times 10^{-2} \text{ D}$ ]	$1.60 \times 10^{-13} \text{ m}^2$ [ $1.62 \times 10^{-1} \text{ D}$ ]	$2.55 \times 10^{-26}$	7.38	56.97
Field Liquid Permeability	83	$2.76 \times 10^{-17} \text{ m}^2$ [ $2.80 \times 10^{-5} \text{ D}$ ]	$1.95 \times 10^{-12} \text{ m}^2$ [1.98 D]	$2.97 \times 10^{-14} \text{ m}^2$ [ $3.01 \times 10^{-2} \text{ D}$ ]	$2.17 \times 10^{-13} \text{ m}^2$ [ $2.20 \times 10^{-1} \text{ D}$ ]	$4.72 \times 10^{-28}$	8.72	77.70
Laboratory Air Permeability	105	$3.81 \times 10^{-16} \text{ m}^2$ [ $3.86 \times 10^{-4} \text{ D}$ ]	$1.01 \times 10^{-13} \text{ m}^2$ [ $1.02 \times 10^{-1} \text{ D}$ ]	$5.71 \times 10^{-15} \text{ m}^2$ [ $5.79 \times 10^{-3} \text{ D}$ ]	$1.56 \times 10^{-14} \text{ m}^2$ [ $1.58 \times 10^{-2} \text{ D}$ ]	$2.44 \times 10^{-28}$	4.84	24.58
Laboratory Liquid Permeability	105	$7.05 \times 10^{-17} \text{ m}^2$ [ $7.14 \times 10^{-5} \text{ D}$ ]	$4.48 \times 10^{-14} \text{ m}^2$ [ $4.54 \times 10^{-2} \text{ D}$ ]	$2.18 \times 10^{-15} \text{ m}^2$ [ $2.21 \times 10^{-3} \text{ D}$ ]	$6.57 \times 10^{-15} \text{ m}^2$ [ $6.66 \times 10^{-3} \text{ D}$ ]	$4.32 \times 10^{-29}$	4.95	26.29
Fracture Frequency	105	$0.00 \text{ m}^{-1}$ [ $0.00 \text{ ft}^{-1}$ ]	$4.33 \text{ m}^{-1}$ [ $1.32 \text{ ft}^{-1}$ ]	$0.766 \text{ m}^{-1}$ [ $0.233 \text{ ft}^{-1}$ ]	$0.833 \text{ m}^{-1}$ [ $0.254 \text{ ft}^{-1}$ ]	0.695	1.97	5.29
Porosity	105	14.3%	27.5%	17.5%	2.34%	5.47	1.49	3.49
van Genuchten Alpha	105	$1.02 \times 10^{-2} \text{ kPa}^{-1}$ [ $7.03 \times 10^{-2} \text{ psi}^{-1}$ ]	$6.43 \times 10^{-2} \text{ kPa}^{-1}$ [ $4.43 \times 10^{-1} \text{ psi}^{-1}$ ]	$2.23 \times 10^{-2} \text{ kPa}^{-1}$ [ $1.54 \times 10^{-1} \text{ psi}^{-1}$ ]	$8.50 \times 10^{-3} \text{ kPa}^{-1}$ [ $5.86 \times 10^{-2} \text{ psi}^{-1}$ ]	$7.22 \times 10^{-5}$	1.94	5.97
Klinkenberg Coefficient	105	$3.50 \times 10^1 \text{ kPa}$ [ $5.08 \times 10^0 \text{ psi}$ ]	$1.28 \times 10^3 \text{ kPa}$ [ $1.86 \times 10^2 \text{ psi}$ ]	$3.22 \times 10^2 \text{ kPa}$ [ $4.67 \times 10^1 \text{ psi}$ ]	$2.67 \times 10^2 \text{ kPa}$ [ $3.87 \times 10^1 \text{ psi}$ ]	$7.11 \times 10^4$	1.62	2.30
Water Content	105	10.1%	17.5%	14.3%	1.61%	2.60	-0.01	-0.46
Dry Thermal Conductivity	105	$0.829 \text{ J/m s K}$ [ $0.479 \text{ Btu/ft h } ^\circ\text{F}$ ]	$1.97 \text{ J/m s K}$ [ $1.14 \text{ Btu/ft h } ^\circ\text{F}$ ]	$1.27 \text{ J/m s K}$ [ $0.734 \text{ Btu/ft h } ^\circ\text{F}$ ]	$0.146 \text{ J/m s K}$ [ $0.084 \text{ Btu/ft h } ^\circ\text{F}$ ]	$2.14 \times 10^{-2}$	0.76	4.64
Saturated Thermal Conductivity	105	$1.29 \text{ J/m s K}$ [ $0.745 \text{ Btu/ft h } ^\circ\text{F}$ ]	$2.49 \text{ J/m s K}$ [ $1.44 \text{ Btu/ft h } ^\circ\text{F}$ ]	$1.82 \text{ J/m s K}$ [ $1.05 \text{ Btu/ft h } ^\circ\text{F}$ ]	$0.195 \text{ J/m s K}$ [ $0.113 \text{ Btu/ft h } ^\circ\text{F}$ ]	$3.79 \times 10^{-2}$	0.02	1.18
Dry Rock Specific Heat	105	$3.45 \times 10^2 \text{ J/kg K}$ [ $0.082 \text{ Btu/lb}_m ^\circ\text{F}$ ]	$1.17 \times 10^3 \text{ J/kg K}$ [ $0.279 \text{ Btu/lb}_m ^\circ\text{F}$ ]	$7.02 \times 10^2 \text{ J/kg K}$ [ $0.168 \text{ Btu/lb}_m ^\circ\text{F}$ ]	$1.62 \times 10^2 \text{ J/kg K}$ [ $0.039 \text{ Btu/lb}_m ^\circ\text{F}$ ]	$2.62 \times 10^4$	0.36	-0.09

\*Rasmussen, T.C., D.D. Evans, P.J. Sheets, and J.H. Blanford. NUREG/CR-5596, "Unsaturated Fractured Rock Characterization Methods and Data Sets at the Apache Leap Tuff Site." Washington, DC: NRC. August 1990.

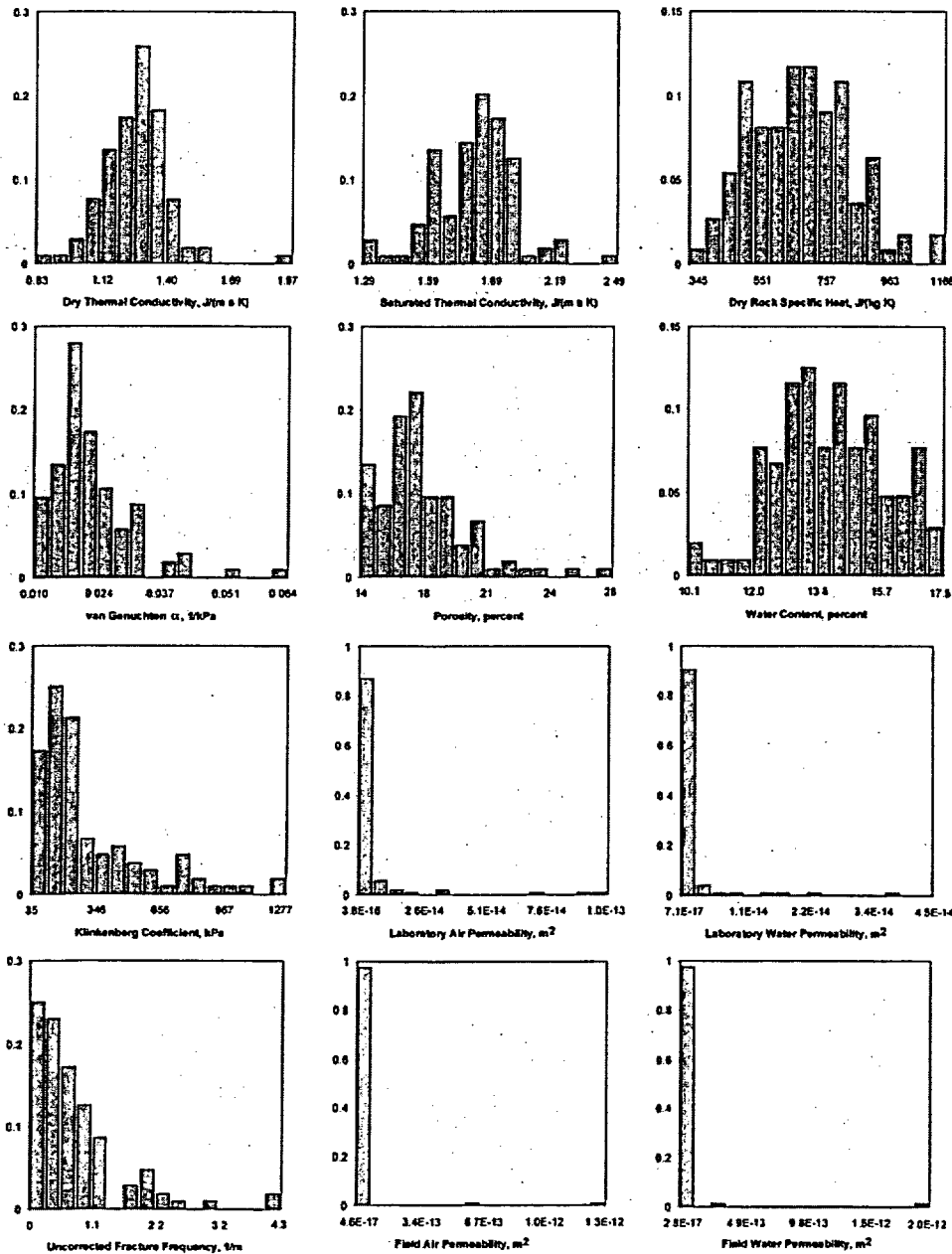


Figure 2-4. Histograms of (a) Dry Thermal Conductivity, (b) Saturated Thermal Conductivity, (c) Dry Rock Specific Heat, (d) van Genuchten  $\alpha$ , (e) Porosity, (f) Water Content, (g) Klinkenberg Coefficient, (h) Laboratory Estimates of Air Permeability, (i) Laboratory Estimates of Water Permeability, (j) Uncorrected Fracture Frequency, (k) Field Estimates of Air Permeability, and (l) Field Estimates of Water Permeability.  
 [1.0 m = 3.2808 ft;  $1.0 \times 10^{12} \text{ m}^2 = 1.01325 \text{ D}$ ;  $1.0 \text{ kPa} = 0.14504 \text{ psi}$ ;  
 $1.0 \text{ J}/(\text{kg} \cdot ^\circ\text{K}) = 2.39 \times 10^4 \text{ Btu}/(\text{lb} \cdot ^\circ\text{F})$ ; and  $1.0 \text{ J}/(\text{m} \cdot \text{s} \cdot ^\circ\text{K}) = 0.57782 \text{ Btu}/(\text{h} \cdot \text{ft} \cdot ^\circ\text{F})$ ]

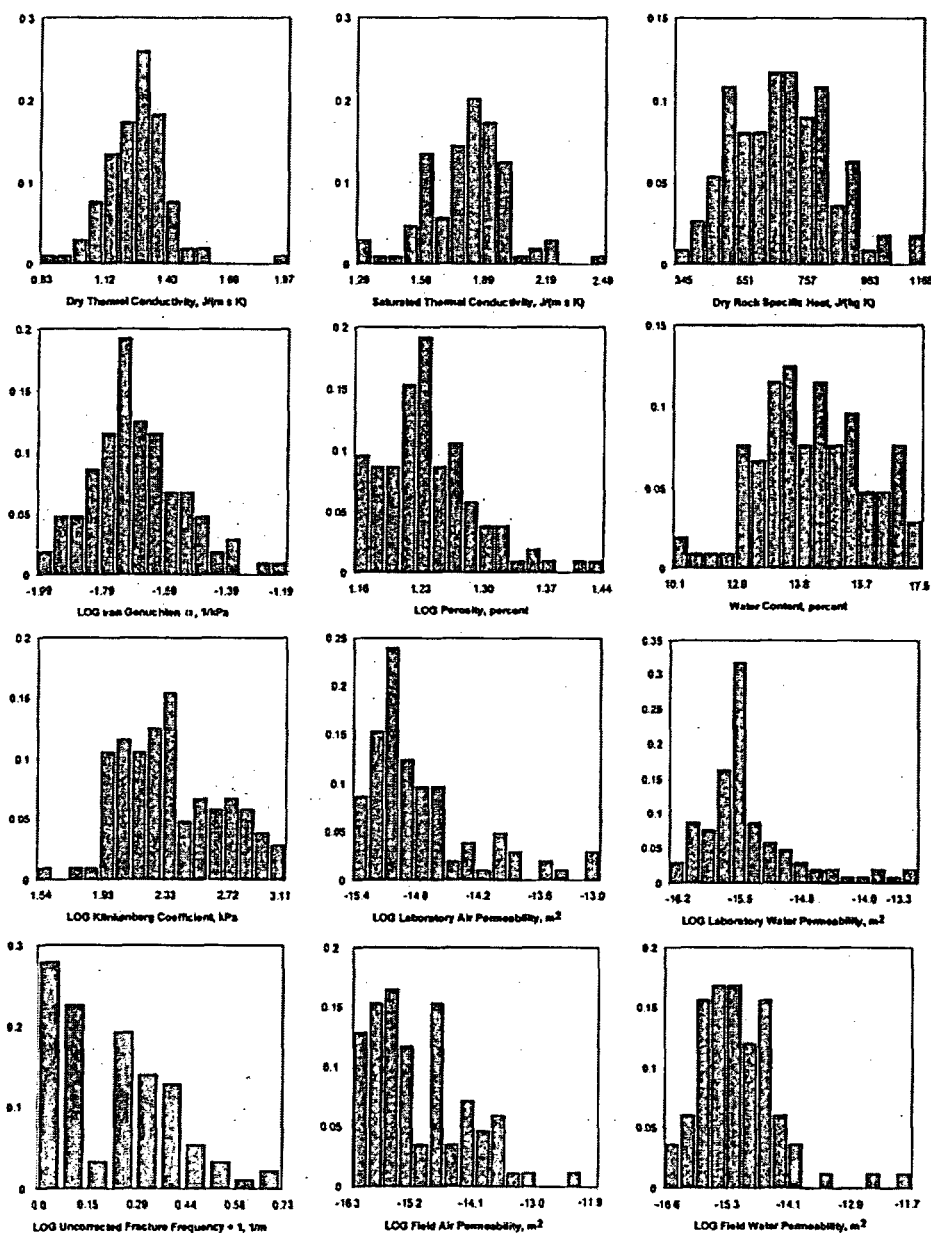


Figure 2-5. Histograms of (a) Dry Thermal Conductivity, (b) Saturated Thermal Conductivity, (c) Dry Rock Specific Heat, (d) LOG<sub>10</sub> van Genuchten  $\alpha$ , (e) LOG<sub>10</sub> Porosity, (f) Water Content, (g) LOG<sub>10</sub> Klinkenberg Coefficient, (h) LOG<sub>10</sub> Laboratory Estimates of Air Permeability, (i) LOG<sub>10</sub> Laboratory Estimates of Water Permeability, (j) LOG<sub>10</sub> Uncorrected Fracture Frequency Plus 1, (k) LOG<sub>10</sub> Field Estimates of Air Permeability, and (l) LOG<sub>10</sub> Field Estimates of Water Permeability. [1.0 m = 3.2808 ft;  $1.0 \times 10^{12} m^2 = 1.01325 D$ ; 1.0 kPa = 0.14504 psi;  $1.0 J/(kg \cdot ^\circ K) = 2.39 \times 10^4 Btu/(lb \cdot ^\circ F)$ ; and  $1.0 J/(m \cdot s \cdot ^\circ K) = 0.57782 Btu/(h \cdot ft \cdot ^\circ F)$ ]

**Table 2-5. Summary Statistics of LOG<sub>10</sub>-Transformed Data Values.\* Pre-LOG<sub>10</sub>-Transformed Units Are Those of Table 2-4.**

Variables	Data	Minimum	Maximum	Mean	Standard Deviation	Variance	Skewness	Kurtosis
LOG <sub>10</sub> (Field $k_a$ )	82	-16.34	-11.87	-15.1	0.95	0.9	1	3.85
LOG <sub>10</sub> (Field $k_w$ )	82	-16.56	-12.45	-15.14	0.68	0.47	0.81	4.75
LOG <sub>10</sub> (Lab $k_a$ )	82	-15.42	-12.99	-14.79	0.55	0.31	1.59	5.03
LOG <sub>10</sub> (Lab $k_w$ )	82	-16.15	-13.35	-15.25	0.58	0.34	1.51	5.08
LOG <sub>10</sub> (Lab $\phi$ )	82	1.16	1.44	1.23	0.05	0.003	1.14	5.07
LOG <sub>10</sub> (Lab $\alpha$ )	82	-1.99	-1.19	-1.68	0.15	0.02	0.64	3.77
LOG <sub>10</sub> ( $b$ )	82	1.54	3.11	2.33	0.31	0.1	0.54	2.99

\*Rasmussen, T.C., D.D. Evans, P.J. Sheets, and J.H. Blanford. NUREG/CR-5596, "Unsaturated Fractured Rock Characterization Methods and Data Sets at the Apache Leap Tuff Site." Washington, DC: NRC. August 1990.

within 10 percent of the geometric mean value of fracture liquid permeability. Laboratory estimates of air permeability (i.e., the permeability of the matrix to air), uncorrected for the gas slippage phenomenon, ranged between  $3.81 \times 10^{-16}$  and  $1.01 \times 10^{-13}$  m<sup>2</sup> [ $3.86 \times 10^{-4}$  and 0.10 Darcies], with a geometric mean of  $1.62 \times 10^{-15}$  m<sup>2</sup> [ $1.64 \times 10^{-3}$  Darcies]. Laboratory estimates of liquid permeability (i.e., the permeability of the matrix to water) ranged between  $7.05 \times 10^{-17}$  and  $4.48 \times 10^{-14}$  m<sup>2</sup> [ $7.14 \times 10^{-5}$  and  $4.54 \times 10^{-2}$  Darcies], with a geometric mean of  $5.62 \times 10^{-16}$  m<sup>2</sup> [ $5.69 \times 10^{-4}$  Darcies]. The geometric mean values of matrix air permeability (uncorrected for gas slippage) and matrix liquid permeability are within the same order of magnitude, but the liquid permeability is 65 percent smaller than the air permeability due to gas slippage. The matrix Klinkenberg coefficient ranged between 35 and 1,280 kPa [5 and 186 psi], with a geometric mean of 214 kPa [31 psi]. Other parameter estimates were spatially variable as well, though to a lesser degree.

In many statistical assessments of site data, the following questions often arise about the fate of outliers: can extreme values in the data set be considered outliers in conducting the geostatistical analysis of the data set? Or should the values be kept because those values are of great interest to the hydrogeologist? The removal or retention of outliers in a data set is a controversial issue because the mean and standard deviation of the distribution can be affected by those outliers. In many environmental applications, however, those outliers are the most interesting measurements in the data set. In the present analysis, the highest values of permeability measured can be due to one or more major fractures, and those features should be kept in the data set. Fast flow paths are of particular interest, and the largest permeability values are an indication of those features. Hence, the decision was made not to remove these values.

As is frequent in a geostatistical investigation, the data set may contain more information than just the primary variable of interest. Thus, instead of examining permeability alone, one can take advantage of the knowledge of other variables in the data set and of the correlation

between these other variables for joint estimation. Components of the correlation matrix, which were computed for all of the Rasmussen et al. (1990) data with the software package ISATIS, are listed in Table 2-6. Individual entries within the symmetric correlation matrix are Pearson Product Moment correlation coefficients, which are a measure of the linear relationship between two stochastic variables. This means that if the relationship between two variables is curvilinear (e.g., laboratory-measured liquid permeability and matrix Klinkenberg coefficient; see Sections 2.2.9 and 2.4), the Pearson Product Moment correlation coefficient cannot adequately describe the degree of association between the two variables. For this reason, and also because the Pearson Product Moment correlation coefficient is susceptible to taking on anomalous values when outliers are present, it is advisable to observe a scatterplot of the data in conjunction with the associated correlation coefficient in order to make a supportable interpretation. If a scatterplot of two stochastic variables indicated a curvilinear relationship, the Spearman Rank correlation coefficient would be better-suited for describing the degree of association between the variables; any such investigation of the Apache Leap Research Site data is reserved for a future report. For now, a discussion of physically meaningful correlation coefficients within Table 2-6 is provided.

A strong correlation is observed between the  $\text{LOG}_{10}$ -transformed field estimates of air and liquid permeability (0.87). The strong correlation implies that air injection experiments conducted in the unsaturated zone can be performed to estimate the value of permeability of the fractured rock to water. Air injection is preferred over water injection in the unsaturated zone, due to negligible gravitational effect, the lower viscosity of air, and the associated shorter duration of air injection tests. A strong correlation is also seen between  $\text{LOG}_{10}$ -transformed laboratory estimates of air and liquid permeability (0.93).

A weak correlation is seen between (i)  $\text{LOG}_{10}$ -transformed effective matrix porosity and laboratory estimates of air permeability (0.68), (ii)  $\text{LOG}_{10}$ -transformed effective matrix porosity and laboratory estimates of liquid permeability (0.70), (iii)  $\text{LOG}_{10}$ -transformed van Genuchten alpha and laboratory estimates of air permeability (0.52), and (iv)  $\text{LOG}_{10}$ -transformed effective van Genuchten alpha and laboratory estimates of liquid permeability (0.54).

The correlation between fracture geometry parameters and permeability is of interest. At the Apache Leap Research Site, the correlations of  $\text{LOG}_{10}$ -transformed fracture frequency (i) with field estimates of  $\text{LOG}_{10}$ -transformed air permeability (0.31), (ii) with field estimates of  $\text{LOG}_{10}$ -transformed liquid permeability (0.21), (iii) with laboratory estimates of  $\text{LOG}_{10}$ -transformed air permeability (0.14), and (iv) with laboratory estimates of  $\text{LOG}_{10}$ -transformed liquid permeability (0.09) are all very weak. It should be noted that laboratory measurements of matrix permeability were conducted only for samples visibly devoid of fractures, thus negligible correlation should be expected. Very weak correlation between field-measured permeability and fracture frequency is expected, as permeability can be highly sensitive to the number and size of fractures present in the measurement interval. However, fracture frequency in a particular interval does not provide a reliable indication of the associated permeability magnitude. Fracture frequency and fracture geometry provide little information on fracture permeability; while they may provide some general indications, only hydraulic and pneumatic tests will provide accurate measures of those parameters. The scatterplot of fracture air permeability versus fracture frequency in Figure 2-6 also suggests a lack of correlation (Illman and Newman, 2001).

Table 2-6. Correlation Matrix of Analyzed Variables

Variable	LOG <sub>10</sub> Field $k_a$	LOG <sub>10</sub> Field $k_w$	LOG <sub>10</sub> Lab $k_a$	LOG <sub>10</sub> Lab $k_w$	Uncorrected Fracture Frequency	LOG <sub>10</sub> Lab $\phi$	LOG <sub>10</sub> $\alpha$	LOG <sub>10</sub> Lab $b$	H <sub>2</sub> O Content	Dry Thermal Conductivity	Saturated Thermal Conductivity	Dry Rock Specific Heat
LOG <sub>10</sub> Field $k_a$	1.00	0.87	0.38	0.29	0.31	0.19	0.14	0.22	-0.02	-0.27	-0.12	0.22
LOG <sub>10</sub> Field $k_w$	0.87	1.00	0.49	0.40	0.21	0.22	0.18	0.18	-0.06	-0.35	-0.20	0.20
LOG <sub>10</sub> Lab $k_a$	0.38	0.49	1.00	0.93	0.14	0.68	0.52	0.06	-0.05	-0.45	-0.31	-0.10
LOG Lab $k_w$	0.29	0.40	0.93	1.00	0.09	0.70	0.54	-0.32	0.10	-0.42	-0.35	-0.11
Uncorrected Fracture Frequency	0.31	0.21	0.14	0.09	1.00	-0.12	0.00	0.10	-0.14	-0.16	-0.05	-0.02
LOG <sub>10</sub> Lab $\phi$	0.19	0.22	0.68	0.70	-0.12	1.00	0.45	-0.13	0.35	-0.46	-0.30	-0.13
LOG <sub>10</sub> $\alpha$	0.14	0.18	0.52	0.54	0.00	0.45	1.00	-0.10	-0.15	-0.37	-0.11	0.05
LOG <sub>10</sub> Lab $b$	0.22	0.18	0.06	-0.32	0.10	-0.13	-0.10	1.00	-0.37	-0.02	0.13	0.06
H <sub>2</sub> O Content	-0.02	-0.06	-0.05	0.10	-0.14	0.35	-0.15	-0.37	1.00	-0.02	-0.26	-0.03
Dry Thermal Conductivity	-0.27	-0.35	-0.45	-0.42	-0.16	-0.46	-0.37	-0.02	-0.02	1.00	0.24	-0.02
Saturated Thermal Conductivity	-0.12	-0.20	-0.31	-0.35	-0.05	-0.30	-0.11	0.13	-0.26	0.24	1.00	0.27
Dry Rock Specific Heat	0.22	0.20	-0.10	-0.11	-0.02	-0.13	0.05	0.06	-0.03	-0.02	0.27	1.00

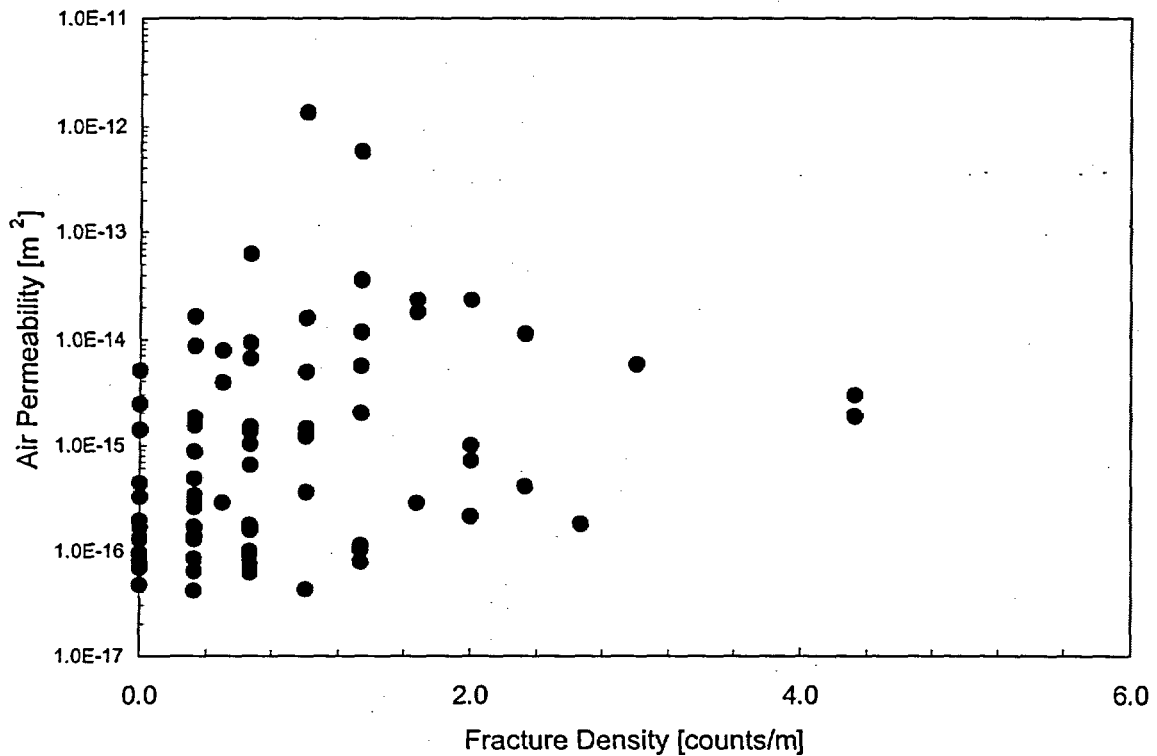


Figure 2-6. Air Permeability Versus Fracture Density  
(Adapted from Illman and Neuman, 2001) [1.0 m = 3.28 ft]

## 2.4 Comparison with Permeability Estimates from Other Tests

This section discusses the differences between air and liquid permeability in the field and in the laboratory and possible explanations for the lack of correlation with fracture characteristics. At first glance, the field permeability values and distributions reported by Rasmussen, et al. (1990) do not appear to differ substantially from their laboratory (matrix only) permeability values and distributions (Figure 2-5). While field permeability values overlap with the laboratory permeability values, they also cover a wider range. Rasmussen, et al. (1990) make the explicit assumption

that field air permeability is a measure of the fracture permeability. They rationalize that the matrix is partially saturated, hence, they assume that there are essentially no air pathways through the matrix pore space. The boreholes were drilled using water as the cooling and chip-circulating fluid, the site was quickly covered with a tarp, facilitating uniformity of saturation, and neutron probe measures of water content support the conclusion that the matrix was greater than 50 percent saturated during the air injection testing by Rasmussen, et al. (1990).

Liquid permeability data plotted versus air permeability data from field and laboratory measurements are illustrated in Figure 2-7. The gas slippage phenomenon, accounted for by the Klinkenberg coefficient, explains the prominent departure of the laboratory air permeability data from that of the laboratory liquid permeability data. The data are shifted below the 1:1 correlation line, indicating that the laboratory air permeability measurements over predict the liquid permeability of the matrix core samples, as is typical for low-permeability granular porous media, particularly at low pore pressures. Figure 2-8 demonstrates a method used to correct the Apache Leap Research Site matrix air permeability data for the gas slippage effect. The Klinkenberg coefficient [determined point-by-point by Rasmussen, et al. (1990) from matrix air and liquid permeability data utilizing Eq. (2-2)] is plotted versus the matrix liquid permeability data. While the data appear highly scattered on the logarithmic scale, one may still fit to them a curve in the form of Eq. (2-3), resulting in the following empirical relationship between Klinkenberg coefficient and liquid permeability:

$$b = 0.5263k_{\infty}^{-0.1747} \quad (2-4)$$

Assigning the empirically determined Klinkenberg coefficient associated with a given matrix liquid permeability measurement location to the matrix air permeability measurement at the same location then allows this coefficient to be employed in Eq. (2-2), such that the intrinsic permeability corrected for gas slippage may be determined from the measured matrix air permeability, by rearranging as follows:

$$k_{\infty} = \frac{k_g}{1 + \frac{b}{P_m}} \quad (2-5)$$

Just as in Figure 2-7, liquid permeability data are plotted versus air permeability data from field and laboratory measurements in Figure 2-9, but now the matrix air permeability data are corrected for the gas slippage effect and fall, on the average, on the 1:1 correlation line. Correcting the air permeability data with the Klinkenberg coefficient results in an overall lowering of the indicated air permeability, as expected given the effect of the gas slippage phenomenon. The majority of the laboratory permeability data lie within one order of magnitude variation  $\{1 \times 10^{-16}$  through  $1 \times 10^{-15} \text{ m}^2 [1 \times 10^{-4}$  through  $1 \times 10^{-3}$  Darcies]}, whereas the majority of the field permeability data lie within three orders of magnitude variation  $\{1 \times 10^{-16}$  through  $1 \times 10^{-13} \text{ m}^2 [1 \times 10^{-4}$  through  $1 \times 10^{-1}$  Darcies]}. That the field data generally span a range of permeability that is an additional two orders of magnitude greater than the range of the laboratory data may provide support for the hypothesis of Rasmussen, et al. (1990) that field air permeability data are indicative of fracture permeability. For large field values that are beyond the range of laboratory matrix values, flow through fractures is a natural explanation. Fracture flow would be expected where there are large positive differences between paired field and laboratory measurements (i.e., outliers in the positive region of Figure 2-10). Because the laboratory measurements were explicitly made on nonfractured cores, the difference between field and laboratory measurements should reflect the flow properties of the fracture system, assuming the matrix is homogeneous. If the fracture network is not responsible for the outliers in Figure 2-10, an alternative explanation is the scale effect, which is related to the nonrepresentativeness of core sampling when compared to the 3-m [10-ft] injection length of borehole permeability measurements. The latter explanation is not considered likely, given the natural distribution of matrix properties, and that poor core recovery was indirectly attributed to fracturing by Rasmussen, et al. (1990).

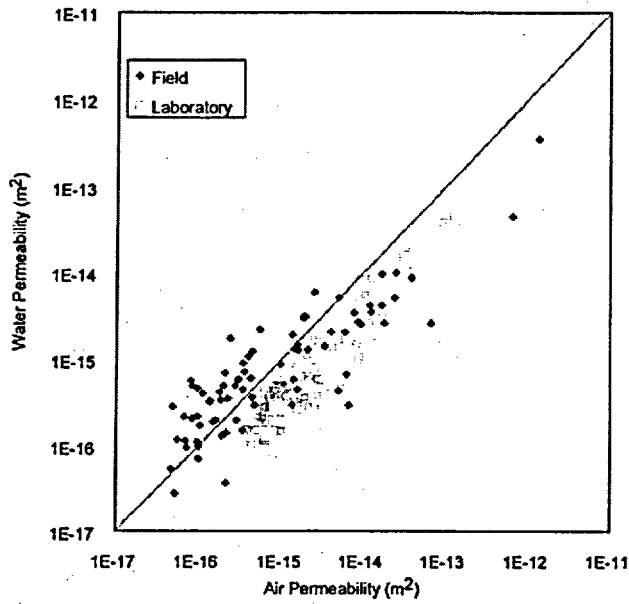


Figure 2-7. Water Permeability Plotted Against Air Permeability for Field and Laboratory Data from Apache Leap Research Site [1.0 m = 3.28 ft]

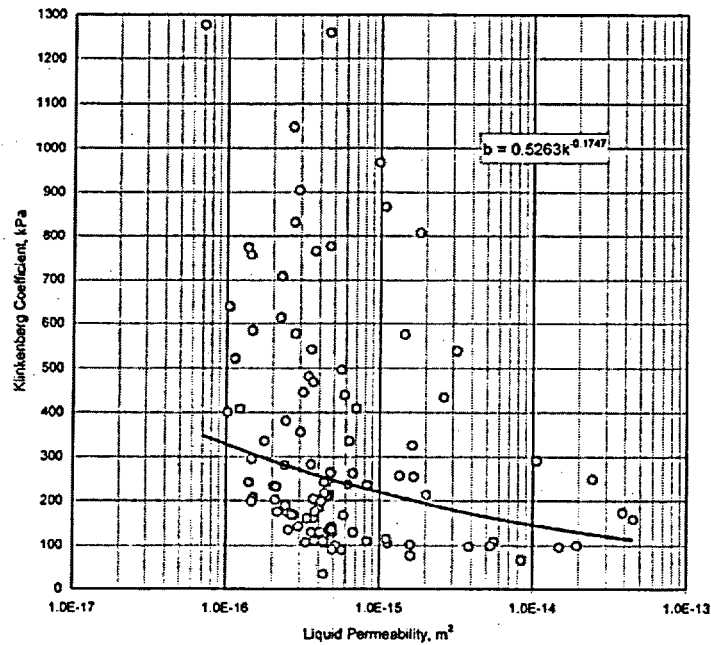


Figure 2-8. Klinkenberg Coefficient Plotted Against Liquid Permeability for Laboratory Data: Apache Leap Research Site [1.0 kPa = 0.145 psi and 1.0 m = 3.28 ft]

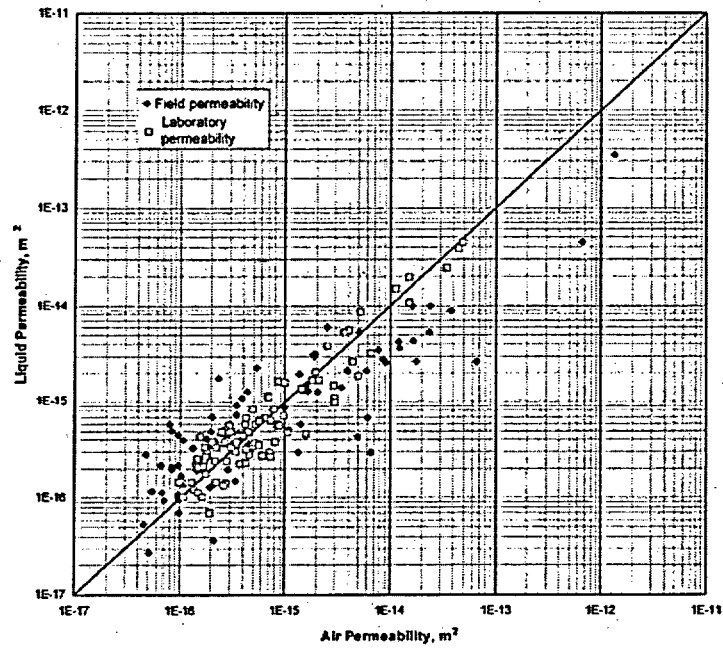


Figure 2-9. Liquid Permeability Plotted Against Air Permeability for Field and Klinkenberg-Corrected Laboratory Data: Apache Leap Research Site [1.0 m = 3.28 ft]

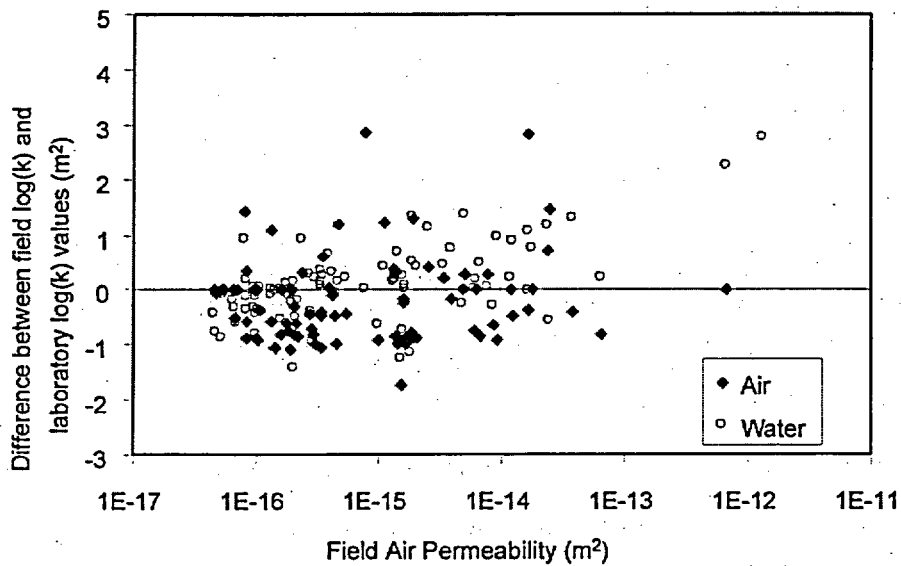


Figure 2-10. Plot of the Field Permeability Versus the Difference Between Field-and-Laboratory Derived Values of Permeability for Both Air and Water at Apache Leap Research Site [1.0 m = 3.28 ft]

A prominent feature of the field data, as illustrated in Figure 2-9, is its behavior at low and high permeability values: air permeability measurements tend to under predict in low-permeability media and over predict in high-permeability media. The reasons for this phenomenon are not clear, but some possible explanations are outlined below.

There are two reasonable hypotheses for field permeability values that are lower than the low end of the range of laboratory (i.e., matrix) permeability values (Figure 2-7). The first possible argument is that the low field permeability values may reflect flow through a fracture system with few fractures and small apertures. The second possibility is that the low field permeability values may reflect the permeability of the matrix. Consistent with the second possibility is that, for porous media with permeability values of  $1 \times 10^{-15} \text{ m}^2$  [ $1 \times 10^{-3}$  Darcies] or less, the field values of air permeability are generally lower than the field values of liquid permeability, possibly reflecting reduced air permeability in a partially saturated rock. Air permeability is known to be a function of saturation. It is clear that the situation in which field air permeability values are generally lower than field liquid permeability values is not consistent with the Klinkenberg effect in either low permeability granular porous media or narrow aperture microfracture systems.

The Rasmussen, et al. (1990) field-measured air permeability data need not be used alone to delineate fracture flow properties at the Apache Leap Research Site. For the Apache Leap Research Site data to be applied to the fracture continuum of the dual-continuum Yucca Mountain flow models, confidence is needed that the field air permeability data reflect only the properties of the fracture network. Permeability data from other Apache Leap Research Site tests will be used to support the assumption that field-measured air permeability is only representative of flow in the fracture network.

As mentioned in Section 2.1, single-hole pneumatic injection tests for determination of fracture permeability were also conducted by Bassett, et al. (1994, Chapter 4) (see also Rasmussen, et al., 1996, pp. 52–91) in 183 intervals of 1.0-m [3.3-ft] length (Guzman, et al., 1996). Six boreholes were tested, including the vertically-oriented V2 and the inclined W2A, X2, Y2, Y3, and Z2 (45° inclination below the horizontal). Additionally, Borehole Y2 was tested with three other sample supports (i.e., injection lengths of 0.5, 2.0, and 3.0 m [1.6, 6.6, and 9.9 ft]) and Borehole X2 was tested with one other sample support (i.e., an injection length of 2.0 m [6.6 ft]) in an effort to determine how the mean permeability depends on the scale of the test. Thus, more than 270 intervals were tested during this venture. Permeability was tested on a much smaller sample support and over many more borehole intervals during this particular effort than during the earlier work by Rasmussen, et al. (1990). These tests were reportedly conducted under highly controlled conditions and were subject to strict quality assurance. Summary statistics from these steady-state permeability tests, as reported by Rasmussen, et al. (1996, pp. 52–91), are provided in Table 2-7. At the time this reference was published, permeability measurements from the 2-m [6.6-ft] length injection intervals of boreholes X2 and Y2 length were not available, and neither were some measurements from the 1-m [3.3-ft] length injection intervals of boreholes W2A and Y3. This situation is indicated in Table 2-7 by the words "Data not available." Data have subsequently become available for Borehole Y2 at the 2-m length injection interval.<sup>1</sup> The geometric mean air permeability resulting from all injection intervals of

---

<sup>1</sup>Vesselinov, V. Email (September 11) to C. Dinwiddie, CNWRA. Los Alamos, New Mexico: Los Alamos National Laboratory. 2002.

Borehole Identification	Measurement Scale, m [ft]	Number of Samples	ln(k, m <sup>2</sup> ) [D]		
			Mean	Median	Variance
Y2	0.5 [1.6]	54	-34.76 [8.12 × 10 <sup>-4</sup> ]	-34.71	2.25
	1.0 [3.3]	28	-34.47 [1.09 × 10 <sup>-3</sup> ]	-34.22	3.07
	2.0 [6.6]	14	-34.43 [1.13 × 10 <sup>-3</sup> ]	-34.43 [1.25 × 10 <sup>-3</sup> ]	2.64
	3.0 [10.0]	9	-34.03 [1.69 × 10 <sup>-3</sup> ]	-34.47	2.00
X2	1.0 [3.3]	30	-34.83 [7.57 × 10 <sup>-4</sup> ]	-34.52	2.93
	2.0 [6.6]	10	Data not available	Data not available	Data not available
Z2	1.0 [3.3]	28	-34.51 [1.04 × 10 <sup>-3</sup> ]	-35.16	4.96
W2A	1.0 [3.3]	31 (now 37)	-34.84 [7.50 × 10 <sup>-4</sup> ] (Data not available)	-35.05 (Data not available)	1.37 (Data not available)
V2	1.0 [3.3]	21	-36.28 [1.78 × 10 <sup>-4</sup> ]	-36.74	3.78
Y3	1.0 [3.3]	23 (now 39)	-34.47 [1.09 × 10 <sup>-3</sup> ] (Data not available)	-34.36 (Data not available)	5.50 (Data not available)
All	1.0 [3.3]	161 (now 183)	-34.85 [7.42 × 10 <sup>-4</sup> ] (Data not available)	-34.90 (Data not available)	3.71 (Data not available)

<sup>\*</sup>Rasmussen, T.C., S.C. Rhodes, A. Guzman, and S.P. Neuman. NUREG/CR-6096, "Apache Leap Tuff INTRAVALEXperiments: Results and Lessons Learned." Washington, DC: NRC. March 1996.  
<sup>†</sup>Guzman, A.G., A.M. Geddis, M.J. Henrich, C.F. Lohrstorfer, and S.P. Neuman. NUREG/CR-6360, "Summary of Air Permeability Data from Single-Hole Injection Tests in Unsaturated Fractured Tuffs at the Apache Leap Research Site: Results of Steady-State Test Interpretation." Washington, DC: NRC. March 1996.  
<sup>‡</sup>Vesselinov, V. Email (September 11) to C. Dinwiddie, CNWRA. Los Alamos, New Mexico: Los Alamos National Laboratory. 2002.

1.0-m [3.3-ft] length {7.33 × 10<sup>-16</sup> m<sup>2</sup> [7.42 × 10<sup>-4</sup> Darcies]; see Table 2-7} is on the same order of magnitude as that originally determined by Rasmussen, et al. (1990) at the 3.0-m [10.0-ft] scale {7.94 × 10<sup>-16</sup> m<sup>2</sup> [8.05 × 10<sup>-4</sup> Darcies]; see Table 2-5}. These data are discussed again in Section 4.3.

Finally, interpretation of cross-hole pneumatic injection tests at the Apache Leap Research Site has yielded geometric mean permeabilities more than a full order of magnitude larger than those determined through single-hole injection tests {3.16 × 10<sup>-14</sup> m<sup>2</sup> [3.2 × 10<sup>-2</sup> Darcies]; recall Table 2-1}.

## 2.5 Summary

The Apache Leap Research Site was described in detail, including its climate and topography, which are similar to that of Yucca Mountain, Nevada. A suite of hydrological and thermal property data previously collected at the Apache Leap Research Site by Rasmussen, et al. (1990) have been described through an exploratory data analysis in order to assess their quality as analog data for the unsaturated zone at Yucca Mountain. These parameters include (i) field estimates of air permeability, (ii) field estimates of liquid permeability, (iii) laboratory estimates of air permeability, (iv) laboratory estimates of liquid permeability, (v) fracture frequency, (vi) effective matrix and fracture porosity, (vii) alpha value of the van Genuchten moisture characteristic function, (viii) matrix Klinkenberg coefficient, (ix) water content, (x) dry thermal conductivity, (xi) saturated thermal conductivity, and (xii) dry rock specific heat. The exploratory data analysis included the computation of summary statistics, including the minimum and maximum values, the mean, the variance, and the standard deviation. Histograms of the data set were plotted, and the shape of the distribution was described with the coefficient of variation, the skewness, and the kurtosis. Univariate and multivariate analyses of the data were presented, as well as the correlation matrix between the thermohydrologic variables. More recent data collection at this site and its interpretation were also presented. Finally, a summary of other statistical analyses of Apache Leap Research Site data, primarily permeability data, was provided in support of the conclusions drawn from the Rasmussen, et al. (1990) data.

Both field and laboratory distributions of air and liquid permeability were highly skewed to the right. Statistical analysis of air and liquid field permeability data indicated that these parameters vary by five orders of magnitude within the test domain, and the majority lie within three orders of magnitude, while the air and liquid laboratory permeability data varied by only three orders of magnitude and the majority lie within one order of magnitude. Fracture frequency, van Genuchten alpha, and the matrix Klinkenberg coefficient were lognormally distributed, and saturated thermal conductivity, dry thermal conductivity, and dry rock specific heat were normally distributed. A strong parameter correlation was observed between field estimates of air and liquid permeability, and between laboratory estimates of air and liquid permeability. Weak correlations were observed between the effective matrix porosity and laboratory estimates of air and liquid permeability, and between the van Genuchten alpha and laboratory estimates of air and liquid permeability. Correlations between all other measured parameters were very weak, including those involving fracture frequency.

### 3 THE YUCCA MOUNTAIN SITE

Before using the Apache Leap Research Site data to represent the heterogeneity of thermohydrologic parameters at Yucca Mountain, a comparison of site properties is needed. This chapter contains a description of Yucca Mountain data pertinent to establishing the Apache Leap Research Site as an analog to Yucca Mountain. Work currently being performed in the Enhanced Characterization of Repository Block drift at Yucca Mountain intends to address the question of spatial variation of properties, particularly in the lower lithophysal unit of the Topopah Spring Tuff. While there is no explicit reason to believe that fracture heterogeneity at the Apache Leap Research Site is exactly the same as that at Yucca Mountain, the Apache Leap Research Site data may be an adequate substitute until the Yucca Mountain data becomes available.

#### 3.1 Site Description and Summary of Data Collection

Yucca Mountain is located approximately 135 km [84 mi] northwest of Las Vegas, Nevada, on land controlled by the U.S. Department of Energy (DOE), the U.S. Air Force, and the U.S. Bureau of Land Management; the crest of the volcanic ridge rises to a maximum elevation of 1,930 m [6,330 ft] above mean sea level. The climate is arid to semiarid with a mean annual precipitation of less than 25.4 cm [10 in]. Most precipitation occurs during summer and winter months, associated with either monsoonal seasons or Pacific Ocean storms. The regional groundwater table beneath the Yucca Mountain crest lies at an elevation of approximately 731 m [2,398 ft] above mean sea level. The proposed repository horizon is located approximately 1,000 m [3,330 ft] above mean sea level, and, except for perched water that exists between depths of 700–800 m [2,297–2,625 ft] above mean sea level, the rock above the water table is unsaturated (CRWMS M&O, 2000d).

In this section, the same suite of parameters will be described for Yucca Mountain as was described for the Apache Leap Research Site in Chapter 2. The testing and data from Yucca Mountain are more extensive and come from a much larger volume of rock than the approximately 20,000-m<sup>3</sup> [700,000-ft<sup>3</sup>] test volume at the Apache Leap Research Site. There is no single locale at Yucca Mountain, however, where all pertinent thermohydrologic parameters were estimated. Different types of tests were performed in different areas, hence, there are no consistent data sets available for Yucca Mountain with which to compare the data from the Apache Leap Research Site. For the estimates reported in this section, parameter values are assembled from different locales at Yucca Mountain, particularly within the proposed repository horizon. For example, cores used for hydraulic testing came from surface-based boreholes separated by kilometers, not by meters as at the Apache Leap Research Site. The field air permeability estimates came from a different set of boreholes, mostly in the Exploratory Studies Facility and Enhanced Characterization of the Repository Block drifts.

##### 3.1.1 Field Estimates of Fracture Air Permeability

Single-hole pneumatic injection tests were conducted near four Exploratory Studies Facility niche sites (35+66, 36+50, 31+07, and 47+88) prior to their excavation, and near two Exploratory Studies Facility alcoves (Alcoves 4 and 6) (CRWMS M&O, 2000a). The location for each niche and Alcove 6 is in the middle nonlithophysal zone of the Topopah Spring welded tuff unit at Yucca Mountain, wherein an estimated 20 to 30 percent of the proposed repository may

eventually be located. Alcove 4 is located in the Paintbrush nonwelded tuff unit above the proposed repository horizon. Each niche borehole is oriented horizontally with its distal end toward the northwest, parallel to the niche axis. The support of the permeability parameter is defined nominally by the length of the injection interval, which was 0.3 m [1 ft] in this case. Air-injection tests {support varies from 4 to 12 m [13 to 39 ft]} were also performed in vertical boreholes and in the Single Heater Test and Drift Scale Test areas of Exploratory Studies Facility Alcove 5 at Yucca Mountain, with the goal of obtaining air permeability values for calibration of the site-scale unsaturated zone model (CRWMS M&O, 2000c). These borehole permeability data, which were collected from the repository horizon (i.e., both the middle nonlithophysal and lower lithophysal zones of the Topopah Spring welded unit), came from vertical boreholes NRG-7a, NRG-6, SD-12, and UZ#16. Steady-state pneumatic injection tests were performed through isolation of an interval with borehole packers, followed by air injection into the isolated interval, and conversion of measured flowrate and injection pressure into air permeability using a modified Hvorslev formula (LeCain, 1995; Hvorslev, 1951). It is assumed that air flows mainly through the fractures, and thus, calculations are for fracture permeability. Geometric mean field estimates of niche, alcove, and unsaturated zone flow model uncalibrated and calibrated fracture air permeability values are listed in Tables 3-1 and 3-2 with units of square meters.

### **3.1.2 Laboratory Estimates of Matrix Liquid Permeability**

Saturated hydraulic conductivity was measured in the laboratory on 750 core samples from 8 deep boreholes at Yucca Mountain (Flint, 1998; CRWMS M&O, 2000c; see also Anderson, 1991). A steady-state permeameter was used to measure hydraulic conductivity of vacuum-saturated cores. The resulting data were converted to liquid permeability, given the viscosity and density of water at atmospheric pressure and 20 °C [68 °F] and gravitational acceleration at sea level (CRWMS M&O, 2000c). These small-scale permeability values were then upscaled (subject to a maximum limit of 1.5 orders of magnitude) according to a scheme outlined by Paleologos, et al. (1996) for highly heterogeneous porous media (CRWMS M&O, 2000c). Unsaturated zone flow model uncalibrated and calibrated matrix liquid permeability values are listed in Table 3-2 with units of square meters.

### **3.1.3 Fracture Frequency**

The Yucca Mountain project primarily uses two-dimensional or full-periphery fracture maps from the Exploratory Studies Facility and the Enhanced Characterization of Repository Block drifts to estimate fracture frequency. However, to maintain consistency in a comparison between the Apache Leap Research Site and Yucca Mountain, borehole fracture frequency data were needed. Borehole data were obtained from the Technical Data Management System for boreholes UZ#14, NRG-6, NRG-7a, SD-7, SD-9, and SD-12 (DTN SNF29041993002.080, SN0101F2941993.085, SNF29041993002.069, SNF29041993002.071, and SNF29041993002.084). These are the only boreholes at Yucca Mountain with fracture plane orientation data available for the middle nonlithophysal Topopah Spring tuff units. Data for the nonwelded Paintbrush tuffs from two of these boreholes also are included in the analysis.

Uncorrected and corrected fracture frequency estimates from available borehole data are presented in Table 3-3. The Terzaghi (1965) factor [Eq. (2-1)] was used to correct the vertical borehole fracture frequency data for orientation bias. As with the Apache Leap Research Site

**Table 3-1. Comparison of Apache Leap Research Site and Yucca Mountain Field-Estimated Air Permeabilities and Their Relationship to Fracture Density and Degree of Welding**

		Fracture Permeability, $k_f$	Fracturing/ Fracture Density	Degree of Welding
Apache Leap Research Site X-, Y-, and Z-series boreholes		$7.94 \times 10^{-16} \text{ m}^2$ [ $8.05 \times 10^{-4} \text{ D}$ ]	$0.98\text{--}3.6 \text{ m}^{-1}$ [ $0.30\text{--}1.1 \text{ ft}^{-1}$ ]	slightly welded
Yucca Mountain PTn*	NRG-6, NRG-7a	—	$3.1\text{--}2.7 \text{ m}^{-1}$ [ $0.9\text{--}0.8 \text{ ft}^{-1}$ ]	nonwelded to partially welded
	ESF <sup>†</sup> Alcove 4 <sup>‡</sup>	$1.00 \times 10^{-13} \text{ m}^2$ [0.10 D]	discretely faulted and fractured	
	Uncalibrated Values <sup>§</sup> (NRG-7a and Alcove 3)	$(0.16\text{--}3.20) \times 10^{-12} \text{ m}^2$ [0.16–3.24 D]		
	Calibrated Basecase <sup>¶</sup>	$(0.26\text{--}20) \times 10^{-12} \text{ m}^2$ [0.26–20 D]		
Yucca Mountain Tptpmn <sup>¶</sup> (tsw34) ESF Data	Alcove 6 <sup>‡</sup>	$1.26 \times 10^{-12} \text{ m}^2$ [1.28 D]	highly fractured	moderately to densely welded
	Niche 35+66 <sup>‡</sup>	$1.00 \times 10^{-13} \text{ m}^2$ [0.10 D]	brecciated; > Niche 36+50	
	Niche 36+50 <sup>‡</sup>	$3.98 \times 10^{-14} \text{ m}^2$ [ $4.03 \times 10^{-2} \text{ D}$ ]	moderately fractured; < Niche 35+66	
	Niche 31+07 <sup>‡</sup>	$3.98 \times 10^{-14} \text{ m}^2$ [ $4.03 \times 10^{-2} \text{ D}$ ]	moderately fractured	
	Niche 47+88 <sup>‡</sup>	$1.00 \times 10^{-13} \text{ m}^2$ [0.10 D]	intensely fractured	
Yucca Mountain Tptpmn (tsw34) Deep Borehole Data	UZ-14, SD-7, SD-9, SD-12, NRG-6, NRG-7a	—	$6.4\text{--}11.2 \text{ m}^{-1}$ [ $2.0\text{--}3.4 \text{ ft}^{-1}$ ]	
	Uncalibrated Values <sup>§</sup> (NRG-7a, NRG-6, SD-12, UZ#16, Alcove 5)	$(1.6 \text{ and } 3.4) \times 10^{-13} \text{ m}^2$ [0.16 and 0.34 D] (two weighted averages)	$4.32 \text{ m}^{-1}$ [ $1.32 \text{ ft}^{-1}$ ]	
	Calibrated Basecase <sup>¶</sup>	$2.76 \times 10^{-13} \text{ m}^2$ [0.280 D]		
Yucca Mountain Tptpl <sup>¶</sup> (tsw35) Deep Borehole Data	Uncalibrated Value <sup>§</sup> (NRG-7a, UZ#16)	$9.0 \times 10^{-13} \text{ m}^2$ [0.91 D]	$3.16 \text{ m}^{-1}$ [ $0.96 \text{ ft}^{-1}$ ]	
	Calibrated Basecase <sup>¶</sup>	$1.29 \times 10^{-12} \text{ m}^2$ [1.31 D]		

\*Paintbrush Nonwelded Tuff

<sup>†</sup>Exploratory Studies Facility

<sup>‡</sup>CRWMS M&O. "In-Situ Field Testing of Processes." ANL-NBS-HS-000005. Rev. 00. Las Vegas, Nevada: TRW Environmental Safety Systems, Inc. 2000a.

<sup>§</sup>\_\_\_\_\_. "Analysis of Hydrologic Properties Data." ANL-NBS-HS-000002. Rev. 00. Las Vegas, Nevada: TRW Environmental Safety Systems, Inc. 2000b.

<sup>¶</sup>\_\_\_\_\_. "Calibrated Properties Model." MDL-NBS-HS-000003. Rev. 00. Las Vegas, Nevada: TRW Environmental Safety Systems, Inc. 2000c.

<sup>‡</sup>Topopah Spring middle nonlithophysal zone

<sup>#</sup>Topopah Spring lower lithophysal zone

Table 3-2. Comparison of Properties Estimated at Apache Leap Research Site and Yucca Mountain					
	Apache Leap Research Site	Yucca Mountain Exploratory Studies Facility and Deep Boreholes (tsw34)		Yucca Mountain Exploratory Studies Facility and Deep Boreholes (tsw35)	
		Uncalibrated	Calibrated Basecase	Uncalibrated	Calibrated Basecase
Welding	Slightly Welded	Moderately to Densely Welded			
Fracture Permeability, $k_f$	$7.94 \times 10^{-16} \text{ m}^2$ [ $8.05 \times 10^{-4} \text{ D}$ ]	$(1.6 \text{ and } 3.4) \times 10^{-13} \text{ m}^2$ [0.16 and 0.34 D] (two weighted averages)	$2.76 \times 10^{-13} \text{ m}^2$ [0.280 D]	$9.0 \times 10^{-13} \text{ m}^2$ [0.91 D]	$1.29 \times 10^{-12} \text{ m}^2$ [1.31 D]
Fracture Permeability, $k_w$	$7.24 \times 10^{-16} \text{ m}^2$ [ $7.34 \times 10^{-4} \text{ D}$ ]	No Data	No Data	No Data	No Data
Matrix Permeability, $k_m$	$1.62 \times 10^{-15} \text{ m}^2$ [ $1.64 \times 10^{-3} \text{ D}$ ]	No Data	No Data	No Data	No Data
Matrix Permeability, $k_w$	$5.62 \times 10^{-16} \text{ m}^2$ [ $5.69 \times 10^{-4} \text{ D}$ ]	$7.5 \times 10^{-18} \text{ m}^2$ [ $7.6 \times 10^{-7} \text{ D}$ ]	$4.07 \times 10^{-18} \text{ m}^2$ [ $4.12 \times 10^{-6} \text{ D}$ ]	$3.1 \times 10^{-17} \text{ m}^2$ [ $3.1 \times 10^{-5} \text{ D}$ ]	$3.04 \times 10^{-17} \text{ m}^2$ [ $3.08 \times 10^{-5} \text{ D}$ ]
Fracture Density, Tunnel Data with Length Threshold	Not Applicable	$4.32 \text{ m}^{-1}$ [1.32 ft <sup>-1</sup> ]		$3.16 \text{ m}^{-1}$ [0.96 ft <sup>-1</sup> ]	
Fracture Frequency in Borehole	$0.77 \text{ m}^{-1}$ [0.23 ft <sup>-1</sup> ]	$2.7\text{--}5.0 \text{ m}^{-1}$ [0.8–1.5 ft <sup>-1</sup> ] (boreholes in Table 3-3)		No Data	
Fracture Density in Borehole, Corrected	$1.85 \text{ m}^{-1}$ [0.56 ft <sup>-1</sup> ]	$6.4\text{--}11.2 \text{ m}^{-1}$ [2.0–3.4 ft <sup>-1</sup> ] (boreholes in Table 3-3)		No Data	
Fracture Porosity	1.7%	1.0%		1.1%	
Matrix Porosity	17.5%	11.0%		13.1%	
Fracture van Genuchten $\alpha$	No Data	$6.8 \times 10^{-1} \text{ kPa}^{-1}$ [4.7 psi <sup>-1</sup> ]	$5.16 \times 10^{-1} \text{ kPa}^{-1}$ [3.56 psi <sup>-1</sup> ]	$1.0 \text{ kPa}^{-1}$ [6.9 psi <sup>-1</sup> ]	$7.39 \times 10^{-1} \text{ kPa}^{-1}$ [5.10 psi <sup>-1</sup> ]
Matrix van Genuchten $\alpha$	$2.23 \times 10^{-2} \text{ kPa}^{-1}$ [ $1.54 \times 10^{-1} \text{ psi}^{-1}$ ]	$3.69 \times 10^{-3} \text{ kPa}^{-1}$ [ $2.54 \times 10^{-2} \text{ psi}^{-1}$ ]	$3.86 \times 10^{-3} \text{ kPa}^{-1}$ [ $2.66 \times 10^{-2} \text{ psi}^{-1}$ ]	$6.41 \times 10^{-3} \text{ kPa}^{-1}$ [ $4.42 \times 10^{-2} \text{ psi}^{-1}$ ]	$6.44 \times 10^{-3} \text{ kPa}^{-1}$ [ $4.44 \times 10^{-2} \text{ psi}^{-1}$ ]
Klinkenburg Coefficient	$3.22 \times 10^2 \text{ kPa}$ [46.7 psi]	Effect assumed negligible due to flow dominated by large aperture fractures			
Matrix Water Content	14.30%	9.3%		10.1%	
Dry Thermal Conductivity	$1.27 \text{ J/m s K}$ [0.73 Btu/ft h °F]	$1.56 \text{ J/m s K}$ [0.90 Btu/ft h °F]		$1.20 \text{ J/m s K}$ [0.69 Btu/ft h °F]	
Saturated Thermal Conductivity	$1.82 \text{ J/m s K}$ [1.05 Btu/ft h °F]	$2.33 \text{ J/m s K}$ [1.35 Btu/ft h °F]		$2.02 \text{ J/m s K}$ [1.17 Btu/ft h °F]	
Dry Rock Specific Heat	$7.02 \times 10^2 \text{ J/kg K}$ [0.168 Btu/lb <sub>m</sub> °F]	$9.48 \times 10^2 \text{ J/kg K}$ [0.226 Btu/lb <sub>m</sub> °F]		$9.00 \times 10^2 \text{ J/kg K}$ [0.215 Btu/lb <sub>m</sub> °F]	

Table 3-3. Frequency of Fractures in Boreholes at Yucca Mountain for the Paintbrush Nonwelded Tuff and the Middle Nonlithophysal Zone of the Topopah Spring Welded Tuff		
	Uncorrected Fracture Frequency m <sup>-1</sup> [ft <sup>-1</sup> ]	Corrected Fracture Frequency m <sup>-1</sup> [ft <sup>-1</sup> ]
Tptpmn,* UZ#14	5.0 [1.5]	10.6 [3.2]
Tptpmn, SD-7	3.2 [1.0]	7.1 [2.2]
Tptpmn, SD-9	2.7 [0.8]	6.4 [1.9]
Tptpmn, SD-12	5.0 [1.5]	11.1 [3.4]
Tptpmn, NRG-6	4.1 [1.3]	11.2 [3.4]
Tptpmn, NRG-7a	3.2 [1.0]	7.7 [2.3]
PTn, <sup>†</sup> NRG-6	2.6 [0.8]	3.1 [0.9]
PTn, NRG-7a	1.4 [0.4]	2.7 [0.8]
*Topopah Spring middle nonlithophysal zone <sup>†</sup> Paintbrush Nonwelded Tuff		

data, the factors are summed along a borehole to obtain, in essence, an estimate of true fracture density representative of the volume through which the borehole crosses. Following the approach of Waiting, et al. (2001) for angles greater than 75°, a value of 4 was assigned as the Terzaghi factor to avoid asymptotic increases in fracture density as angles of 90° are approached.

Tables 3-1 and 3-2 contain summaries of both the uncorrected and corrected fracture frequency values. The borehole estimates from Yucca Mountain should be compared with the borehole estimates from the Apache Leap Research Site. For reference, the estimates provided by CRWMS M&O (2000c) from the Exploratory Studies Facility are also included in these tables. The estimates of fracture frequency from the Exploratory Studies Facility are generally believed to be one order of magnitude less than estimates from boreholes because only fractures longer than 1.0 m [3.3 ft] in length were counted in the Exploratory Studies Facility and because of the likelihood that fewer fractures were induced during excavation.

### 3.1.4 Effective Fracture Porosity

Effective fracture porosity of the middle nonlithophysal zone of the Topopah Spring welded unit,  $\phi_{\text{middle nonlithophysal}}$ , was determined from gas tracer tests in the Exploratory Studies Facility.

Because gas tracer tests were not performed within other Yucca Mountain units, this field-determined value for effective fracture porosity was modified through its projection to the

other unsaturated zone model layers (e.g., the lower lithophysal zone) subject to a study of their fracture networks (CRWMS M&O, 2000c). That is,

$$\phi_{\text{layer } x} = \phi_{\text{middle nonlithophysal}} \left( \frac{\phi_{2D_{\text{layer } x}}}{\phi_{2D_{\text{middle nonlithophysal}}}} \right), \quad (3-1)$$

where  $\phi_{2D}$  is the two-dimensional porosity, defined by the product of fracture intensity and fracture aperture. Unsaturated zone model estimates of effective fracture porosity are listed in Table 3-2. When fracture intensity data were unavailable, the ratio of one-dimensional porosity was used, where one-dimensional porosity is defined by the product of fracture frequency and fracture aperture.

### 3.1.5 Effective Matrix Porosity

Effective matrix porosity values for the middle nonlithophysal and lower lithophysal zones of the Topopah Spring welded unit were determined through laboratory measurement of borehole core sample saturated and dry weights (Flint, 1998; CRWMS M&O, 2000c). Unsaturated zone model estimates of effective matrix porosity are listed in Table 3-2.

### 3.1.6 Fracture van Genuchten Alpha

The van Genuchten fracture alpha is calculated via a form of the Young-LaPlace equation that has been recast in a more elementary manner (CRWMS M&O, 2000c). Use of the Young-LaPlace equation requires knowledge of the effective hydraulic fracture aperture, which may be determined (see Bear, et al., 1993) when the mean fracture frequency and fracture permeability are known. Exploratory Studies Facility seepage tests performed in Niche 36+50 were used to independently determine the van Genuchten fracture alpha for the middle nonlithophysal zone of the Topopah Spring welded unit (CRWMS M&O, 2000c). Water release fluxes and seepage rates were used to quantify a seepage threshold flux; the threshold fluxes and arrival times were used to then determine the van Genuchten fracture alpha (Philip, et al., 1989). Unsaturated zone flow model uncalibrated and calibrated fracture van Genuchten alphas are listed in Table 3-2 with units of  $\text{kPa}^{-1}$ . The fracture van Genuchten alpha determined for Niche 36+50 was  $6.9 \times 10^{-1} \text{ kPa}^{-1}$  [ $4.8 \text{ psi}^{-1}$ ] (CRWMS M&O, 2000c), only 1.45 percent greater than that calculated for the unsaturated zone flow model as an uncalibrated value.

### 3.1.7 Matrix van Genuchten Alpha

The  $\alpha$  and  $m$  fitting parameters of the middle nonlithophysal and lower lithophysal zones of the Topopah Spring welded unit were determined through laboratory measurement of saturation, water potential, and desaturation data at various times during the borehole core sample drying process. By minimizing the sum of the squared saturation residuals, the best fit matrix van Genuchten  $\alpha$  and  $m$  could be deduced (CRWMS M&O, 2000c). *In-situ* borehole measurements of water potential were used to amend these results for field conditions, providing a better representation of actual field behavior. Unsaturated zone flow model uncalibrated and calibrated matrix van Genuchten alphas are listed in Table 3-2.

### 3.1.8 Field Estimates of Fracture Volumetric Water Content

A finite pulse of water was released above Niche 36+50 during the drift seepage test, in order to simulate the approach of an episodic percolation front through preferential flow pathways. Volumetric water content of fractures was estimated from the niche seepage data via a time-dependent analytical solution, derived by Braester (1973), for a surface source that generates a constant flux (CRWMS M&O, 2000a). Niche estimates of fracture volumetric water content ranged from 0.09 to 2.4 percent.

### 3.1.9 Laboratory Estimates of Matrix Gravimetric and Volumetric Water Content

Volumetric water content may be related to gravimetric water content by the ratio of water density to rock bulk density (the bulk densities of the Topopah Spring middle nonlithophysal zone and lower lithophysal zone are  $2,250 \text{ kg/m}^3$  [ $140 \text{ lb/ft}^3$ ] and  $2,210 \text{ kg/m}^3$  [ $138 \text{ lb/ft}^3$ ], respectively). Flint (1998) conducted experimental determinations of volumetric water content via laboratory measurement of borehole core sample initial and dry weights, using the previously mentioned conversion from gravimetric to volumetric. Unsaturated zone flow model estimates of matrix volumetric water content are listed in Table 3-2.

### 3.1.10 Dry Thermal Conductivity

Dry thermal conductivity was determined experimentally from borehole cores UE25 NRG-4, UE25 NRG-5, USW NRG-6, and USW NRG-7/7A. Measurements were made at temperatures both below and in excess of  $100 \text{ }^\circ\text{C}$  [ $212 \text{ }^\circ\text{F}$ ]. Measured dry thermal conductivities at both temperatures were then arithmetically averaged to arrive at final basecase values for the middle nonlithophysal and lower lithophysal zones of the Topopah Spring welded unit<sup>1</sup> (Brodsky, et al., 1997; CRWMS M&O, 2000c). Dry thermal conductivities are listed in Table 3-2.

### 3.1.11 Saturated Thermal Conductivity

Saturated thermal conductivity was determined experimentally from borehole cores UE25 NRG-4, UE25 NRG-5, USW NRG-6, and USW NRG-7/7A. Measured saturated thermal conductivities were arithmetically averaged to provide values for the middle nonlithophysal and lower lithophysal zones of the Topopah Spring welded unit<sup>2</sup> (CRWMS M&O, 2000c). For the lithophysal zone, the experimental values were amended based on the increased porosity of the zone due to the presence of lithophysae.<sup>3</sup> Saturated thermal conductivities are listed in Table 3-2.

---

<sup>1</sup>Francis, N.D. "The Base-Case Thermal Properties for TSPA-VA Modeling." Memorandum (April 16) to Distribution. Albuquerque, New Mexico: Sandia National Laboratories. 1997.

<sup>2</sup>ibid.

<sup>3</sup>ibid.

### 3.1.12 Dry Rock Specific Heat

Measured bulk thermal capacitance data (the product of bulk density and specific heat) provided the means to calculate dry rock specific heat (or grain specific heat)<sup>4</sup> (CRWMS M&O, 2000c). Dry rock specific heats are listed in Table 3-2.

## 3.2 Comparison of Apache Leap Research Site and Yucca Mountain Data

### 3.2.1 Comparison of Properties

#### 3.2.1.1 Fracture Permeability

Because the tuff at the Apache Leap Research Site is only partially welded, it is generally expected to be less fractured than the proposed repository horizon at Yucca Mountain, which exhibits greater degrees of welding. Thus, a comparison of the geometric mean fracture air permeability values at the two sites indicates that while the fracture air permeability of Apache Leap Research Site is two orders of magnitude smaller than the air permeability measurements of the moderately welded Niche 36+50 and Niche 31+07, it is three to four orders of magnitude smaller than permeability values measured in the discretely faulted and fractured Alcove 4 (located above the repository horizon), the highly fractured Alcove 6, the brecciated Niche 35+66, and the intensely fractured Niche 47+88 (Table 3-2). The geometric mean fracture air permeability of Apache Leap Research Site is three orders of magnitude smaller than the uncalibrated and calibrated basecase fracture permeability values for modeling the middle nonlithophysal zone of the Topopah Spring unit, in which 20 to 30 percent of the proposed repository may be located. And, it is four orders of magnitude smaller than the uncalibrated and calibrated basecase (drift scale) fracture permeability values for the Topopah Spring lower lithophysal zone, in which 70 percent of the proposed repository may be located (Table 3-2). The geometric mean fracture air permeability of the Apache Leap Research Site is five orders of magnitude smaller than the mountain scale fracture permeability  $\{4.51 \times 10^{-11} \text{ m}^2$  [45.7 Darcies]] of the Topopah Spring lower lithophysal zone. It is important to keep in mind the scale at which various measurements were made and any upscaling employed in arriving at model parameters when making such comparisons—this will be discussed further in Section 3.2.2.

In addition to the fracture air permeability data discussed previously, LeCain (1997) reports the following borehole-based data for the Topopah Spring welded unit as a whole: the geometric mean of data collected from borehole UZ-16 is  $9 \times 10^{-13} \text{ m}^2$  [0.9 Darcies]; the geometric mean of data collected from borehole SD-12 is  $1.7 \times 10^{-12} \text{ m}^2$  [1.7 Darcies]; the geometric mean of data collected from borehole NRG-6 is  $8 \times 10^{-13} \text{ m}^2$  [0.8 Darcies], and the geometric mean of data collected from borehole NRG-7a is  $3 \times 10^{-13} \text{ m}^2$  [0.3 Darcies]. When the permeabilities of the Topopah Spring middle nonlithophysal zone were analyzed as a subset of this borehole data, the borehole-based geometric average was determined to be  $4.27 \times 10^{-13} \text{ m}^2$  [ $4.33 \times 10^{-1}$  Darcies], as reported in CRWMS M&O (1997). Similarly, the borehole-based

---

<sup>4</sup>Francis, N.D. "The Base-Case Thermal Properties for TSPA-VA Modeling." Memorandum (April 16) to Distribution. Albuquerque, New Mexico: Sandia National Laboratories. 1997.

geometric average of the Topopah Spring lower lithophysal zone was determined to be  $9.12 \times 10^{-13} \text{ m}^2$  [ $9.24 \times 10^{-1}$  Darcies]. Rousseau, et al. (1999) report arithmetic mean estimates for the Topopah Spring middle nonlithophysal zone in the range of  $0.6 \times 10^{-12} \text{ m}^2$  [0.6 Darcies] (Borehole NRG-6) to  $1.1 \times 10^{-12} \text{ m}^2$  [1.1 Darcies] (Borehole NRG-7a); for the lower lithophysal zone, they report  $0.4 \times 10^{-12} \text{ m}^2$  [0.4 Darcies] as the arithmetic mean estimate from Borehole NRG-7a (see also, Ahlers, et al., 1996). LeCain, et al. (1999) report the following geometric means from single-hole pneumatic testing at the Ghost Dance fault:  $5 \times 10^{-13} \text{ m}^2$  [0.5 Darcies] for the hanging wall,  $7 \times 10^{-13} \text{ m}^2$  [0.7 Darcies] for the foot wall, and  $1 \times 10^{-11} \text{ m}^2$  [10 Darcies] for the fault zone. Likewise, cross-hole testing yielded  $4.1 \times 10^{-12} \text{ m}^2$  [4.1 Darcies] for the hanging wall,  $7.8 \times 10^{-12} \text{ m}^2$  [7.8 Darcies] for the foot wall, and  $1.46 \times 10^{-11} \text{ m}^2$  [14.8 Darcies] for the fault zone.

Unfortunately, there are no fracture/field liquid permeability data available from Yucca Mountain with which to compare the Apache Leap Research Site data.

### 3.2.1.2 Matrix Permeability

There are no matrix air permeability data available from Yucca Mountain. In general, this would have required core plug measurements of permeability via the one-dimensional Hassler-sleeve method, which was used at the Apache Leap Research Site, or outcrop/drift wall measurements of permeability via the multidimensional gas minipermeameter. To the authors' knowledge, neither of these approaches have been employed at Yucca Mountain.

The geometric mean of the Apache Leap Research Site matrix liquid permeability is much greater than those measured and calibrated for Yucca Mountain (Table 3-2). The uncalibrated estimate of permeability for the Topopah Spring middle nonlithophysal zone is three orders of magnitude smaller than that determined at the Apache Leap Research Site, while the calibrated basecase value used to model this layer is approximately two orders of magnitude smaller. The uncalibrated estimate of permeability for the Topopah Spring lower lithophysal zone and the calibrated basecase value used to model this layer are both one order of magnitude smaller than the geometric mean determined at the Apache Leap Research Site. Flint (1998) estimates geometric mean matrix permeabilities of the Topopah Spring middle nonlithophysal and lower lithophysal zones to be  $4.09 \times 10^{-18} \text{ m}^2$  [ $4.14 \times 10^{-6}$  Darcies] and  $2.35 \times 10^{-17} \text{ m}^2$  [ $2.38 \times 10^{-5}$  Darcies].

### 3.2.1.3 Fracture Frequency

Borehole data indicate that there is a two- or three-fold increase in both corrected and uncorrected fracture frequency for Yucca Mountain relative to the Apache Leap Research Site. The range of average fracture frequencies for boreholes at the Apache Leap Research Site was  $0.98\text{--}3.59 \text{ m}^{-1}$  [ $0.30\text{--}1.09 \text{ ft}^{-1}$ ], while at Yucca Mountain it was  $6.4\text{--}11.2 \text{ m}^{-1}$  [ $2.0\text{--}3.4 \text{ ft}^{-1}$ ] for the middle nonlithophysal zone of the Topopah Spring unit, and  $2.7$  to  $3.1 \text{ m}^{-1}$  [ $0.8$  to  $0.9 \text{ ft}^{-1}$ ] for the Paintbrush nonwelded tuff.

The variation of fracture frequency at Yucca Mountain is also larger than at the Apache Leap Research Site. A meaningful comparison of the variation in fracture frequency is constrained by the type of data recorded for each site. The Apache Leap Research Site data were listed as a strike and dip for each fracture in every borehole. The Yucca Mountain borehole data are

comprised of the number of fractures in 10° bins (fracture plane attitude relative to borehole axis) for 3-m [10-ft] sections of core. The fracture frequency for 3-m [10-ft] sections of core range from 0 to 4.5 m<sup>-1</sup> [0 to 1.4 ft<sup>-1</sup>] for the Apache Leap Research Site and from 0 to 28 m<sup>-1</sup> [0 to 8.5 ft<sup>-1</sup>] for the middle nonlithophysal zone of the Topopah Spring welded tuff at Yucca Mountain. The data for Yucca Mountain come from a much larger than that of the Apache Leap Research Site, hence, more variation is expected in the Yucca Mountain data.

The overprint of surficial processes also affects the structural features of the Apache Leap Research Site (e.g., stress release overburden unloading). The Apache Leap Research Site measurement volume is located between the surface and a 30-m [98-ft] depth, whereas, the Yucca Mountain fracture frequency data are gathered from depths below the surface on the order of 150–250 m [490–820 ft].

Fracture intensity generally increases with degree of welding at Yucca Mountain, which is reflective of the degree of brittleness of the rock. The variation of fracturing with degree of welding is supported by Yucca Mountain borehole and Exploratory Studies Facility data (CRWMS M&O, 2000c). Vague nomenclature used to describe degree of welding can be misleading when terminology is not consistently applied between sites. The Apache Leap Research Site has been described as slightly-welded (Rasmussen, et al., 1990), and may fall somewhere between the degree of welding observed in the Paintbrush nonwelded tuffs and the moderately welded Tiva Canyon tuffs of Yucca Mountain, or it may be similar to the degree of welding observed in the Topopah Spring tuffs. Hence, a description of the degree of welding should not be used to infer fracture properties.

#### **3.2.1.4 Effective Fracture and Matrix Porosity**

In addition to the Yucca Mountain fracture porosity data reported in Table 3-2, LeCain, et al. (1999) determined the following fracture porosity arithmetic and geometric means in the vicinity of the Ghost Dance fault: 4.0 and 3.0 percent for the hanging wall, 4.0 and 3.0 percent for the foot wall, and 13.0 and 10.0 percent for the fault zone. Fracture porosity determined through a single cross-hole pneumatic injection test (i.e., PP4, see Table 2-1) at the Apache Leap Research Site (Illman and Neuman, 2001) compares well with those determined for the repository horizons of Yucca Mountain; specifically, the parameter ranged between 0.003 and 7 percent, while the arithmetic mean value of air-filled fracture porosity determined from the Apache Leap Research Site (1.7 percent) is only 35–41 percent greater than that reported for the lower lithophysal (1.1 percent) and middle nonlithophysal (1.0 percent) zones of the Topopah Spring unit. Vesselinov, et al. (2001b) report the arithmetic mean air-filled fracture porosity for a total of five cross-hole pneumatic injection tests conducted at the Apache Leap Research site to be 2.34 percent.

Flint (1998) reports that arithmetic average matrix porosity values in the Topopah Spring middle nonlithophysal zone for each borehole ranged between 10 and 12 percent, whereas, arithmetic average matrix porosity values in the lower lithophysal zone ranged between 12 and 14 percent. Estimated arithmetic mean matrix porosity at the Apache Leap Research Site is 37 percent and 25 percent greater than the respective porosity of each Topopah Spring repository horizon zone (Table 3-2). The arithmetic average matrix porosity values from the Apache Leap Research Site are similar to the partially- to moderately-welded units of the Tiva Canyon (e.g., upper lithophysal

unit) and the less welded portions of the Topopah Spring welded tuff (e.g., the crystal-rich rounded unit, Tptrn).

### 3.2.1.5 Fracture and Matrix van Genuchten Alpha

While fracture van Genuchten alphas were determined at Yucca Mountain, they were not investigated at the Apache Leap Research Site. In addition to the uncalibrated fracture van Genuchten alpha values provided in Table 3-2, CRWMS M&O (1997) reports values for the Topopah Spring middle nonlithophysal zone and lower lithophysal zone of  $9.73 \times 10^{-1} \text{ kPa}^{-1}$  [ $6.71 \text{ psi}^{-1}$ ] and  $1.26 \text{ kPa}^{-1}$  [ $8.69 \text{ psi}^{-1}$ ], respectively. Calibrated fracture van Genuchten alphas in the proposed repository horizon of Yucca Mountain were on the order of  $10^{-1} \text{ kPa}^{-1}$  [ $10^0 \text{ psi}^{-1}$ ]; in addition to the calibrated fracture van Genuchten alpha values provided in Table 3-2, CRWMS M&O (1997) reports values for the Topopah Spring middle nonlithophysal zone of  $0.83 \times 10^{-1} \text{ kPa}^{-1}$  [ $0.57 \text{ psi}^{-1}$ ] and  $0.98 \times 10^{-1} \text{ kPa}^{-1}$  [ $0.68 \text{ psi}^{-1}$ ] for two different inversions. It also reports calibrated fracture van Genuchten alphas for the lower lithophysal zone of  $1.02 \times 10^{-1} \text{ kPa}^{-1}$  [ $0.70 \text{ psi}^{-1}$ ] and  $1.10 \times 10^{-1} \text{ kPa}^{-1}$  [ $0.76 \text{ psi}^{-1}$ ] for two different inversions.

The matrix van Genuchten alpha of the Apache Leap Research Site was on the order  $10^{-2} \text{ Pa}^{-1}$  [ $10^{-1} \text{ psi}^{-1}$ ], but the reader is cautioned against directly comparing this value to those estimated for Yucca Mountain because the Apache Leap Research Site method arbitrarily assumed all other van Genuchten parameters to be constant (i.e.,  $n = 1.6$  and  $\theta_r = 0$ ). In addition to the uncalibrated matrix van Genuchten alpha values provided in Table 3-2, CRWMS M&O (1997) reports values for the Topopah Spring middle nonlithophysal zone and lower lithophysal zone of  $6.4 \times 10^{-4} \text{ kPa}^{-1}$  [ $4.4 \times 10^{-3} \text{ psi}^{-1}$ ] and  $2.73 \times 10^{-3} \text{ kPa}^{-1}$  [ $1.88 \times 10^{-2} \text{ psi}^{-1}$ ]. Matrix van Genuchten alphas for the proposed repository horizon of Yucca Mountain were on the order of  $10^{-3} \text{ kPa}^{-1}$  [ $10^{-2} \text{ psi}^{-1}$ ]. In addition to the calibrated matrix van Genuchten alpha values provided in Table 3-2, CRWMS M&O (1997) reports values for the Topopah Spring middle nonlithophysal zone of  $1.07 \times 10^{-3} \text{ kPa}^{-1}$  [ $7.38 \times 10^{-3} \text{ psi}^{-1}$ ] and  $1.02 \times 10^{-3} \text{ kPa}^{-1}$  [ $7.03 \times 10^{-3} \text{ psi}^{-1}$ ] for two different inversions, and it reports calibrated matrix van Genuchten alphas for the lower lithophysal zone of  $3.24 \times 10^{-3} \text{ kPa}^{-1}$  [ $2.23 \times 10^{-2} \text{ psi}^{-1}$ ] and  $3.31 \times 10^{-3} \text{ kPa}^{-1}$  [ $2.28 \times 10^{-2} \text{ psi}^{-1}$ ] for two different inversions.

### 3.2.1.6 Fracture and Matrix Klinkenberg Coefficient

Just as at the Apache Leap Research Site, pneumatic testing of fracture permeability at Yucca Mountain assumed that the Klinkenberg (or gas slippage) effect was essentially negligible due to gas flow dominated by large aperture fractures.

Recalling from Section 3.2.1.2 that there are no matrix permeability data from Yucca Mountain, it is not possible to investigate the matrix Klinkenberg coefficient.

### 3.2.1.7 Fracture and Matrix Water Content

The volumetric water content measurements conducted by Flint (1998) were within the same order of magnitude as those determined for the Apache Leap Research Site. Matrix volumetric water content measured at the Apache Leap Research Site is 35 percent greater than that of the Topopah Spring middle nonlithophysal zone and 29 percent greater than that of the Topopah Spring lower lithophysal zone, as determined by Flint (1998). The water content determined for

Niche 36+50 (CRWMS M&O, 2000a), which ranged from 0.09 to 2.4 percent, represents fracture water content in the Topopah Spring middle nonlithophysal zone; as would be expected, it is substantially smaller than the matrix water content of the same zone (i.e., fracture water content is only 1 to 25 percent of the estimated matrix water content).

#### **3.2.1.8 Dry and Saturated Thermal Conductivity**

Dry thermal conductivity at the Apache Leap Research Site compares well with that of both Yucca Mountain zones encompassing the proposed repository horizon (Table 3-2). The dry thermal conductivity of the Topopah Spring middle nonlithophysal zone is 19 percent greater than that at the Apache Leap Research Site, and the dry thermal conductivity of the Apache Leap Research Site is six percent greater than that of the Topopah Spring lower lithophysal zone. The Topopah Spring thermal-mechanical unit Tsw2 encompasses both the middle nonlithophysal zone and the lower lithophysal zone. In testing borehole core from this unit (Boreholes UE25 NRG-5 and USW NRG-6), Brodsky, et al. (1997) found the dry thermal conductivity to be 1.50 J/s m K [0.87 Btu/h ft °F] at low temperature {<100 °C [<212 °F]}, and 1.59 J/s m K [0.92 Btu/h ft °F] at high temperature {100 °C < T < 300 °C [212 °F < T < 572 °F]}.

Saturated thermal conductivity compares well with that of both Yucca Mountain zones encompassing the proposed repository horizon (Table 3-2). The dry thermal conductivity of the Apache Leap Research Site is 22 percent less than that of the Topopah Spring middle nonlithophysal zone and 10 percent less than that of the Topopah Spring lower lithophysal zone. In testing borehole core from the Tsw2 thermal-mechanical unit (Boreholes UE25 NRG-5 and USW NRG-6), Brodsky, et al. (1997) found the saturated thermal conductivity to be 2.29 J/s m K [1.32 Btu/h ft °F] at low temperature {<100 °C [<212 °F]}.

#### **3.2.1.9 Dry Rock Specific Heat**

The Apache Leap Research Site dry rock specific heat compares well with that of both Yucca Mountain zones encompassing the repository horizon (Table 3-2). The dry rock specific heat of the Topopah Spring middle nonlithophysal zone is 26 percent greater than that of the Apache Leap Research Site, and the dry rock specific heat of the Topopah Spring lower lithophysal zone is 22 percent greater than that of the Apache Leap Research Site. In testing borehole core from the Tsw2 thermal-mechanical unit (Borehole UE25 NRG-5), Brodsky, et al. (1997) found the arithmetic average of dry rock specific heat to vary as a function of temperature between  $1.79 \times 10^3$  and  $2.46 \times 10^3$  J/kg K [ $4.28 \times 10^{-1}$  and  $5.88 \times 10^{-1}$  Btu/lb °F].

#### **3.2.2 Comparison of Scales**

As mentioned in Section 3.1, data from Yucca Mountain come from a much larger volume of rock than the test volume at the Apache Leap Research Site. For example, boreholes used for hydraulic testing at Yucca Mountain are separated by kilometers, rather than the several meter separation typical of the Apache Leap Research Site. The entire Apache Leap Research Site test domain spans a surface area of approximately 55 × 35 m [180 × 115 ft] and a volume of rock on the order of 60,000 m<sup>3</sup> [2.1 million ft<sup>3</sup>], while the Rasmussen, et al. (1990) subdomain spans a surface area of approximately 35 × 20 m [115 × 66 ft] and a volume on the order of 20,000 m<sup>3</sup> [700,000 ft<sup>3</sup>]. In comparison, the repository block at Yucca Mountain is approximately 3 × 5 km [2 × 3 mi]. Fracture distributions at Yucca Mountain occur as swarms, both the cooling

joints on scales of approximately 100 m [300 ft] (Waiting, et al., 2001) and the tectonic fractures on scales related to the distribution of faults. The Apache Leap Research Site may not exhibit the same level of variability in fracture patterns observed at Yucca Mountain simply because the Apache Leap Research Site fracture network characterization was obtained from a small rock volume.

A comparison of Yucca Mountain and Apache Leap Research Site fracture air permeability measurement scales is provided in Table 3-4. Information on heterogeneity in the test volume at the Apache Leap Research Site is directly amenable for use with drift-scale models at Yucca Mountain; both the isothermal and the thermohydrologic numerical models use grids that contain cells on the order of meters. The site-scale unsaturated zone flow model (CRWMS M&O, 2000b), on the other hand, uses horizontal grid spacings greater than 100 m [330 ft]. This limits the utility of the Apache Leap Research Site data to use in upscaling exercises for estimation of equivalent fracture permeability for the site-scale model.

### 3.2.3 Parameter Correlations

From Yucca Mountain data, Flint (1998) found strong correlations between matrix porosity and degree of fracturing, matrix permeability and matrix porosity, matrix water saturation and matrix permeability, and matrix van Genuchten alpha and matrix permeability.

The matrix porosity of volcanic tuff is inversely related to the degree of welding exhibited by the rock (Table 3-2), while the degree of welding is directly related to the degree of fracturing (Table 3-1).

For the hydrogeologic units encompassing the proposed repository, matrix permeability is directly related to matrix porosity (Table 3-2). Flint (1998) arrived at the following regression equation for the prediction of saturated hydraulic conductivity ( $K_s$ ) as a function of porosity ( $\phi$ ):

$$\text{LOG}_{10}(K_s) = -14.2 + 69.0(\phi) - 63.3(\phi)^{1.3} \quad (3-2)$$

Eq. (3-2) is applicable to the Topopah Spring middle nonlithophysal and lower lithophysal zones, which have undergone minimal diagenetic alteration via mineral precipitation and formation of clays, and which are without significant microfractures.

Matrix permeability is inversely related to matrix water saturation (Table 3-2). For rocks with nonnegligible clay contents, significant amounts of water are sequestered within the clay network, reducing the effective permeability of the rock. Conversely, when pores are large and unobstructed, drainage is unhindered (high permeability) and the associated saturations are low.

For the hydrogeologic units encompassing the proposed repository, the matrix van Genuchten alpha is directly related to matrix porosity (Table 3-2). Flint (1998) arrived at the following regression equation for the prediction of the van Genuchten alpha ( $\alpha$ ) as a function of matrix porosity ( $\phi$ ):

$$\text{LOG}_{10}(\alpha) = -2.0 + 28.6(\phi) - 28.6(\phi)^{1.3} \quad (3-3)$$

Table 3-4. Comparison of Fracture Air Permeability, Variance, and Measurement Scales					
			Measurement Scale	Fracture Permeability, $k_a$	Variance
Apache Leap Research Site	Single-Hole Data	Rasmussen, et al. (1990)*	3.0 m [10.0 ft]	$7.94 \times 10^{-16} \text{ m}^2$ [ $8.05 \times 10^{-4} \text{ D}$ ]	0.9 for $\text{LOG}_{10}(k_a)$
		Guzman, et al. (1996) <sup>†</sup>	0.5–3.0 m [1.6–10.0 ft]	$7.33 \times 10^{-16} \text{ m}^2$ [ $7.42 \times 10^{-4}$ ]	3.71 for $\text{LN}(k_a)$
	Cross-Hole Data	Illman and Neuman (2001) <sup>‡</sup>	30 m [100 ft]	$3.16 \times 10^{-14} \text{ m}^2$ [ $3.20 \times 10^{-2} \text{ D}$ ]	0.36 for $\text{LOG}_{10}(k_a)$
Yucca Mountain PTn <sup>§</sup>	ESF <sup>¶</sup> Single-Hole Data	Alcove 4 <sup>¶</sup>	0.3 m [1.0 ft]	$1.00 \times 10^{-13} \text{ m}^2$ [0.10 D]	0.86 for $\text{LOG}_{10}(k_a)$
Yucca Mountain Tptpmn <sup>¶</sup> (tsw34)	ESF Single-Hole Data	Alcove 6 <sup>¶</sup>	0.3 m [1.0 ft]	$1.26 \times 10^{-12} \text{ m}^2$ [1.28 D]	0.45 for $\text{LOG}_{10}(k_a)$
		Niche 35+66 <sup>¶</sup>	0.3 m [1.0 ft]	$1.00 \times 10^{-13} \text{ m}^2$ [0.10 D]	0.86 for $\text{LOG}_{10}(k_a)$
		Niche 36+50 <sup>¶</sup>	0.3 m [1.0 ft]	$3.98 \times 10^{-14} \text{ m}^2$ [ $4.03 \times 10^{-2} \text{ D}$ ]	0.66 for $\text{LOG}_{10}(k_a)$
		Niche 31+07 <sup>¶</sup>	0.3 m [1.0 ft]	$3.98 \times 10^{-14} \text{ m}^2$ [ $4.03 \times 10^{-2} \text{ D}$ ]	0.49 for $\text{LOG}_{10}(k_a)$
		Niche 47+88 <sup>¶</sup>	0.3 m [1.0 ft]	$1.00 \times 10^{-13} \text{ m}^2$ [0.10 D]	0.72 for $\text{LOG}_{10}(k_a)$
	ESF Cross-Hole Data	Single Heater Test, <sup>**</sup> Drift Scale Test <sup>††</sup>	» 4.0–12.0 m [» 13.0–39.0 ft]	$(0.5, 2.32) \times 10^{-13} \text{ m}^2$ [(5, 23) $\times 10^{-2} \text{ D}$ ]	0.9, 2.0 for $\text{LOG}_{10}(k_a)$
Deep Borehole Single-Hole Data and ESF Cross-Hole Data Combined	NRG-6, NRG-7a, SD-12, UZ#16, Single Heater Test, Drift Scale Test <sup>††</sup>	3.5–4.9 m [11.5–16 ft] » 4.0–12.0 m [» 13.0–39.0 ft]	$(1.6 \text{ and } 3.4) \times 10^{-13} \text{ m}^2$ [0.16 and 0.32 D] (two weighted averages)	0.3 for $\text{LOG}_{10}(k_a)$	

\*Rasmussen, T.C., D.D. Evans, P.J. Sheets, and J.H. Blanford. NUREG/CR-5596, "Unsaturated Fractured Rock Characterization Methods and Data Sets at the Apache Leap Tuff Site." Washington, DC: NRC. August 1990.

<sup>†</sup>Guzman, A.G., A.M. Geddis, M.J. Henrich, C.F. Lohrstorfer, and S.P. Neuman. NUREG/CR-6360, "Summary of Air Permeability Data From Single-Hole Injection Tests in Unsaturated Fractured Tuffs at the Apache Leap Research Site: Results of Steady-State Test Interpretation." Washington, DC: NRC. March 1996.

<sup>‡</sup>Illman, W.A. and S.P. Neuman. "Type-Curve Interpretation of a Cross-Hole Pneumatic Injection Test in Unsaturated Fractured Tuff." *Water Resources Research*. Vol. 37, No. 3. pp. 583–603. 2001.

<sup>§</sup>Paintbrush Nonwelded Tuff

<sup>¶</sup>Exploratory Studies Facility

<sup>¶</sup>CRWMS M&O. "In Situ Field Testing of Processes." ANL-NBS-HS-000005. Rev. 00. Las Vegas, Nevada: TRW Environmental Safety Systems, Inc. 2000a.

<sup>¶</sup>Topopah Spring middle nonlithophysal zone

<sup>\*\*</sup>Tsang, Y.W., K. Huang, and G.S. Bodvarsson. "Estimation of the Heterogeneity of Fracture Permeability by Simultaneous Modeling of Multiple Air-Injection Tests in Partially Saturated Fractured Tuff." *Dynamics of Fluids in Fractured Rocks*. B. Faybishenko, P.A. Witherspoon, and S.M. Benson, eds. *Geophysical Monograph 122*. Washington, DC: American Geophysical Union. 2001.

<sup>††</sup>Huang, K., Y.W. Tsang, and G.S. Bodvarsson. "Simultaneous Inversion of Air-Injection Tests in Fractured Unsaturated Tuff at Yucca Mountain." *Water Resources Research*. Vol. 35, No. 8. pp. 2,375–2,386. 1999.

<sup>††</sup>CRWMS M&O. "Analysis of Hydrologic Properties Data." ANL-NBS-HS-000002. Rev. 00. Las Vegas, Nevada: TRW Environmental Safety Systems, Inc. 2000b.

Just as before, Eq. (3-3) is applicable to the Topopah Spring middle nonlithophysal and lower lithophysal zones. Inspection of the model calibrated results reported in Tables 3-1 and 3-2 supports the generalized relationships between the parameters discussed in this section. Additionally, it appears that dry rock specific heat is inversely related to matrix porosity. Statistical analysis of variables from the Apache Leap Research Site revealed a strong correlation between the  $\text{LOG}_{10}$ -transformed field estimates of air and water permeability values (0.87). The strong correlation implies that air injection experiments conducted in the unsaturated zone can be performed to estimate the value of permeability of the fractured rock to water, at least at the Apache Leap Research Site. Similar assessments are being made at Yucca Mountain in both the middle nonlithophysal and the lower lithophysal zones of the Topopah Spring Tuff. Preliminary results indicate that there may be differences between air and liquid permeability test results from the lower lithophysal zone.

The correlation between fracture geometry parameters and permeability is very slight. Some correlation between those variables is expected, because the permeability values can be highly sensitive to the number and size of fractures present in the measurement interval. The slight correlation suggests, however, that the number of fractures in a particular interval provides an insufficient indication of the permeability magnitude for that interval.

Although fracture frequency should conceptually be correlated with fracture permeability, other physical characteristics such as fracture connectivity and fracture aperture are not included in the fracture characterization data, yet, these characteristics are also important contributors to the magnitude of fracture permeability. Methods for estimating permeability in classic porous media have included descriptions of the pore space. The most common descriptors of pore space in granular porous media rely on an indirect approach where determination of the grain size distribution of the media is used as an analog for the pore space size distribution. In fractured porous media, no such approach has been developed for describing fracture pore size distribution. Although fracture connectivity and fracture aperture data are difficult to obtain, conceptually, these data, in combination with fracture frequency data, would lead to better estimates of permeability.

### **3.3 Summary**

Yucca Mountain, Nevada, was described, including its climate and topography, which are similar to that of the Apache Leap Research Site. Although there was no explicit reason to believe that parameter heterogeneity at the Apache Leap Research Site was exactly the same as that at Yucca Mountain, the Apache Leap Research Site data should prove useful, given that geospatial analyses of Yucca Mountain data have not been performed to date. Tests and methods of hydrological and thermal property data collection used at Yucca Mountain by the DOE were explored, and much of the available data were presented for comparison with that collected from the Apache Leap Research Site. Data from Yucca Mountain were more extensive and came from a much larger volume of rock than did the data from the test volume at the Apache Leap Research Site. There is no single locale at Yucca Mountain where all pertinent thermohydrologic parameters were estimated. Different types of tests were performed in different areas, and the support volumes of similar types of tests differed between the two sites. Issues of scale and parameter correlations were examined. For the estimates reported in this chapter, parameter values were assembled from different locales at Yucca Mountain, particularly within the proposed repository horizon and the nonwelded Paintbrush Tuff. The Apache Leap

Research Site is a reasonable analog site for Yucca Mountain given the similarities between the two sites and the completeness of the available data, even though the tuffs of the Apache Leap appear to be less welded than those of the repository horizon and more welded than the nonwelded Paintbrush Tuff. Given the issue of scale, information on heterogeneity at the Apache Leap Research Site is particularly amenable for direct use with drift-scale models of Yucca Mountain.

## 4 GEOSPATIAL ANALYSIS OF APACHE LEAP RESEARCH SITE DATA

### 4.1 Experimental Variograms

An experimental variogram is a measure of spatial correlation between data points. Experimental variograms were calculated for all variables using default values in ISATIS. Several lag intervals were selected arbitrarily for plotting experimental variograms to obtain the maximum detail at small distances without being misled by structural artifacts due to the particular class interval used. In most cases, the omni-directional variogram was calculated for 10 lags of the default value.

Directional variograms were also calculated to examine the directionality in correlation lengths of several variables. In general, all directional variograms calculated in directions parallel to the reference direction appeared to share similar characteristics with the omni-directional variograms. While one could use fracture orientation data to develop anisotropic variogram models, this has not been done to date. In the anisotropic case, the separation between two points is characterized not only by distance, but also by orientation; thus, anisotropic models require more parameters than corresponding isotropic models. Good fits were not always achieved during these preliminary efforts, which used simple omni-directional variograms, and future work may involve the development of anisotropic models.

The precise definition of principal directions of statistical anisotropy in correlation lengths appears to be very difficult, especially when analyzing data in three -dimensions. For example, Tsang, et al. (1996) indicate that directional variograms were not calculated for their data set, which consisted of packer injection data (similar to the Apache Leap Research Site data set), because of the clustering nature of their data {close spacings of 3-m [10-ft] consecutive sections within each borehole, yet wide spacings on the order of 100 m [98 ft] between boreholes}. They further comment that no attempt was made to determine the anisotropy, if any, of the correlation structure.

### 4.2 Model Fitting

Model fitting of experimental variograms was accomplished using a suite of empirical models available in ISATIS. Models were selected by visually comparing the experimental variogram to the empirical model. The automatic sill-fitting option of ISATIS was employed once a suitable model was found for a given experimental variogram. Journel and Huijbregts (1978) note that the calculated experimental variogram should only be considered for small distances  $\{L/2$ , where  $L$  equals the sample transect length, or approximately 30 m [100 ft] in this case} in relation to the dimension of the field on which it has been computed. Application of this rule to the experimental variograms computed herein gives a lag of up to 15 m [49 ft].

A fitted experimental variogram of field-estimated  $\text{LOG}_{10}$ -transformed air permeability is shown in Figure 4-1. The lag is set to the default value of 1.12 m [3.67 ft] calculated by ISATIS. The number of pairs employed for the variogram computation is also shown in the figure. A power model with a scale of 0.60 m [1.98 ft] and an exponent of 0.45 m [1.48 ft] is fit using the automatic sill-fitting option of ISATIS. Default values of the scale parameter were used to fit all models to the experimental variogram. (Table 4-1 summarizes all of the model fits described in this section.) The principle of the automatic sill-fitting procedure is to minimize the distance

Table 4-1. Summary of Variogram Parameters					
Variable	Model	Lag	Scale	Exponent	Sill
Field LOG <sub>10</sub> Air Permeability	Power	1.12 m [3.67 ft]	0.61 m [2.00 ft]	0.45	NA
Field LOG <sub>10</sub> Air Permeability	Power	2.00 m [6.56 ft]	0.61 m [2.00 ft]	0.45	NA
Field LOG <sub>10</sub> Air Permeability	Power	3.00 m [9.84 ft]	0.61 m [2.00 ft]	0.45	NA
Field LOG <sub>10</sub> Air Permeability	Power	4.00 m [13.12 ft]	0.61 m [2.00 ft]	0.45	NA
Field LOG <sub>10</sub> Air Permeability	Power	5.00 m [16.40 ft]	0.61 m [2.00 ft]	0.45	NA
Field LOG <sub>10</sub> Water Permeability	Power	5.00 m [16.40 ft]	6.00 m [19.69 ft]	0.60	NA
Lab LOG <sub>10</sub> Air Permeability	Exponential	3.00 m [9.84 ft]	4.48 m [14.70 ft]	NA	0.28
Laboratory LOG <sub>10</sub> Water Permeability	Exponential	3.00 m [9.84 ft]	1.48 m [4.86 ft]	NA	0.32
Fracture Counts/m	Exponential	3.00 m [9.84 ft]	7.50 m [24.61 ft]	NA	0.72
LOG <sub>10</sub> Porosity	Exponential	3.00 m [9.84 ft]	6.48 m [21.26 ft]	NA	0.003
LOG <sub>10</sub> van Genuchten $\alpha$	Exponential	3.00 m [9.84 ft]	4.48 m [14.70 ft]	NA	0.02
LOG <sub>10</sub> Klinkenberg Coefficient	Exponential	3.00 m [9.84 ft]	9.50 m [31.17 ft]	NA	0.11
Water Content	Exponential	3.00 m [9.84 ft]	27.48 [90.16 ft]	NA	3.30
Dry Thermal Conductivity	Exponential	3.00 m [9.84 ft]	5.50 [18.04 ft]	NA	0.02
Saturated Thermal Conductivity	Exponential	3.00 m [9.84 ft]	6.50 m [21.33 ft]	NA	0.04
Dry Rock Specific Heat	Exponential	3.00 m [9.84 ft]	6.00 m [19.69 ft]	NA	26,975.62

between the experimental value of the variogram lag and the corresponding value of the model (Geostatistics, 1997). Periodic behavior, also known as the hole effect, is observed in the computed experimental variogram at this lag interval. While some occurrences of the hole effect may indicate noise in the variogram, true periodicity is indicative of the presence of correlation at multiple scales, which in turn implies strong heterogeneity in the permeability distribution. In the fractured tuff environment of the Apache Leap Research Site, cyclic variations in associated variograms may be likely if there are discrete bands of fractures (i.e., discrete fracture zones separated by matrix). However, if the first two data points of Figure 4-1 are neglected due to an insufficient number of pairs (i.e., less than 30), true periodicity may be difficult to ascertain.

Fitted experimental variograms of field-based  $\text{LOG}_{10}$ -transformed air permeabilities with lags of 2.0, 3.0, 4.0, and 5.0 m [6.6, 9.9, 13.1, and 16.4 ft] are shown in Figures 4-2 through 4-5. The dashed line indicates the value of variance computed using ISATIS. It is evident from these variograms that a finite correlation length does not appear to exist. Stationary stochastic processes are characterized by means and moments that are spatially independent, whereas nonstationary stochastic processes are characterized by means and moments that are spatially dependent. Data which can be described through a power-law variogram, such as those illustrated in Figures 4-1 through 4-5, are nonstationary in a probabilistic sense and form a random fractal field of the fractional Brownian motion type. While the stochastic process itself is nonstationary, the increments of the process are stationary (e.g., fractional Gaussian noise) and, thus, lend themselves to a more useful analysis. A finite variance and correlation scale do not exist for nonstationary data; a power-law model describes a self-similar stochastic process, the realizations of which appear the same at any scale (Kitanidis, 1997).

Nonstationarity can be observed in sample variograms when the growth rate of the variogram is larger than quadratic. In this case, the intrinsic hypothesis is met but strong stationarity conditions are not met. Nonstationarity and anisotropy are sometimes difficult to distinguish (the rationale for using a power-law model is that a sill does not appear to exist for the experimental variogram, yet the growth rate is less than quadratic).

In some of the experimental variograms, the growth rate appeared to approach a quadratic rate, thus a nonergodic, omni-relative variogram model was computed and compared to the experimental variogram. According to Myers (1991), the algorithm locally estimates drift at each sample location, computes a residual, and then computes an estimate of the variogram. Comparison of the experimental and nonergodic variogram model revealed little difference, thus it is concluded that there is no measurable drift in the  $\text{LOG}_{10}$ -transformed air permeability data set.

A preliminary fitted experimental variogram of field-based  $\text{LOG}_{10}$ -transformed liquid permeability with lag of 6.0 m [20 ft] is shown in Figure 4-6. A power-law model is fitted with emphasis on smaller lag values. Removal of the larger lag values (i.e., lags greater than 15.0 m [50 ft]) should result in considerable improvement to the model fit.

Preliminary omni-directional variograms for laboratory estimates of  $\text{LOG}_{10}$ -transformed air (Figure 4-7) and liquid (Figure 4-8) permeability are also computed with different lag values. Here we show variograms with lag values of 3.0 m [10 ft]. A very large nugget value is seen in Figure 4-7, and a pure nugget effect is evident in Figure 4-8. The nugget effect is used to

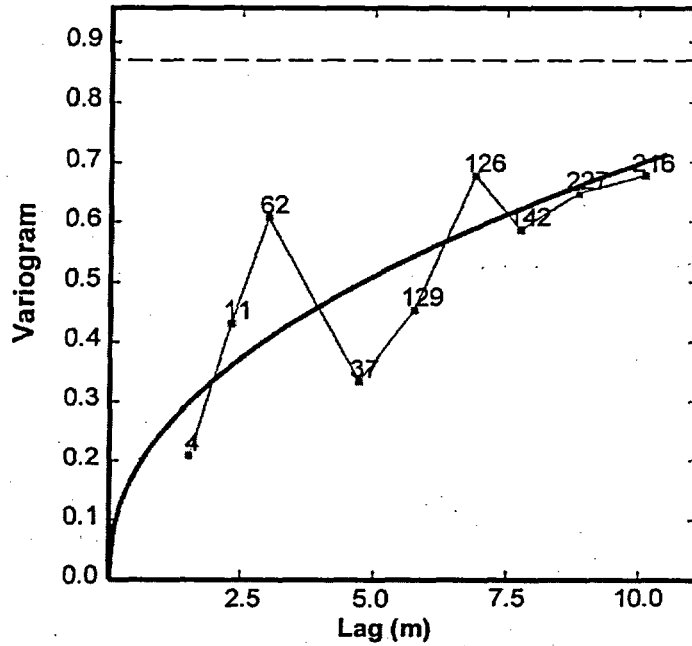


Figure 4-1. Fitted Experimental Variogram for Field Estimates of  $\text{LOG}_{10}$  Air Permeability with Lag of 1.12 m [1.0 m = 3.28 ft]. The Number of Pairs Employed for the Variogram Computation Are Shown.

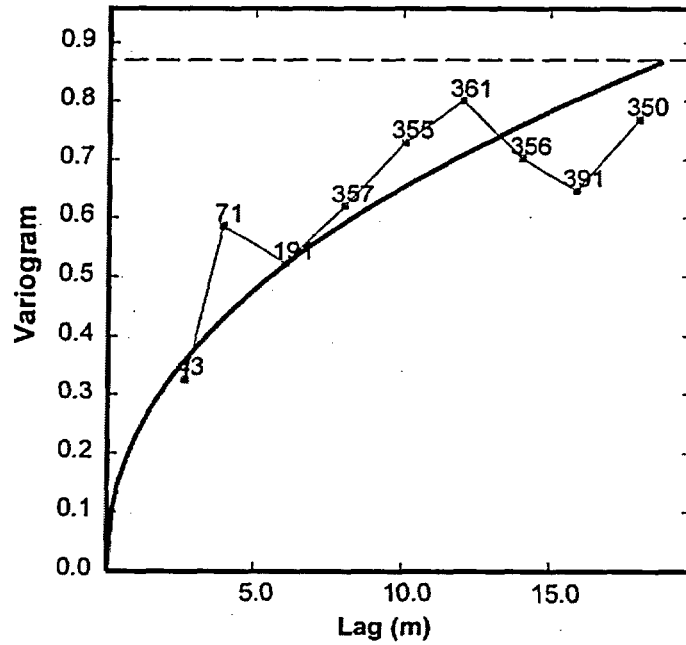


Figure 4-2. Fitted Experimental Variogram for Field Estimates of  $\text{LOG}_{10}$  Air Permeability with Lag of 2.0 m [1.0 m = 3.28 ft]. The Number of Pairs Employed for the Variogram Computation Are Shown.

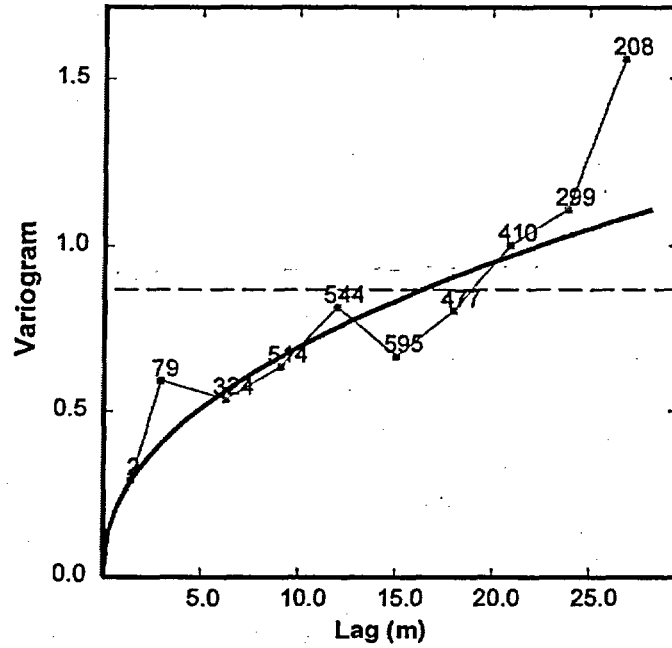


Figure 4-3. Fitted Experimental Variogram for Field Estimates of  $\text{LOG}_{10}$  Air Permeability with Lag of 3.0 m [1.0 m = 3.28 ft]. The Number of Pairs Employed for the Variogram Computation Are Shown.

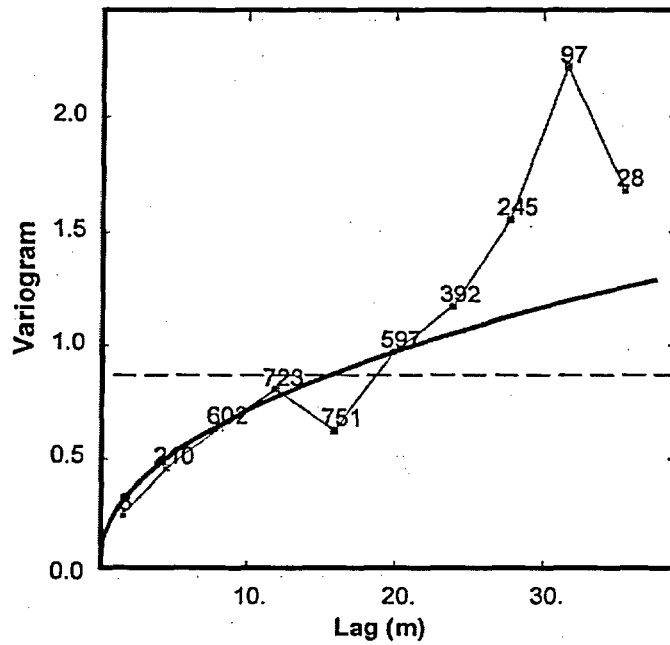


Figure 4-4. Fitted Experimental Variogram for Field Estimates of  $\text{LOG}_{10}$  Air Permeability with Lag of 4.0 m [1.0 m = 3.28 ft]. The Number of Pairs Employed for the Variogram Computation Are Shown.

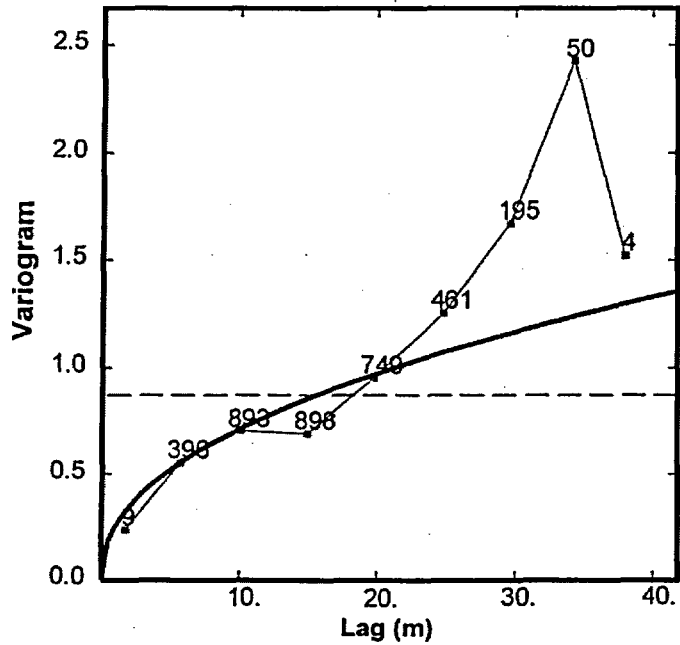


Figure 4-5. Fitted Experimental Variogram for Field Estimates of  $\text{LOG}_{10}$  Air Permeability with Lag of 5.0 m [1.0 m = 3.28 ft]. The Number of Pairs Employed for the Variogram Computation Are Shown.

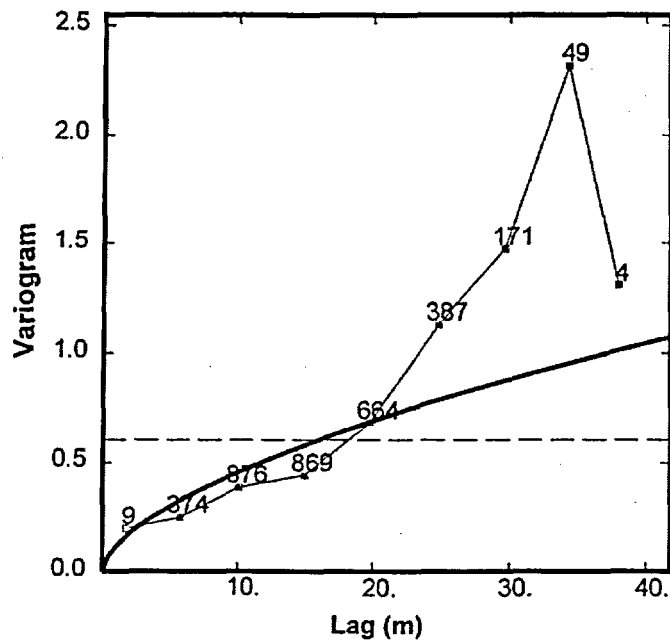


Figure 4-6. Fitted Experimental Variogram for Field Estimates of  $\text{LOG}_{10}$  Liquid Permeability with Lag of 6.0 m [1.0 m = 3.28 ft]. The Number of Pairs Employed for the Variogram Computation Are Shown.

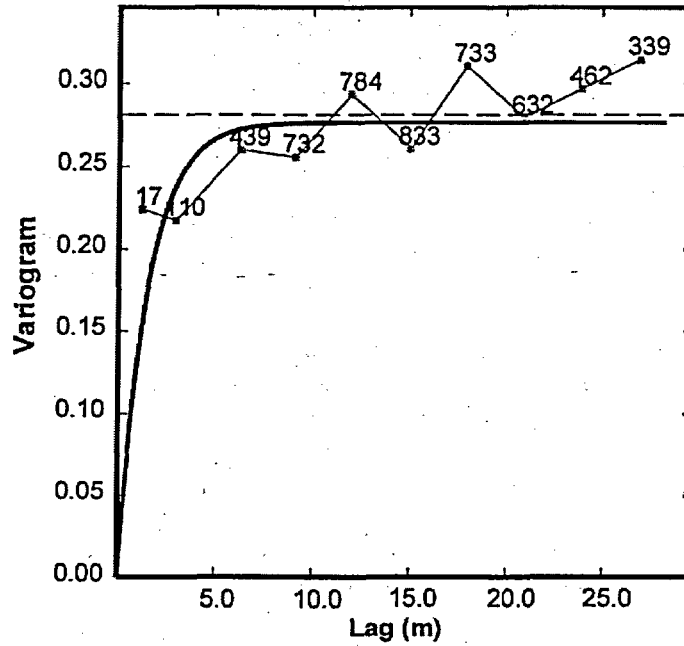


Figure 4-7. Fitted Experimental Variogram for Laboratory Estimates of  $\text{LOG}_{10}$  Air Permeability with Lag of 3.0 m [1.0 m = 3.28 ft]. The Number of Pairs Employed for the Variogram Computation Are Shown.

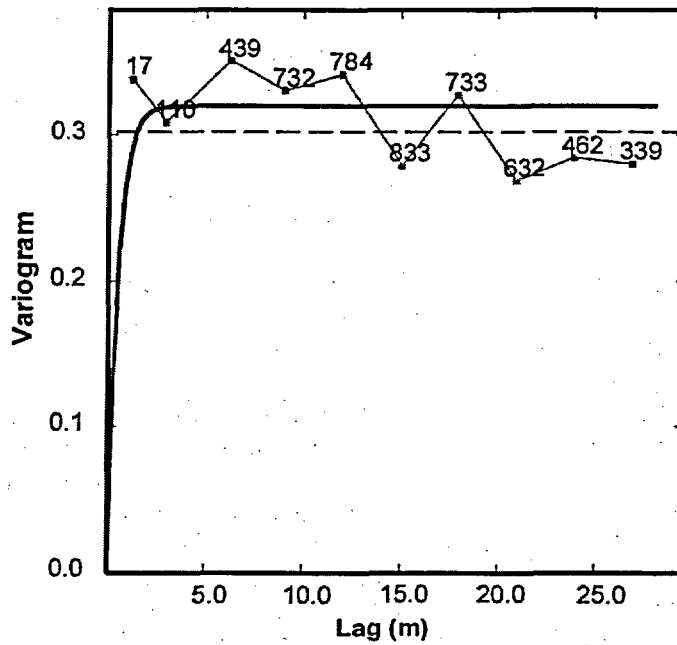


Figure 4-8. Fitted Experimental Variogram for Laboratory Estimates of  $\text{LOG}_{10}$  Liquid Permeability with Lag of 3.0 m [1.0 m = 3.28 ft]. The Number of Pairs Employed for the Variogram Computation Are Shown.

characterize the residual influence of all variabilities that have ranges much smaller than the available distances of observations (Journel and Huijbregts, 1978). The pure nugget effect suggests a total absence of spatial correlation, and in practice it is very rare; it suggests undersampling and variability at a scale shorter than the sampling interval {note that the sampling interval for these laboratory data was approximately 3.0 m [10 ft]; standard practice in the petroleum industry is to sample matrix permeability in the lab at 0.30-m [1-ft] intervals, but even this frequency commonly fails to identify the presence of thin high- or low-permeability zones}. A precursory exponential model without nugget is fitted to both experimental variograms.

Preliminary omni-directional variograms for fracture density (Figure 4-9) and porosity (Figure 4-10) were also calculated and fitted using a similar procedure. A precursory exponential model is fitted to both experimental variograms. Examination indicates that the first data point of each variogram should be neglected due to an insufficient number of pairs (i.e., less than 30); thus, the next step would be to include a nugget in both model fits. Here, the variogram tends to increase at a relatively low rate with numerous pairs for short lag distances but oscillates in a haphazard manner at larger values of lag. Removal of lag values larger than 15.0 m [50 ft] should result in considerable improvement to the model fit.

Preliminary omni-directional variograms for the van Genuchten alpha (Figure 4-11) and matrix Klinkenberg coefficients (Figure 4-12) were also calculated and fitted using a similar procedure. An exponential model is fitted to both experimental variograms. In both cases, the nugget component is relatively large. Again, the first data point of each variogram should be neglected due to an insufficient number of pairs, and removal of lag values larger than 15.0 m [50 ft] should result in considerable improvement to the model fit.

The omni-directional variogram of water content (Figure 4-13) computed with a 3.0-m [10-ft] lag is found to fit well with the exponential model, but the first data point of the variogram should be neglected.

Preliminary omni-directional variograms of dry thermal conductivity (Figure 4-14), saturated thermal conductivity (Figure 4-15), and dry rock specific heat (Figure 4-16) all exhibit a small nugget effect and are oscillatory at larger lag values. While neglecting the nugget, the exponential model fits the variograms quite well at a lag value of 3.0 m [10 ft]. Again, the first data point of each variogram should be neglected due to an insufficient number of pairs and removal of lag values larger than 15.0 m [50 ft] is warranted.

There is a dichotomy of approaches for experimental variogram model fitting. In cases where the structure of the variogram appears to be clear and there is prior information about the distribution of the random variable, model fitting should probably emphasize capturing much of the structure. In cases where the structure of the variogram is unclear or there is little information about the random variable, the preference should be to use the simplest model with the fewest number of parameters. Considering the oscillatory and intricate nature of these experimental variograms, the model-fitting strategy was to pick simple models that fit through the middle of the oscillation, weighting the model-fit towards points with large numbers of pairs. Fitting was done visually, by trying different models and employing the automatic sill-fitting option given in ISATIS after a model was selected. In general, the variogram model is more important for shorter lags because the kriging estimator has the property that it assigns larger weights to data at points close to the location where the variable is estimated and lesser

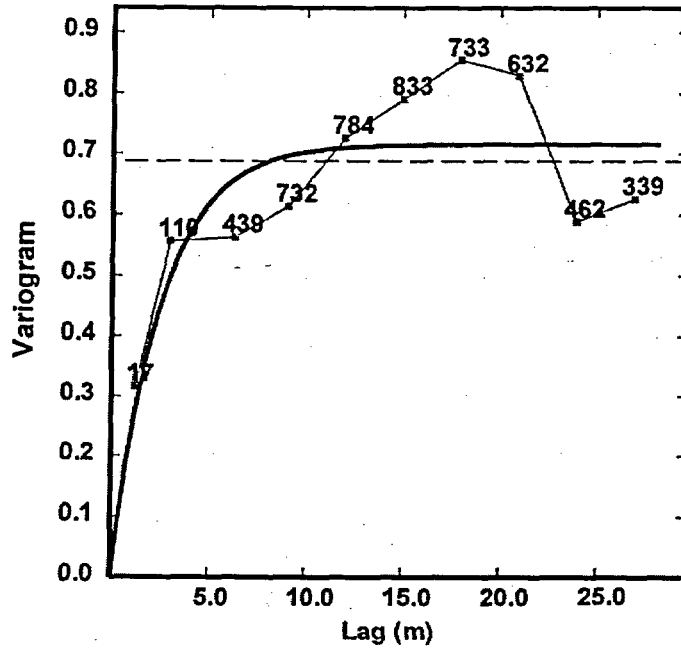


Figure 4-9. Fitted Experimental Variogram of Fracture Density with Lag of 3.0 m [1.0 m = 3.28 ft]. The Number of Pairs Employed for the Variogram Computation Are Shown.

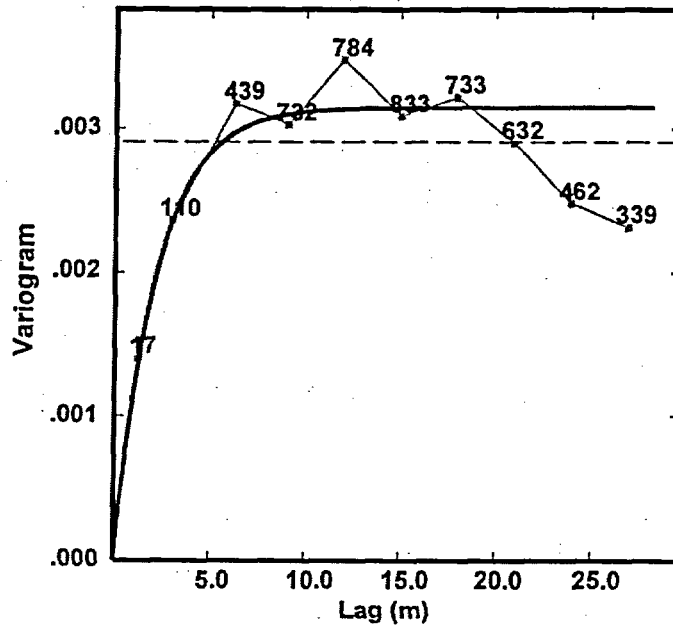


Figure 4-10. Fitted Experimental Variogram of  $\text{LOG}_{10}$  Porosity with Lag of 3.0 m [1.0 m = 3.28 ft]. The Number of Pairs Employed for the Variogram Computation Are Shown.

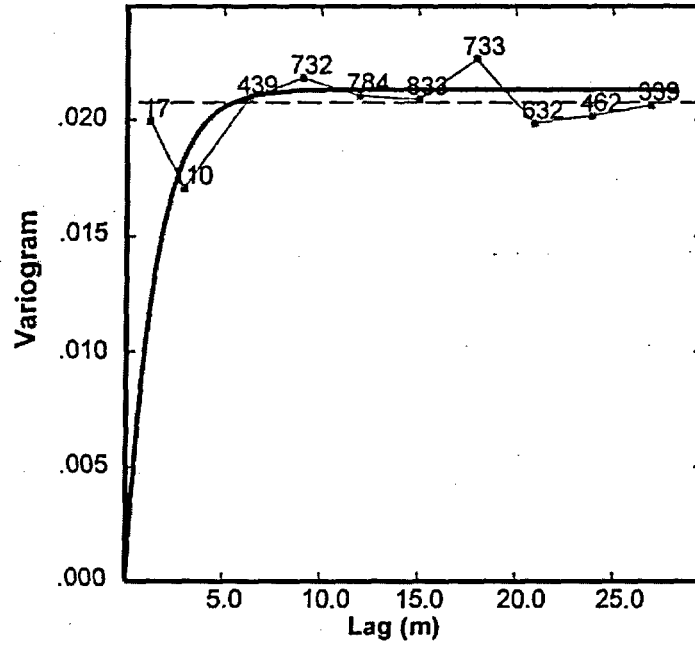


Figure 4-11. Fitted Experimental Variogram of  $\text{LOG}_{10}$  van Genuchten  $\alpha$  Coefficient with Lag of 3.0 m [1.0 m = 3.28 ft]. The Number of Pairs Employed for the Variogram Computation Are Shown.

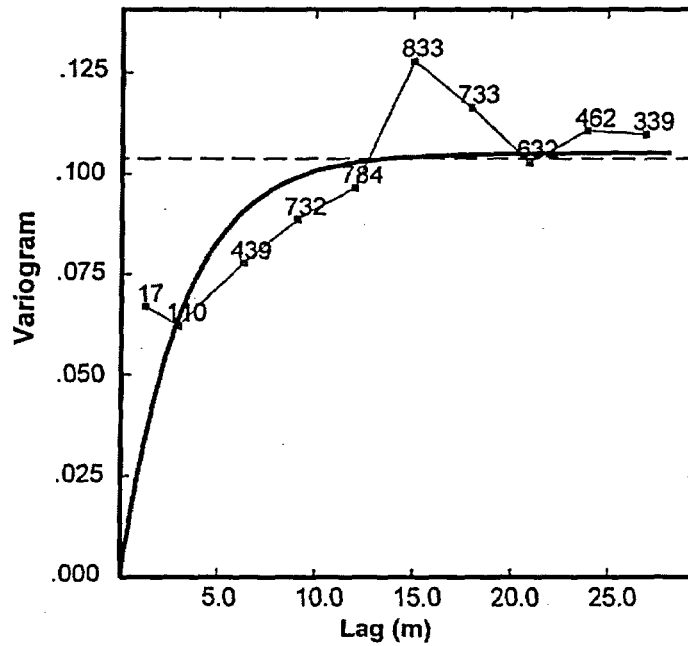


Figure 4-12. Fitted Experimental Variogram of  $\text{LOG}_{10}$  Klinkenberg Coefficient with Lag of 3.0 m [1.0 m = 3.28 ft]. The Number of Pairs Employed for the Variogram Computation Are Shown.

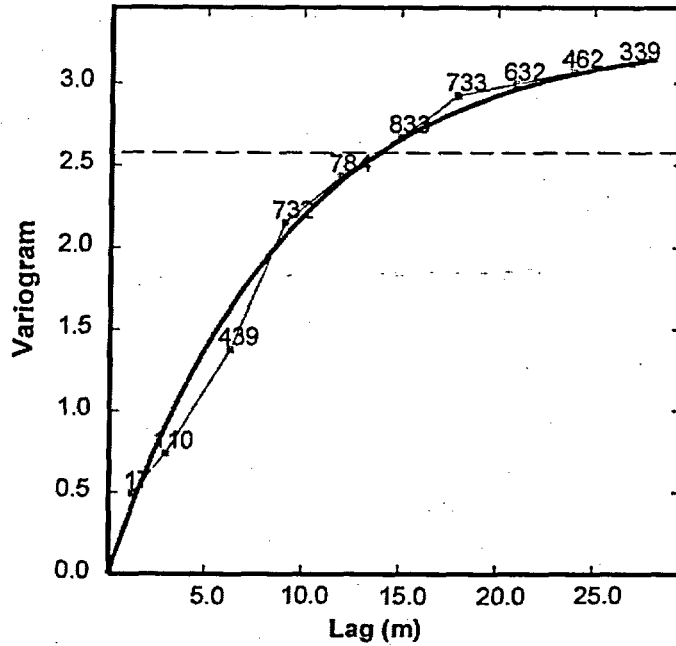


Figure 4-13. Fitted Experimental Variogram of Water Content with Lag of 3.0 m [1.0 m = 3.28 ft]. The Number of Pairs Employed for the Variogram Computation Are Shown.

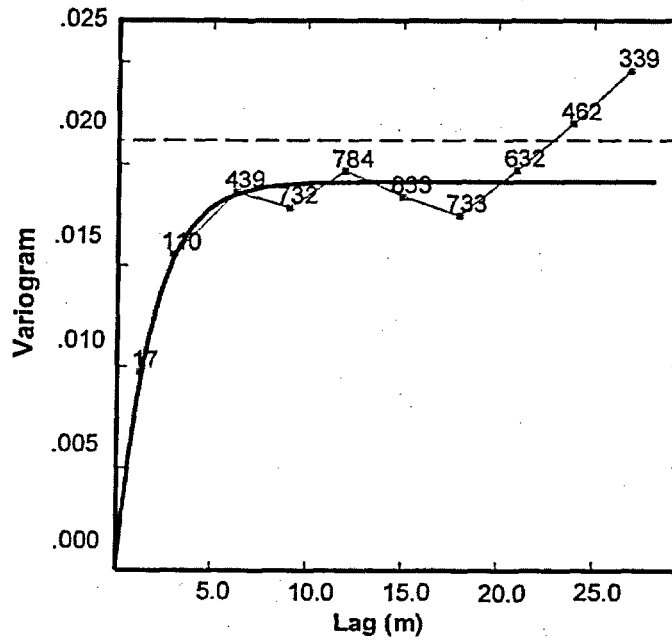


Figure 4-14. Fitted Experimental Variogram of Dry Thermal Conductivity with Lag of 3.0 m [1.0 m = 3.28 ft]. The Number of Pairs Employed for the Variogram Computation Are Shown.

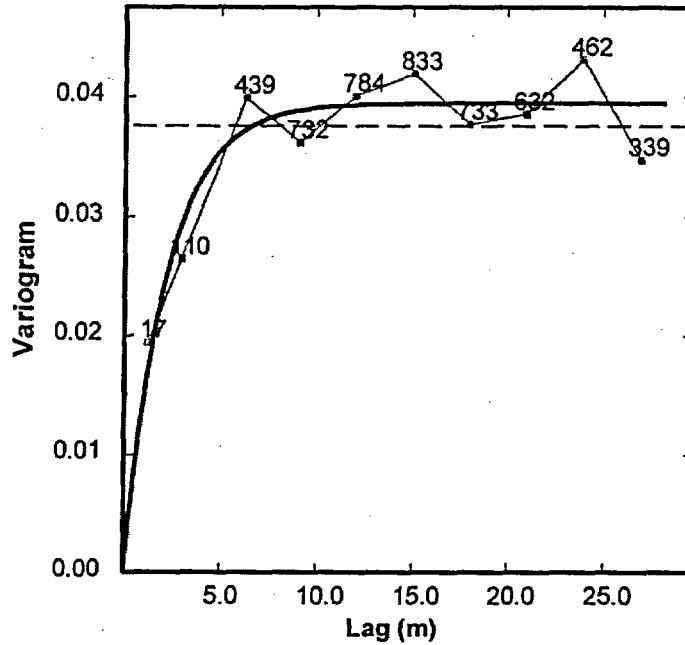


Figure 4-15. Fitted Experimental Variogram of Saturated Thermal Conductivity with Lag of 3.0 m [1.0 m = 3.28 ft]. The Number of Pairs Employed for the Variogram Computation Are Shown.

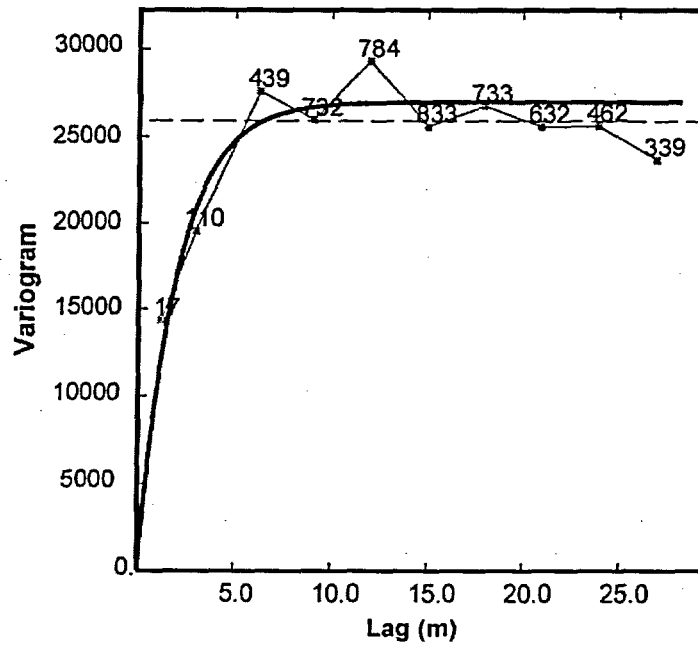


Figure 4-16. Fitted Experimental Variogram of Dry Rock Specific Heat with Lag of 3.0 m [1.0 m = 3.28 ft]. The Number of Pairs Employed for the Variogram Computation Are Shown.

weights to those farther away.<sup>1</sup> Consequently, emphasis was placed on fitting the model at shorter rather than longer lags. The degree to which the model fits the experimental variograms depends on the investigated variable, and there can be great variation in quality-of-fit. Some model ranking system may be useful to quantify the quality of the model fit.

### **4.3 Comparison with Other Apache Leap Research Site Geostatistical Analyses**

#### **4.3.1 Geostatistical Analysis of Bassett, et al. (1994, Chapter 4) and Rasmussen, et al. (1996, pp. 52–91)**

Bassett, et al. (1994, Chapter 4) and Rasmussen, et al. (1996, pp. 52–91) performed preliminary geostatistical analysis of their single-hole air permeability data. As permeability data had been collected at three scales {i.e., 0.5, 1.0, and 3.0 m [1.6, 3.3, and 10.0 ft]} within borehole Y2 at that time, they examined semivariograms of permeability at each measurement scale. With only nine data points available at the 3.0-m [10-ft] scale (Table 2-7), this semivariogram was poorly defined. However, the semivariograms for permeability at the 0.5- and 1.0-m [1.6- and 3.3-ft] scales reveal a nested structure. Bassett, et al. (1994, Chapter 4) attribute the lower sill to the matrix and discontinuous microfractures, and the upper sill to well-connected macrofractures, whereas Rasmussen, et al. (1996, pp. 52–91) provide the alternative explanation of possible heterogeneities at different scales originating in different depositional processes. A power-law semivariogram model may be fit to the data, capturing its fractal nature (Hurst coefficient,  $w \approx 0.285$ ), if not the specific nested multiscale structure (Rasmussen, et al., 1996, pp. 52–91).

#### **4.3.2 Geostatistical Analysis by Bassett, et al. (1997)**

Bassett, et al. (1997) utilized a model ranking system known as the Maximum Likelihood Cross Validation (Samper and Neuman, 1989a,b) in combination with four model identification criteria (Akaike, 1974, 1977; Hannan, 1980; Kashyap, 1982) to select the best conceptual geostatistical model of natural log-transformed air permeability, as determined by Guzman, et al. (1996), and of the water content and natural log-transformed porosity and van Genuchten alpha parameter, as determined by Rasmussen, et al. (1990). The ln-transformed field-estimated air permeability was found to be most accurately modeled as a random fractal by a power-law semivariogram, just as demonstrated in Section 4.2. Again, the power model represents a statistically nonhomogeneous field that, while it possesses neither a finite variance nor a finite spatial correlation scale, does possess statistically homogeneous spatial increments. Water content was determined to be well-represented by a more traditional spherical model with quadratic spatial drift, which treats the data as belonging to a statistically homogeneous random field. Both the ln-transformed porosity and the ln-transformed alpha parameter were found to be well-represented by exponential models without spatial drift. Bassett, et al. (1997) estimated spatial distributions of the above parameters through kriging. Recognizing that the kriging interpolation method smoothes the inherent natural variability of parameters like permeability, Chen, et al. (2000) utilized conditional simulations to superimpose random fluctuations on kriged distributions such that more realistic parameter distributions might be achieved.

---

<sup>1</sup>Myers, D.E. "Introduction to Geostatistics—Math 577." Classroom notes (1995) to W.A. Illman, Department of Geoscience, University of Iowa. Tucson, Arizona: University of Arizona.

### 4.3.3 Geostatistical Analyses of Illman, et al. (1998) and Chen, et al. (2000)

High-resolution air permeability data collected by Guzman, et al. (1996), and geostatistically analyzed by Bassett, et al. (1997) originated from a total of six boreholes at the Apache Leap Research Site (X2, Y2, Y3, Z2, V2, and W2A), spanning a lateral area of 32 × 20 m [105 × 66 ft]. However, lower spatial resolution air permeability data collected by Rasmussen, et al. (1990) span a greater lateral area, because these data originated from all of the X-, Y-, and Z-series boreholes. Illman, et al. (1998) demonstrated that the air permeability data with 1.0-m [3.3-ft] sample support from Guzman, et al. (1996) could be justifiably combined with the lower spatial resolution 3.0-m [10.0-ft] sample support data from Rasmussen, et al. (1990) because the resulting omni-directional variograms are quite similar, especially at small separation distances or lags. Illman, et al. (1998) proceeded by kriging the combined set of 227 1.0-m [3.3-ft] and 3.0-m [10.0-ft] air permeability data jointly, using the power variogram model as determined by Bassett, et al. (1997) for the 1.0-m [3.3-ft] data. The combined set of LOG<sub>10</sub>-transformed permeability data is summarized in Table 4-2, as are the statistics of the kriged estimates. Note that while the arithmetic mean of the data and of the kriged estimates are the same, the variance and coefficient of variation are lower due to the smoothing effect of kriging.

Illman, et al. (1998) also illustrate an omni-directional sample and model variogram for uncorrected fracture frequency, as measured at the Apache Leap Research Site. They report that an exponential model without spatial drift provides an accurate representation of the variability of this parameter.

	Minimum LOG <sub>10</sub> (k, m <sup>2</sup> ) [D]	Maximum LOG <sub>10</sub> (k, m <sup>2</sup> ) [D]	Arithmetic Mean LOG <sub>10</sub> (k, m <sup>2</sup> ) [D]	Variance	Coefficient of Variation
Statistics of Combined Data Sets	-17.13 [7.5 × 10 <sup>-6</sup> ]	-11.62 [2.43 × 10 <sup>0</sup> ]	-15.22 [6.39 × 10 <sup>-4</sup> ]	8.7 × 10 <sup>-1</sup>	-6.1 × 10 <sup>-2</sup>
Kriged Distribution	—	—	-15.22 [6.39 × 10 <sup>-4</sup> ]	5.1 × 10 <sup>-1</sup>	-4.7 × 10 <sup>-2</sup>

\*Rasmussen, T.C., D.D. Evans, P.J. Sheets, and J.H. Blanford. NUREG/CR-5596, "Unsaturated Fractured Rock Characterization Methods and Data Sets at the Apache Leap Tuff Site." Washington, DC: NRC. August 1990.  
 †Guzman, A.G., A.M. Geddis, M.J. Henrich, C.F. Lohrstorfer, and S.P. Neuman. NUREG/CR-6360, "Summary of Air Permeability Data From Single-Hole Injection Tests in Unsaturated Fractured Tuffs at the Apache Leap Research Site: Results of Steady-State Test Interpretation." Washington, DC: NRC. March 1996.  
 ‡Illman, W.A., D.L. Thompson, V.V. Vesselinov, and S.P. Neuman. NUREG/CR-5559, "Single-Hole and Cross-Hole Pneumatic Tests in Unsaturated Fractured Tuffs at the Apache Leap Research Site: Phenomenology, Spatial Variability, Connectivity and Scale." Washington, DC: NRC. September 1998.

## 5 DISCUSSION

Presently, there are a number of ways to numerically represent flow and transport of fluids and contaminants through fractured rocks. Traditionally, fractures have been idealized as parallel plates (discrete fracture network model), but this idealization suffers from numerous shortcomings stemming from the variable nature of fracture apertures, fracture orientation, fracture frequency, and trace length. Fractures have been conceptualized as parallel, discrete features because the fluid flow properties of fractures are remarkably different from the surrounding matrix. In general, fractures tend to be highly permeable with very little fluid storage capacity, whereas the surrounding matrix tends to be very low in permeability, but has a much higher storage capacity. Neuman (1987) proposed an alternative to the classical continuum approach based on the Representative Elementary Volume concept and discrete fracture network model by employing the stochastic continuum concept. He postulated that hydraulic test data obtained from single-hole tests with short intervals are amenable to quantitative analysis by treating them as realizations of a stochastic (random) process defined over a continuum, despite the fact that the rock is fractured and therefore mechanically discontinuous. Clearly there are not enough fractures within a measurement volume to support a continuum assumption. The most general definition of stochastic continuum does not make a distinction between fractures and matrix, but instead idealizes a block of rock containing both fractures and matrix as a single continuum.

The dual-permeability and fracture-only models used at Yucca Mountain assume separate continua for the matrix and the fractures, though stochastic realizations of properties within each separate continua can be created. To apply the geostatistical data from the Apache Leap Research Site to Yucca Mountain, the assumption that air injection tests only measure characteristics of the fracture system must be made. As supported by conceptual arguments of water retention in matrix versus fractures, and by the data of Guzman, et al. (1996), air injection test results are thought to reflect the properties of the fracture network at the Apache Leap Research Site. In particular, numerical simulations by these authors (Bassett, et al., 1994, Chapter 4) show that, whereas the intrinsic permeability one determines from such tests is generally lower than the intrinsic permeability of fractures to water within the test interval, it nevertheless approaches the latter as the applied pressure increases. Capillary forces tend to draw water from fractures into the porous (matrix) blocks of rock between the fractures, thereby leaving the latter saturated primarily with air. Water saturation in the matrix blocks is therefore typically much higher than that within the fractures, making it relatively difficult for air to flow through such blocks. It follows that the air moves primarily through fractures (most of which contain relatively little water) during a pneumatic injection test, and the test therefore yields flow and transport parameters that are only slightly below the intrinsic properties of these predominantly air-filled fractures. By accepting the stochastic continuum hypothesis for the fracture network, a three-dimensional stochastic field of variable permeability (and other parameters described herein) can be generated using measurements of flow parameters.

Single-hole pneumatic and hydraulic injection tests conducted over short segments of a borehole and core data obtained near the centroids of the injection intervals provide information about a very small volume of rock in the immediate vicinity of each measurement interval. Available data from the Apache Leap Research Site indicate that rock properties, which are measured on such small scales, vary erratically in space in a manner which renders the rock

randomly heterogeneous. A major question is how to describe this spatial and directional dependence of porous medium properties in untested portions of the rock.

The analyses to date that are presented in this report and elsewhere (Bassett, et al., 1994, 1997; Guzman, et al., 1996; Chen, et al., 2000) suggest that it is possible to interpolate some of the measurements at the Apache Leap Research Site between boreholes by means of geostatistical methods that view the corresponding variables as correlated random fields. This is especially true for: (i) field estimates of air permeability, (ii) field estimates of liquid permeability, (iii) laboratory estimates of air permeability, (iv) laboratory estimates of liquid permeability, (v) fracture frequency, (vi) effective matrix porosity, (vii) matrix alpha-value of the van Genuchten moisture characteristic function, (viii) matrix Klinkenberg coefficient, (ix) water content, (x) dry thermal conductivity, (xi) saturated thermal conductivity, and (xiii) dry rock specific heat. For each of these variables, enough measurements are available to constitute a workable geostatistical sample.

The preliminary geostatistical analysis of data analyzed herein yielded statistical parameters and geostatistical model structure of unsaturated fractured tuffs that potentially may be considered analogous to those of the tuffs found at Yucca Mountain. Standard geostatistical analysis provides best (minimum variance) linear unbiased estimates of how each such quantity varies in three-dimensional space, including information about the quality of these estimates. The nugget effect observed in some of the experimental variograms suggests discontinuous behavior, which is commonly attributed to random measurement error or micro-variability in data that probably cannot be resolved with 3-m [10-ft] scale injection tests. Similar results were found by Tsang, et al. (1996) in their paper on indicator geostatistics using 3-m [10-ft] support scale packer-test data collected at the Stripa Mine site in Sweden. Therefore, to improve the geostatistical analysis, some data would need to be collected at a finer scale.

Such information can be used to construct a number of three-dimensional stochastic fields of permeability and other parameters for Yucca Mountain through the application of existing geostatistical simulation techniques such as those of Robin, et al. (1993), Gomez-Hernandez and Cassiraga (1994), and Painter (1996). The validity of stochastic fields generated by means of kriging and geostatistical simulation techniques cannot be assessed unless one conducts flow and transport experiments on a scale that encompasses the entire volume of the geological formation under controlled conditions.

Using an alternative approach for obtaining geostatistical information, Vesselinov, et al. (2001a,b) used a three-dimensional numerical inverse model to interpret several cross-hole pneumatic injection tests at the Apache Leap Research Site. Their model solves the airflow equations in their original nonlinear form, and accounts directly for the ability of all packed-off borehole intervals to store and conduct air through the system. The authors analyzed pneumatic cross-hole test data in two ways: (i) by considering pressure records from individual borehole monitoring intervals one at a time, while treating the rock as being spatially uniform, and (ii) by considering pressure records from multiple tests and borehole monitoring intervals simultaneously, while treating the rock as a random fractal characterized by a power variogram. The first approach yielded a series of equivalent  $\text{LOG}_{10}$ -transformed air permeabilities and  $\text{LOG}_{10}$ -transformed air-filled porosities for fractures that connect the corresponding monitoring and injection intervals, representing rock volumes with length-scales at least as large as the distances between these intervals (meters to tens of meters). The second approach yielded a high-resolution estimate of how air permeability and air-filled porosity vary spatially throughout

the tested rock volume, based on grid blocks having a length scale of 1.0 m [3.3 ft]. This approach amounts to three-dimensional pneumatic tomography (or stochastic imaging) of the rock, a concept originally proposed in the context of hydraulic cross-hole tests by Neuman (1987). The geostatistical inverse results have shown that values estimated from this type of cross-hole experiment were consistent with the estimated values using single-hole data collected on various scales {0.5-, 1.0-, 2.0-, and 3.0-m [1.6-, 3.3-, 6.6- and 9.9-ft]}. The principle behind this methodology is general and the inversion of cross-hole test data is a viable alternative method for assessing heterogeneity using pneumatic properties of welded, unsaturated fractured tuffs at Yucca Mountain at scales appropriate for seepage models or for intralayer heterogeneity of larger-scale models.

To obtain spatial information on hydraulic and pneumatic flow/transport parameters and continuity/connectivity of permeable pathways, extensive field studies of major lithological units at Yucca Mountain are being conducted by U.S. Department of Energy (DOE) researchers by means of hydraulic and pneumatic injection tests. The field tests include a large number of single- and cross-hole pneumatic injection and gaseous tracer tests under isothermal conditions, borehole infiltration tests, and pneumatic tests during the single-heater and the ongoing drift scale heating experiments. Determination of geostatistical model structure through the spatial analysis of air permeability estimates obtained from single- and cross-hole pneumatic injection tests can be an important component in understanding deep percolation processes.

Results of these field tests have shown considerable spatial variability in hydraulic and pneumatic properties of the unsaturated fractured tuffs. In particular, air permeabilities determined from air injection tests conducted in the Exploratory Studies Facility varied over at least five orders of magnitude within a single hydrostratigraphic unit (CRWMS M&O, 2000a). It appears that this full range of variability and uncertainty has not been accounted for in permeabilities, in other calibrated properties, and in model results computed using these calibrated properties. A thorough evaluation of uncertainty, including uncertainty in calibrated properties and thermohydrologic variables calculated from those properties, would greatly assist in obtaining a more credible total system performance assessment. Chapter 3 summarized and analyzed available data from Yucca Mountain, but it is clear that geospatial information is severely lacking.

In order to investigate the applicability of the dual continuum approach and the effect of simplifying fracture permeability distributions on deep percolation processes at Yucca Mountain, random field simulations of flow in unsaturated fractured rocks were previously conducted using the two-phase, nonisothermal flow simulator MULTIFLO (Illman and Hughson, 2001; Fedors, et al., 2002b). The fractured rock is idealized as a dual-continuum porous media in this simulator, in which the matrix and fracture constitute two distinct continua represented by two overlapping, interacting numerical grids. Darcy's law and the area of the matrix-fracture interface open to flow govern the exchange of fluids between the two continua. Grid blocks with dimensions of 1.0 m [3.3 ft] were used, which is commensurate with the support volume of fracture permeabilities estimated from single-hole pneumatic injection tests. The aforementioned researchers investigated the consequences of simplifying fracture permeability on unsaturated flow by comparing the model results using uniform formation properties to a stochastic model that represents spatial variability of the fracture permeability within the layers as a multivariate lognormal random field. With little data available to constrain geostatistical parameter values, a sensitivity-type approach was taken to assess the effect of intralayer heterogeneity on flow rates and distributions.

From the modeling (Illman and Hughson, 2001; Fedors, et al., 2002b), it was concluded that the variability in fracture permeability causes the development of preferential flow paths in the fracture continuum for the welded tuff units and in the matrix continuum for the nonwelded unit. This occurs despite the steady and spatially uniform application of water at the top boundary, and without explicitly built-in high permeability pathways or discrete features that represent fractures. It was also found that the magnitude of variance in fracture permeability correlates well with the degree of flow focusing. Water flow rates in preferential flow pathways were found to be locally very high (more than ten times the input flow rate), while they varied the input flow rate by a factor of three. Flow focusing due to the development of preferential pathways increases saturation locally. This local increase in saturation causes an increase in relative permeability to water along the pathway and may reduce the wetted surface area for fracture-matrix interaction. Comparison of results obtained from the homogeneous and heterogeneous model of unsaturated flow through thick vadose zones shows that deep percolation can take place rapidly through persistent preferential flow paths. These pathways are hard to detect and may carry large volumes of water.

Clearly, the simplification of site hydrogeology can lead to erroneous conclusions about fluid flow and solute transport through unsaturated fractured rocks. Therefore, in order to further investigate the consequences of model simplification on repository performance, it is suggested that complete geostatistical analyses of air injection test data and other available data from Yucca Mountain be undertaken. Accounting for variability in matrix permeabilities, fracture porosities, and other rock properties may affect performance assessment calculations. It is suggested that those variabilities be considered in future modeling studies. According to Hughson, et al. (2000), accounting for variability and heterogeneity within both welded and nonwelded units and transecting faults would undoubtedly increase the variability in computed thermohydrologic variables.

In summary, it is not clear what the effect of heterogeneity is on percolation, seepage, refluxing due to thermal pulse, transport of radionuclides, and overall performance of the proposed repository. Use of the Apache Leap Research Site data for fracture property heterogeneity will help assess the need for the DOE to adequately incorporate spatial variability in key parameters on deep percolation, coupled liquid and gas flow, radionuclide transport, and thermal effects on flow. Site-specific data may have to be analyzed, and additional data collected if the effects of heterogeneity are demonstrated through modeling studies to be significant for repository performance.

## 6 SUMMARY

Geostatistical analyses of pneumatic, hydraulic, interstitial, and thermal properties of unsaturated fractured tuffs has been undertaken because the results of field tests at Yucca Mountain have shown considerable spatial variation of hydraulic and pneumatic properties. In particular, air permeability data determined from air injection tests conducted in the Exploratory Studies Facility varied over at least five orders of magnitude within a single hydrostratigraphic unit (CRWMS M&O, 2000a). Accounting for variability and heterogeneity within both welded and nonwelded units and transecting faults will increase the variability in computed thermohydrologic variables. Using hypothetical data, previous modeling efforts (Illman and Hughson, 2001; Fedors, et al., 2002b) illustrated the importance of including fracture heterogeneity in evaluating flow rate and distribution through unsaturated fractured rocks. Using limited data from above the ceiling of Niche 36+50, sensitivity analyses for heterogeneity of fracture permeability have been documented (CRWMS M&O, 2001). More recently, the U.S. Department of Energy has begun to evaluate the effect of intralayer heterogeneity of thermal conductivity on in-drift temperature and relative humidity conditions using the thermohydrologic model.

This report summarizes the geostatistical analysis of interstitial, hydraulic, pneumatic, and thermal properties of unsaturated fractured tuffs collected by Rasmussen, et al. (1990) at the Apache Leap Research Site. Analyzed parameters include: (i) field estimates of air permeability, (ii) field estimates of liquid permeability, (iii) laboratory estimates of air permeability, (iv) laboratory estimates of liquid permeability, (v) fracture frequency, (vi) effective porosity, (vii) van Genuchten alpha, (viii) matrix Klinkenberg coefficient, (ix) water content, (x) dry thermal conductivity, (xi) saturated thermal conductivity, and (xii) dry rock specific heat. The data set consisted of field tests involving 3-m [10-ft] packer injection tests and a variety of laboratory tests performed on oriented cores. Descriptive statistics, histograms, experimental variograms, and preliminary model fits are provided for each variable.

The available data from Yucca Mountain are also summarized, analyzed, and compared with characteristics of the Apache Leap Research Site. Adequate geospatial data sets from Yucca Mountain are lacking for site-specific analyses. However, when geospatial data from the Systematic Testing Program currently running in the Enhanced Characterization of the Repository Block drift become available, they should prove valuable. The Apache Leap Research Site should be considered a reasonable analog site for Yucca Mountain, even though the tuffs at Apache Leap appear to be less welded than those in the repository horizon of Yucca Mountain and more welded than the nonwelded Paintbrush Tuffs above the repository horizon.

## 7 REFERENCES

Ahlers, C.F., C. Shan, C. Haukwa, A.J.B. Cohen, and G.S. Bodvarsson. "Calibration and Prediction of Pneumatic Response at Yucca Mountain, Nevada Using the LBNL/USGS Three-Dimensional Site-Scale Model of the Unsaturated Zone." Yucca Mountain Project Milestone OB12M. Berkeley, California: Lawrence Berkeley National Laboratory. 1996.

Akaike, H. "An Entropy Maximization Principle." White State University Proceedings: Applications in Statistics, Dayton, Ohio, June 14-18, 1976. P.R. Krishnaiah, ed. Amsterdam, Holland: North-Holland. 1977.

\_\_\_\_\_. "A New Look at Statistical Model Identification." *IEEE Transactions on Automatic Control*. Vol. AC-19. pp. 716-722. 1974.

Anderson, L.A. "Results of Rock Property Measurements Made on Core Samples from Yucca Mountain Boreholes, Nevada Test Site, Nevada." U.S. Geological Survey Open-File Report 90-474. 1991.

Bandurraga, T.M. and G.S. Bodvarsson. "Calibrating Hydrogeologic Parameters for the 3-D Site-Scale Unsaturated Zone Model of Yucca Mountain, Nevada." *Journal of Contaminant Hydrology*. Vol. 38. pp. 25-46. 1999.

Bassett, R.L., S.P. Neuman, P.J. Wierenga, G. Chen, G.R. Davidson, E.L. Hardin, W.A. Illman, M.T. Murrell, D.M. Stephens, M.J. Thomasson, D.L. Thompson, and E.G. Woodhouse. NUREG/CR-6497, "Data Collection and Field Experiments at the Apache Leap Research Site, May 1995-1996." Chapter 4, Infiltration Tests in Fractured Porous Tuffs at the ALRS. Washington, DC: NRC. 1997.

Bassett, R.L., S.P. Neuman, T.C. Rasmussen, A. Guzman, G.R. Davidson, and C.F. Lohrstorfer. NUREG/CR-6203, "Validation Studies for Assessing Unsaturated Flow and Transport Through Fractured Rock." E.G. Woodhouse, et al., eds. Washington, DC: NRC. 1994.

Bear, J., C.F. Tsang, and G. de Marsily, eds. *Flow and Contaminant Transport in Fractured Rock*. San Diego, California: Academic Press. 1993.

Braester, C. "Moisture Variation at the Soil Surface and the Advance of the Wetting Front During Infiltration at Constant Flux." *Water Resources Research*. Vol. 9, No. 3. pp. 687-694. 1973.

Brodsky, N.S., M. Riggins, J. Connolly, and P. Ricci. "Thermal Expansion, Thermal Conductivity, and Heat Capacity Measurements for Boreholes UE25 NRG-4, UE25 NRG-5, USW NRG-6, and USW NRG-7/7A Yucca Mountain Site Characterization Report." SAND95-1955/UC-814. Albuquerque, New Mexico: Sandia National Laboratories. 1997.

Chen, G., W.A. Illman, D.L. Thompson, V.V. Vesselinov, and S.P. Neuman. "Geostatistical, Type Curve and Inverse Analyses of Pneumatic Injection Tests in Unsaturated Fractured Tuffs at the Apache Leap Research Site Near Superior, Arizona, 73-98." *Dynamics of Fluids in Fractured Rocks*. B. Faybishenko, et al., eds. *Geophysical Monograph 122*. Washington, DC: American Geophysical Union. 2000.

Chuang, Y., W.R. Haldeman, T.C. Rasmussen, and D.D. Evans. NUREG/CR-5482, "Laboratory Analysis of Fluid Flow and Solute Transport Through a Variably Saturated Fracture Embedded in Porous Tuff." Washington, DC: NRC. February 1990.

CRWMS M&O. "Multiscale Thermohydrologic Model." ANL-EBS-MD-000049. Rev. 00 ICN 02. Las Vegas, Nevada: Bechtel-SAIC, Inc., 2001.

———. "In Situ Field Testing of Processes." ANL-NBS-HS-000005. Rev. 00. Las Vegas, Nevada: TRW Environmental Safety Systems, Inc. 2000a.

———. "Unsaturated Zone Flow and Transport Process Model Report." TDR-NBS-HS-000002. Rev. 00 ICN 02. Las Vegas, Nevada: TRW Environmental Safety Systems, Inc. 2000b.

———. "Analysis of Hydrologic Properties Data." ANL-NBS-HS-000002. Rev. 00. Las Vegas, Nevada: TRW Environmental Safety Systems, Inc. 2000c.

———. "Calibrated Properties Model." MDL-NBS-HS-000003. Rev. 00. Las Vegas, Nevada: TRW Environmental Safety Systems, Inc. 2000d.

———. "The Site-Scale Unsaturated Zone Model of Yucca Mountain, Nevada, for the Viability Assessment." Las Vegas, Nevada: CRWMS M&O. 1997.

Dachler, R. *Grundwasserströmung* (Flow of Groundwater). Wien, German: Julius Springer. 1936.

Evans, D.D. and T.C. Rasmussen. NUREG/CR-5581, "Unsaturated Flow and Transport Through Fractured Rock Related to High-Level Waste Repositories, Final Report—Phase III." Washington, DC: NRC. 1991.

Fedors, R., C. Manepally, and C. Dinwiddie. "Review of the Multiscale Thermohydrologic Model Analysis Model Report." Rev. 00 ICN 02. San Antonio, Texas: CNWRA. 2002a.

Fedors, R.W., J.R. Winterle, W.A. Illman, C.L. Dinwiddie, and D.L. Hughson. "Unsaturated Zone Flow at Yucca Mountain, Nevada: Effects of Fracture Heterogeneity and Flow in the Nonwelded Paintbrush Tuff Unit." San Antonio, Texas: CNWRA. 2002b.

Flint, L.E. "Characterization of Hydrogeologic Units Using Matrix Properties, Yucca Mountain, Nevada." U.S. Geological Survey Water Resources Investigations Report 97-4243. 1998.

Geddis, A.M. "Rapid estimate of solid volume in large tuff cores using a gas pycnometer." Master's thesis. University of Arizona, Department of Hydrology and Water Resources. Tucson, Arizona. 1994.

- Geovariances. "ISATIS User's Guide." Version 3.1. Avon, France: Geovariances. 1997.
- Gomez-Hernandez, J.J., and E.F. Cassiraga. "The Theory of Practice of Sequential Simulation." *Geostatistical Simulations*. M. Armstrong and P.A. Dowd, eds. pp. 111–124. Norwell, Massachusetts: Kluwer Academic. 1994.
- Guzman, A.G., A.M. Geddis, M.J. Henrich, C.F. Lohrstorfer, and S.P. Neuman. NUREG/CR–6360, "Summary of Air Permeability Data from Single-Hole Injection Tests in Unsaturated Fractured Tuffs at the Apache Leap Research Site: Results of Steady-State Test Interpretation." Washington, DC: NRC. March 1996.
- Haldeman, W.R., Y. Chuang, T.C. Rasmussen, and D.D. Evans. "Laboratory Analysis of Fluid Flow and Solute Transport Through a Fracture Embedded in Porous Tuff." *Water Resources Research*. Vol. 27, No. 1. pp. 53–65. 1991.
- Hannan, E.S. "The Estimation of the Order of an ARMA Process." *The Annals of Statistics*. Vol. 8, No. 5. pp 1,071–1,081. 1980.
- Hughson, D.L., R.T. Green, G.I. Ofoegbu, D.A. Farrell, and S. Mayer. "Review of Analysis/Models Reports Relevant to the Thermal Effects on Flow Key Technical Issue." San Antonio, Texas: CNWRA. 2000.
- Hvorslev, M.J. "Time Lag and Soil Permeability in Ground-Water Observations." *U.S. Army Corps of Engineers Bulletin 36*. Vicksburg, Mississippi: U.S. Army Corps of Engineers. 1951.
- Hyun, Y., S.P. Neuman, V.V. Vesselinov, W.A. Illman, D.M. Tartakovsky, and V. Di Federico. "Theoretical Interpretation of a Pronounced Permeability Scale Effect in Unsaturated Fractured Tuff." *Water Resources Research*. Vol. 38, No. 6. pp. 28-1 through 28-8. 2002.
- Illman, W.A. "Single- and cross-hole pneumatic injection tests in unsaturated fractured tuffs at the Apache Leap research site near Superior, Arizona." Ph.D. dissertation. University of Arizona, Department of Hydrology and Water Resources. Tucson, Arizona. 1999.
- Illman, W.A., and D.L. Hughson. "Monte Carlo Analyses of Unsaturated Flow in Thick Vadose Zones of Layered, Fractured Rocks." Proceedings of the American Geophysical Union Fall Meeting, San Francisco, California, December 10–14, 2001. *EOS Transactions Supplement*. American Geophysical Union. Vol. 82, No. 47. 2001.
- Illman, W.A. and S.P. Neuman. "Type-Curve Interpretation of a Cross-Hole Pneumatic Injection Test in Unsaturated Fractured Tuff." *Water Resources Research*. Vol. 37, No. 3. pp. 583–603. 2001.
- . "Type-Curve Interpretation of Multi-Rate Single-Hole Pneumatic Injection Tests in Unsaturated Fractured Rock." *Ground Water*. Vol. 38, No. 6. pp. 899–911. 2000.
- Illman, W.A., D.L. Thompson, V.V. Vesselinov, and S.P. Neuman. NUREG/CR–5559, "Single-Hole and Cross-Hole Pneumatic Tests in Unsaturated Fractured Tuffs at the Apache Leap Research Site: Phenomenology, Spatial Variability, Connectivity and Scale." Washington, DC: NRC. September 1998.

Journel, A.G. and Ch.J. Huijbregts. *Mining Geostatistics*. New York City, New York: Academic Press. 1978.

Kashyap, R.L. "Optimal Choice of AR and MA Parts in Autoregressive Moving Average Models." *IEEE Transactions on Pattern Analysis and Machine Intelligence*. Vol. 4, No. 2. pp. 99–104. 1982.

Kitanidis, P.K. *Introduction to Geostatistics—Application in Hydrogeology*. New York City, New York: Cambridge University Press. 1997.

Klinkenberg, L.J. "The Permeability of Porous Media to Liquids and Gases." *American Petroleum Institute Drilling and Production Practice*. pp. 200–213. 1941.

LeCain, G.D. "Air-Injection Testing in Vertical Boreholes in Welded and Nonwelded Tuff, Yucca Mountain, Nevada." U.S. Geological Survey Water Resources Investigations Report 95-4262. 1997.

———. "Pneumatic Testing in 45-Degree-Inclined Boreholes in Ash-Flow Tuff near Superior, Arizona." U.S. Geological Survey Water Resources Investigations Report 95-4073. 1995.

LeCain, G.D., L.O. Anna, M.F. Fahy. "Results from Geothermal Logging, Air and Core-Water Chemistry Sampling, N Testing and Tracer Testing in the northern Ghost Dance Fault, Yucca Mountain, Nevada." U.S. Geological Survey Water Resources Investigations Report 99-4210. 1999.

Lichtner, P.C., M.S. Seth, and S. Painter. "MULTIFLO User's Manual." MULTIFLO, Version 1.2: Two-Phase Nonisothermal Coupled Thermal-Hydrologic-Chemical Flow Simulator. Rev. 2, Change 0. San Antonio, Texas: CNWRA. 2000.

Myers, D.E. "Interpolation and Estimation with Spatially Located Data." *Chemometrics and Intelligent Laboratory Systems*. Vol. 11. pp. 209–228. 1991.

Neuman, S.P. "Stochastic Continuum Representation of Fractured Rock Permeability as an Alternative to the REV and Fracture Network Concepts." Proceedings of the 28th U.S. Rock Mechanics Symposium, Tucson, Arizona, June 29–July 1, 1987. I.W. Farmer, J.J.K. Daemen, C.S. Desai, C.E. Glass, and S.P. Neuman, eds. Rotterdam, Holland: A.A. Balkema. pp. 533–561. 1987.

Nitao, J.J. "Reference Manual for the NUFT Flow and Transport Code." UCRL-MA-130651. Livermore, California: Lawrence Livermore National Laboratory. 1998.

Painter, S. "Stochastic Interpolation of Aquifer Properties Using Fractional Lévy Motion." *Water Resources Research*. Vol. 32, No. 5. pp. 1,323–1,332. 1996.

Paleologos, E.K., S.P. Neuman, and D. Tartakovsky. "Effective Hydraulic Conductivity of Bounded, Strongly Heterogeneous Porous Media." *Water Resources Research*. Vol. 32. No. 5. pp. 1,333–1,341. 1996.

Peterson, D.W. "Dacitic Ash-Flow Sheet Near Superior and Globe, Arizona." Ph.D. dissertation. Stanford University. Palo Alto, California. 1961.

Philip, J.R., J.H. Knight, and R.T. Waechter. "Unsaturated Seepage and Subterranean Holes: Conspectus, and Exclusion Problem for Cylindrical Cavities." *Water Resources Research*. Vol. 25, No. 1. pp. 16-28. 1989.

Pruess, K. "TOUGH2—A General Purpose Numerical Simulator for Multiphase Fluid and Heat Flow." LBL-29400 UC-251. Livermore, California: Lawrence Livermore National Laboratory. 1991.

Rasmussen, T.C. and D.D. Evans. NUREG/CR-5880, "Nonisothermal Hydrologic Transport Experimental Plan." Washington, DC: NRC. September 1992.

———. NUREG/CR-5239, "Fluid Flow and Solute Transport Modeling Through Three-Dimensional Networks of Variably Saturated Discrete Fractures." Washington, DC: NRC. 1989.

———. NUREG/CR-4655, "Unsaturated Flow and Transport Through Fractured Rock-Related to High-Level Waste Repositories, Final Report—Phase II." Washington, DC: NRC. May 1987.

Rasmussen, T.C., D.D. Evans, P.J. Sheets, and J.H. Blanford. "Permeability of Apache Leap Tuff: Borehole and Core Measurements Using Water and Air." *Water Resources Research*. Vol. 29, No. 7. pp. 1,997-2,006. 1993.

———. NUREG/CR-5596, "Unsaturated Fractured Rock Characterization Methods and Data Sets at the Apache Leap Tuff Site." Washington, DC: NRC. August 1990.

Rasmussen T.C., S.C. Rhodes, A. Guzman, and S.P. Neuman. NUREG/CR-6096, "Apache Leap Tuff INTRAVAL Experiments: Results and Lessons Learned." Washington, DC: NRC. March 1996.

Robin, M.J.L., A.L. Gutjahr, E.A. Sudicky, and J.L. Wilson. "Cross-Correlated Random Field Generation with the Direct Fourier Transform Method." *Water Resources Research*. Vol. 29, No. 7. pp. 2,385-2,397. 1993.

Rousseau, J.P., E.M. Kwicklis, and D.C. Gillies. "Hydrogeology of the Unsaturated Zone, North Ramp Area of the Exploratory Studies Facility, Yucca Mountain, Nevada." U.S. Geological Survey Water Resources Investigations Report 98-4050. 1999.

Samper, F.J. and S.P. Neuman. "Estimation of Spatial Covariance Structures by Adjoint State Maximum Likelihood Cross-Validation: 1—Theory." *Water Resources Research*. Vol. 25, No. 3. pp. 351-362. 1989a.

———. "Estimation of Spatial Covariance Structures by Adjoint State Maximum Likelihood Cross-Validation: 3—Application to Hydrochemical and Isotopic Data." *Water Resources Research*. Vol. 25, No. 3. pp. 373-384. 1989b.

Terzaghi, R. "Source of Error in Joint Surveys." *Geotechnique*. Vol. 15. p. 287. 1965

Tidwell, V.C., T.C. Rasmussen, and D.D. Evans. "Saturated Hydraulic Conductivity Estimates for Fractured Rocks in the Unsaturated Zone." Proceedings of International Conference and Workshop on the Validation of Flow and Transport Models for the Unsaturated Zone, Las Cruces, New Mexico. P.J. Wierenga, ed. Las Cruces, New Mexico: New Mexico State University. 1988.

Tsang, Y.W., C.F. Tsang, F.V. Hale, and B. Dverstorp. "Tracer Transport in a Stochastic Continuum Model of Fractured Media." *Water Resources Research*. Vol. 32, No. 10. pp. 3,077–3,092. 1996.

van Genuchten, M.Th. "A Closed-Form Equation for Predicting the Hydraulic Conductivity of Unsaturated Soils." *Soil Science Society of America Journal*. Vol. 44. pp. 892–898. 1980.

Vesselinov, V.V., S.P. Neuman, and W.A. Illman. "Three-Dimensional Numerical Inversion of Pneumatic Cross-Hole Tests in Unsaturated Fractured Tuff: 1—Methodology and Borehole Effects." *Water Resources Research*. Vol. 37, No. 12. pp. 3,001–3,017. 2001a.

———. "Three-Dimensional Numerical Inversion of Pneumatic Cross-Hole Tests in Unsaturated Fractured Tuff: 2—Equivalent Parameters, High-Resolution Stochastic Imaging and Scale Effects." *Water Resources Research*. Vol. 37, No. 12. pp. 3,019–3,041. 2001b.

Waiting, D.J., R. Chen, J.G. Crider, W.M. Dunne, R.W. Fedors, D.A. Ferrill, M.B. Gray, B.E. Hill, P.C. LaFemina, H.L. McKague, A.P. Morris, D.W. Sims, and J.A. Stamatakos. "Technical Assessment of Structural Deformation and Seismicity at Yucca Mountain, Nevada." San Antonio, Texas: CNWRA. 2001.

Weber, D. "Mineralogic, Isotopic, and Spatial Properties of Fractures in an Unsaturated Partially-Welded Tuff Near Superior, Arizona. Master's thesis. University of Arizona. Tucson, Arizona. 1986.

Weber, D.S. and D.D. Evans. NUREG/CR-5255, "Stable Isotopes of Authigenic Minerals in Variably-Saturated Fractured Tuff." Washington, DC: NRC. November 1988.

Wu, Y.S., C. Haukwa, G.S. Bodvarsson. "A Site-Scale Model for Fluid and Heat Flow in the Unsaturated Zone of Yucca Mountain, Nevada." *Journal of Contaminant Hydrology*. Vol. 38. pp. 185–215. 1999.

Yeh, T.C., T.C. Rasmussen, and D.D. Evans. NUREG/CR-5097, "Simulation of Liquid and Vapor Movement in Unsaturated Fractured Rock at the Apache Leap Tuff Site—Models and Strategies." Washington, DC: NRC. March 1988.

## APPENDIX

**Table 1. Published\* Field and Laboratory Estimates of Air and Liquid Permeability and Fracture Frequency from the Apache Leap Research Site. Spatial Locations are Based on a Local Coordinate System Using the Lower Lip of the Z3 Borehole Casing as the Origin and Oriented 8° West of North.**

[Note that 1.0 m = 3.28 ft and  $1.0 \times 10^{-12} \text{ m}^2 = 1.01325 \text{ D}$ ]

Borehole	x (m)	y (m)	z (m)	Field Air	Field Water	Lab Air	Lab Water	Uncorrected
				Permeability (m <sup>2</sup> )	Permeability (m <sup>2</sup> )	Permeability (m <sup>2</sup> )	Permeability (m <sup>2</sup> )	Fracture Frequency (counts/m)
X1	8.84	10.04	-1.46			$8.43 \times 10^{-15}$	$1.46 \times 10^{-15}$	1.00
	8.20	10.04	-2.10			$1.51 \times 10^{-15}$	$4.80 \times 10^{-16}$	0.00
	7.64	10.04	-2.67	$4.73 \times 10^{-16}$	$3.00 \times 10^{-16}$	$1.36 \times 10^{-15}$	$2.24 \times 10^{-16}$	0.00
	5.44	10.04	-4.86	$2.13 \times 10^{-16}$	$3.68 \times 10^{-17}$	$5.35 \times 10^{-16}$	$1.23 \times 10^{-16}$	2.67
	3.25	10.04	-7.05	$6.63 \times 10^{-15}$	$2.97 \times 10^{-16}$	$4.40 \times 10^{-16}$	$1.02 \times 10^{-16}$	0.67
	1.34	10.04	-8.96	$1.00 \times 10^{-16}$	$1.06 \times 10^{-16}$	$4.17 \times 10^{-16}$	$1.41 \times 10^{-16}$	0.00
	-0.85	10.04	-11.15	$5.44 \times 10^{-17}$	$1.16 \times 10^{-16}$	$3.98 \times 10^{-16}$	$1.50 \times 10^{-16}$	0.00
X2	19.17	10.03	-1.29			$2.55 \times 10^{-14}$	$1.49 \times 10^{-14}$	1.00
	18.46	10.03	-2.00			$1.71 \times 10^{-15}$	$3.43 \times 10^{-16}$	2.00
	17.97	10.03	-2.49	$2.54 \times 10^{-15}$	$5.92 \times 10^{-15}$	$1.35 \times 10^{-15}$	$4.57 \times 10^{-16}$	0.00
	15.77	10.03	-4.68	$7.92 \times 10^{-17}$	$5.74 \times 10^{-16}$	$8.19 \times 10^{-16}$	$7.05 \times 10^{-17}$	0.67
	13.37	10.03	-7.09	$1.59 \times 10^{-15}$	$4.42 \times 10^{-16}$	$6.03 \times 10^{-16}$	$2.51 \times 10^{-16}$	0.33
	11.46	10.03	-9.00	$6.61 \times 10^{-14}$	$2.62 \times 10^{-15}$	$2.50 \times 10^{-15}$	$1.61 \times 10^{-15}$	0.67
	9.06	10.03	-11.40	$1.37 \times 10^{-15}$	$1.94 \times 10^{-15}$	$2.04 \times 10^{-15}$	$1.14 \times 10^{-15}$	0.67
	7.36	10.03	-13.10	$9.83 \times 10^{-16}$	$8.75 \times 10^{-16}$	$6.63 \times 10^{-15}$	$3.84 \times 10^{-15}$	0.33
	5.17	10.03	-15.29	$2.06 \times 10^{-15}$	$1.27 \times 10^{-15}$	$9.94 \times 10^{-16}$	$4.94 \times 10^{-16}$	1.33
	2.97	10.03	-17.48	$1.59 \times 10^{-16}$	$1.96 \times 10^{-16}$	$1.35 \times 10^{-15}$	$6.75 \times 10^{-16}$	0.33
	0.71	10.03	-19.74	$1.98 \times 10^{-16}$	$4.87 \times 10^{-16}$	$1.52 \times 10^{-15}$	$8.31 \times 10^{-16}$	0.67
-1.34	10.03	-21.79	$9.87 \times 10^{-17}$	$9.81 \times 10^{-17}$	$6.51 \times 10^{-16}$	$2.79 \times 10^{-16}$	0.67	
X3	29.15	10.04	-1.23			$3.07 \times 10^{-15}$	$7.04 \times 10^{-16}$	0.00
	28.52	10.04	-1.87			$1.27 \times 10^{-15}$	$4.70 \times 10^{-16}$	0.00
	27.74	10.04	-2.64	$3.97 \times 10^{-15}$	$2.07 \times 10^{-15}$	$2.76 \times 10^{-15}$	$3.75 \times 10^{-16}$	0.50
	25.62	10.04	-4.76	$9.18 \times 10^{-15}$	$2.54 \times 10^{-15}$	$1.63 \times 10^{-15}$	$2.81 \times 10^{-16}$	0.67
	23.43	10.04	-6.96	$1.44 \times 10^{-15}$	$1.32 \times 10^{-15}$	$2.17 \times 10^{-15}$	$2.74 \times 10^{-16}$	1.00
	21.31	10.04	-9.08	$1.79 \times 10^{-16}$	$4.10 \times 10^{-16}$	$1.48 \times 10^{-15}$	$3.17 \times 10^{-16}$	0.67
	19.25	10.04	-11.13	$9.90 \times 10^{-17}$	$7.05 \times 10^{-17}$	$9.92 \times 10^{-16}$	$4.75 \times 10^{-16}$	0.67
	17.13	10.04	-13.25	$2.21 \times 10^{-16}$	$3.46 \times 10^{-16}$	$9.51 \times 10^{-16}$	$5.71 \times 10^{-16}$	0.33
	15.15	10.04	-15.23	$8.30 \times 10^{-17}$	$2.09 \times 10^{-16}$	$6.30 \times 10^{-16}$	$2.98 \times 10^{-16}$	0.33
	12.96	10.04	-17.42	$8.32 \times 10^{-17}$	$4.98 \times 10^{-16}$	$6.00 \times 10^{-16}$	$3.32 \times 10^{-16}$	0.67
	10.84	10.04	-19.54	$6.75 \times 10^{-17}$	$1.14 \times 10^{-16}$	$5.27 \times 10^{-16}$	$2.56 \times 10^{-16}$	0.33
	8.51	10.04	-21.88	$1.33 \times 10^{-15}$	$2.92 \times 10^{-16}$	$6.01 \times 10^{-16}$	$2.09 \times 10^{-16}$	2.00
	6.60	10.04	-23.79	$2.87 \times 10^{-16}$	$1.98 \times 10^{-16}$	$9.04 \times 10^{-16}$	$5.16 \times 10^{-16}$	1.67
	4.33	10.04	-26.05	$1.66 \times 10^{-15}$		$7.20 \times 10^{-16}$	$3.82 \times 10^{-16}$	0.67
	2.21	10.04	-28.17	$1.60 \times 10^{-16}$		$8.50 \times 10^{-16}$	$4.43 \times 10^{-16}$	0.00
0.09	10.04	-30.29	$5.18 \times 10^{-17}$	$2.76 \times 10^{-17}$	$5.20 \times 10^{-16}$	$2.17 \times 10^{-16}$	0.67	
Y1	8.93	5.08	-1.30			$6.59 \times 10^{-16}$	$1.77 \times 10^{-16}$	0.00
	7.87	5.08	-2.36			$3.52 \times 10^{-15}$	$4.71 \times 10^{-16}$	1.00
	7.30	5.08	-2.93	$3.40 \times 10^{-16}$	$4.40 \times 10^{-16}$	$1.78 \times 10^{-15}$	$3.66 \times 10^{-16}$	0.50
	5.54	5.08	-4.69	$3.43 \times 10^{-16}$	$1.51 \times 10^{-16}$	$6.02 \times 10^{-16}$	$1.13 \times 10^{-16}$	0.33
	3.20	5.08	-7.03	$2.09 \times 10^{-16}$	$1.37 \times 10^{-16}$	$6.56 \times 10^{-16}$	$1.04 \times 10^{-16}$	0.33

**Table 1. Published\* Field and Laboratory Estimates of Air and Liquid Permeability and Fracture Frequency from the Apache Leap Research Site. Spatial Locations are Based on a Local Coordinate System Using the Lower Lip of the Z3 Borehole Casing as the Origin and Oriented 8° West of North.**

[Note that 1.0 m = 3.28 ft and  $1.0 \times 10^{-12} \text{ m}^2 = 1.01325 \text{ D}$ ] (continued)

Borehole	x (m)	y (m)	z (m)	Field Air Permeability (m <sup>2</sup> )	Field Water Permeability (m <sup>2</sup> )	Lab Air Permeability (m <sup>2</sup> )	Lab Water Permeability (m <sup>2</sup> )	Uncorrected Fracture Frequency (counts/m)
	1.58	5.08	-8.65	$1.92 \times 10^{-16}$	$1.29 \times 10^{-16}$	$4.99 \times 10^{-16}$	$1.47 \times 10^{-16}$	0.67
	-0.90	5.08	-11.13	$9.69 \times 10^{-17}$	$1.08 \times 10^{-16}$	$6.18 \times 10^{-16}$	$2.45 \times 10^{-16}$	0.67
Y2	18.76	5.20	-1.58			$6.01 \times 10^{-15}$	$1.65 \times 10^{-15}$	1.00
	17.70	5.20	-2.64			$1.42 \times 10^{-14}$	$1.83 \times 10^{-15}$	1.00
	17.14	5.20	-3.21	$5.10 \times 10^{-15}$	$5.25 \times 10^{-15}$	$1.56 \times 10^{-15}$	$2.27 \times 10^{-16}$	0.00
	15.65	5.20	-4.69	$4.21 \times 10^{-16}$	$5.96 \times 10^{-16}$	$2.51 \times 10^{-15}$	$2.94 \times 10^{-16}$	1.00
	13.46	5.20	-6.88	$1.10 \times 10^{-15}$	$5.11 \times 10^{-16}$	$5.88 \times 10^{-16}$	$2.04 \times 10^{-16}$	0.67
	11.34	5.20	-9.00	$1.65 \times 10^{-15}$	$1.28 \times 10^{-15}$	$2.10 \times 10^{-15}$	$1.12 \times 10^{-15}$	0.00
	9.22	5.20	-11.12	$1.68 \times 10^{-14}$	$4.27 \times 10^{-15}$	$9.74 \times 10^{-16}$	$3.71 \times 10^{-16}$	0.33
	6.95	5.20	-13.39	$1.57 \times 10^{-15}$	$1.48 \times 10^{-15}$	$1.25 \times 10^{-14}$	$8.44 \times 10^{-15}$	1.00
	4.97	5.20	-15.37	$3.45 \times 10^{-16}$	$9.15 \times 10^{-16}$	$8.39 \times 10^{-16}$	$4.29 \times 10^{-16}$	0.33
	2.71	5.20	-17.63	$4.46 \times 10^{-16}$	$3.63 \times 10^{-16}$	$7.81 \times 10^{-16}$	$4.34 \times 10^{-16}$	0.00
	0.73	5.20	-19.61	$6.55 \times 10^{-17}$	$2.20 \times 10^{-16}$	$7.26 \times 10^{-16}$	$3.62 \times 10^{-16}$	0.33
	-1.39	5.20	-21.73	$9.70 \times 10^{-17}$	$2.20 \times 10^{-16}$	$9.85 \times 10^{-16}$	$4.76 \times 10^{-16}$	0.00
Y3	28.65	5.35	-1.68			$2.72 \times 10^{-15}$	$5.88 \times 10^{-16}$	0.00
	27.88	5.35	-2.46			$8.84 \times 10^{-15}$	$1.08 \times 10^{-15}$	0.00
	27.17	5.35	-3.17	$7.82 \times 10^{-15}$	$3.48 \times 10^{-15}$	$1.74 \times 10^{-14}$	$3.19 \times 10^{-15}$	0.50
	25.68	5.35	-4.65	$1.54 \times 10^{-15}$	$1.34 \times 10^{-15}$	$7.40 \times 10^{-14}$	$2.45 \times 10^{-14}$	1.00
	23.49	5.35	-6.84	$1.91 \times 10^{-15}$	$2.98 \times 10^{-15}$	$1.05 \times 10^{-15}$	$1.43 \times 10^{-16}$	0.33
	21.30	5.35	-9.03	$1.86 \times 10^{-15}$	$3.12 \times 10^{-15}$	$1.01 \times 10^{-13}$	$4.48 \times 10^{-14}$	0.33
	18.75	5.35	-11.58	$5.41 \times 10^{-16}$	$2.23 \times 10^{-15}$	$4.20 \times 10^{-15}$	$1.36 \times 10^{-15}$	0.33
	17.20	5.35	-13.14	$1.09 \times 10^{-16}$	$3.98 \times 10^{-16}$	$6.91 \times 10^{-16}$	$3.77 \times 10^{-16}$	1.33
	14.94	5.35	-15.40	$1.85 \times 10^{-16}$	$3.33 \times 10^{-16}$	$5.25 \times 10^{-16}$	$4.33 \times 10^{-16}$	0.67
	12.96	5.35	-17.38	$2.71 \times 10^{-16}$	$4.93 \times 10^{-16}$	$6.30 \times 10^{-16}$	$2.69 \times 10^{-16}$	2.00
	10.69	5.35	-19.64	$1.35 \times 10^{-16}$	$3.26 \times 10^{-16}$	$7.92 \times 10^{-16}$	$4.31 \times 10^{-16}$	0.33
	8.64	5.35	-21.69	$3.01 \times 10^{-16}$	$5.80 \times 10^{-16}$	$8.49 \times 10^{-16}$	$3.72 \times 10^{-16}$	0.33
	6.59	5.35	-23.74	$1.45 \times 10^{-16}$	$1.91 \times 10^{-16}$	$5.49 \times 10^{-16}$	$2.10 \times 10^{-16}$	0.00
	4.26	5.35	-26.08	$1.04 \times 10^{-16}$	$1.68 \times 10^{-16}$	$9.95 \times 10^{-16}$	$4.02 \times 10^{-16}$	0.00
	2.28	5.35	-28.06	$7.09 \times 10^{-17}$	$9.60 \times 10^{-17}$	$8.21 \times 10^{-16}$	$4.10 \times 10^{-16}$	0.00
	0.30	5.35	-30.04	$4.58 \times 10^{-17}$	$5.41 \times 10^{-17}$	$3.81 \times 10^{-16}$	$1.47 \times 10^{-16}$	0.33
Z1	20.79	0.00	-1.60			$2.86 \times 10^{-15}$	$5.61 \times 10^{-16}$	0.00
	21.64	0.00	-2.45			$1.95 \times 10^{-15}$	$3.56 \times 10^{-16}$	0.00
	22.35	0.00	-3.16	$1.65 \times 10^{-14}$	$9.80 \times 10^{-15}$	$3.55 \times 10^{-14}$	$1.06 \times 10^{-14}$	1.00
	23.69	0.00	-4.50	$1.79 \times 10^{-14}$	$2.63 \times 10^{-15}$	$5.31 \times 10^{-15}$	$4.60 \times 10^{-16}$	1.67
	26.02	0.00	-6.83	$6.62 \times 10^{-13}$	$4.43 \times 10^{-14}$	$1.01 \times 10^{-15}$	$2.44 \times 10^{-16}$	1.33
	28.29	0.00	-9.10	$1.20 \times 10^{-14}$	$4.24 \times 10^{-15}$	$1.20 \times 10^{-14}$	$2.63 \times 10^{-15}$	2.33
	30.34	0.00	-11.15		$1.95 \times 10^{-12}$	$2.60 \times 10^{-15}$	$2.67 \times 10^{-16}$	1.33
Z2	11.21	0.03	-1.61			$8.56 \times 10^{-16}$	$1.47 \times 10^{-16}$	0.00
	11.92	0.03	-2.32			$1.19 \times 10^{-15}$	$3.05 \times 10^{-16}$	0.33

**Table 1. Published\* Field and Laboratory Estimates of Air and Liquid Permeability and Fracture Frequency from the Apache Leap Research Site. Spatial Locations are Based on a Local Coordinate System Using the Lower Lip of the Z3 Borehole Casing as the Origin and Oriented 8° West of North.**

[Note that 1.0 m = 3.28 ft and  $1.0 \times 10^{-12} \text{ m}^2 = 1.01325 \text{ D}$ ] (continued)

Borehole	x (m)	y (m)	z (m)	Field Air Permeability (m <sup>2</sup> )	Field Water Permeability (m <sup>2</sup> )	Lab Air Permeability (m <sup>2</sup> )	Lab Water Permeability (m <sup>2</sup> )	Uncorrected Fracture Frequency (counts/m)
	12.63	0.03	-3.02	$4.73 \times 10^{-17}$	$2.82 \times 10^{-16}$	$5.16 \times 10^{-15}$	$1.68 \times 10^{-15}$	1.00
	14.40	0.03	-4.79	$8.29 \times 10^{-17}$	$2.00 \times 10^{-16}$	$1.03 \times 10^{-15}$	$4.88 \times 10^{-16}$	1.33
	16.38	0.03	-6.77	$8.71 \times 10^{-15}$	$2.74 \times 10^{-15}$	$1.02 \times 10^{-14}$	$5.57 \times 10^{-15}$	0.33
	18.57	0.03	-8.96	$2.45 \times 10^{-14}$	$1.00 \times 10^{-14}$	$9.16 \times 10^{-14}$	$3.84 \times 10^{-14}$	2.00
	20.62	0.03	-11.01	$1.94 \times 10^{-15}$	$3.12 \times 10^{-15}$	$8.97 \times 10^{-15}$	$9.88 \times 10^{-16}$	4.33
	23.02	0.03	-13.42	$3.77 \times 10^{-14}$	$8.68 \times 10^{-15}$	$1.29 \times 10^{-15}$	$4.36 \times 10^{-16}$	1.33
	24.86	0.03	-15.26	$2.37 \times 10^{-14}$	$5.26 \times 10^{-15}$	$1.18 \times 10^{-15}$	$3.58 \times 10^{-16}$	1.67
	27.12	0.03	-17.52	$2.34 \times 10^{-16}$	$1.75 \times 10^{-15}$	$6.14 \times 10^{-16}$	$2.13 \times 10^{-16}$	0.67
	29.17	0.03	-19.57	$6.17 \times 10^{-15}$	$6.72 \times 10^{-16}$	$1.23 \times 10^{-15}$	$4.57 \times 10^{-16}$	3.00
	31.37	0.03	-21.76	$4.95 \times 10^{-15}$	$4.28 \times 10^{-16}$	$2.41 \times 10^{-15}$	$8.31 \times 10^{-16}$	1.0
Z3	1.41	0.00	-1.41			$1.02 \times 10^{-15}$	$1.37 \times 10^{-16}$	0.00
	2.12	0.00	-2.12			$2.09 \times 10^{-15}$	$6.69 \times 10^{-16}$	0.00
	2.69	0.00	-2.69	$2.03 \times 10^{-16}$	$6.89 \times 10^{-16}$	$3.38 \times 10^{-14}$	$1.94 \times 10^{-14}$	0.00
	4.67	0.00	-4.67	$2.95 \times 10^{-16}$	$5.76 \times 10^{-16}$	$9.23 \times 10^{-15}$	$5.31 \times 10^{-15}$	0.33
	6.93	0.00	-6.93	$3.89 \times 10^{-16}$	$1.08 \times 10^{-15}$	$7.92 \times 10^{-16}$	$2.41 \times 10^{-16}$	0.67
	8.98	0.00	-8.98	$4.40 \times 10^{-16}$	$1.26 \times 10^{-15}$	$2.82 \times 10^{-15}$	$1.60 \times 10^{-15}$	2.33
	11.17	0.00	-11.17	$5.95 \times 10^{-15}$	$2.09 \times 10^{-15}$	$5.50 \times 10^{-15}$	$2.03 \times 10^{-15}$	1.33
	13.29	0.00	-13.29	$3.48 \times 10^{-16}$	$7.26 \times 10^{-16}$	$1.08 \times 10^{-15}$	$4.16 \times 10^{-16}$	0.33
	15.27	0.00	-15.27	$1.34 \times 10^{-16}$	$3.28 \times 10^{-16}$	$7.66 \times 10^{-16}$	$3.38 \times 10^{-16}$	1.33
	17.47	0.00	-17.47	$3.42 \times 10^{-15}$	$1.40 \times 10^{-15}$	$8.24 \times 10^{-16}$	$4.93 \times 10^{-16}$	4.33
	19.59	0.00	-19.59	$1.23 \times 10^{-14}$	$3.62 \times 10^{-15}$	$1.02 \times 10^{-15}$	$4.92 \times 10^{-16}$	1.33
	21.71	0.00	-21.71	$1.40 \times 10^{-15}$	$5.79 \times 10^{-16}$	$9.14 \times 10^{-16}$	$3.80 \times 10^{-16}$	1.00
	23.83	0.00	-23.83	$7.90 \times 10^{-16}$		$2.37 \times 10^{-15}$	$6.35 \times 10^{-16}$	2.00
	26.02	0.00	-26.02	$1.92 \times 10^{-16}$		$1.35 \times 10^{-15}$	$5.81 \times 10^{-16}$	0.00
	28.07	0.00	-28.07	$1.34 \times 10^{-12}$	$3.51 \times 10^{-13}$	$1.83 \times 10^{-15}$	$6.27 \times 10^{-16}$	1.00
	30.33	0.00	-30.33	$9.60 \times 10^{-17}$	$4.56 \times 10^{-16}$	$1.21 \times 10^{-15}$	$4.40 \times 10^{-16}$	0.00

\*Rasmussen, T.C., D.D. Evans, P.J. Sheets, and J.H. Blanford. NUREG/CR-5596, "Unsaturated Fractured Rock Characterization Methods and Data Sets at the Apache Leap Tuff Site." Washington, DC: NRC. August 1990.

**Table 2. Published\* Laboratory Estimates of Matrix Porosity, van Genuchten Alpha, Matrix Klinkenberg Coefficient, and Water Content from the Apache Leap Research Site. Spatial Locations are Based on a Local Coordinate System Using the Lower Lip of the Z3 Borehole Casing as the Origin and Oriented 8° West of North.**  
 [Note that 1.0 m = 3.28 ft, and 1.0 kPa = 0.14504 psi]

Borehole	x (m)	y (m)	z (m)	Porosity (cm <sup>3</sup> /cm <sup>3</sup> , percent)	van Genuchten alpha (kPa <sup>-1</sup> )	Klinkenberg coefficient (kPa)	Water content (cm <sup>3</sup> /cm <sup>3</sup> , percent)
X1	8.84	10.04	-1.46	17.61	0.0289	575.00	12.14
	8.20	10.04	-2.10	16.34	0.0289	264.00	12.52
	7.64	10.04	-2.67	17.45	0.0157	613.00	12.21
	5.44	10.04	-4.86	16.63	0.0154	408.00	12.35
	3.25	10.04	-7.05	15.16	0.0177	401.00	13.94
	1.34	10.04	-8.96	16.23	0.0240	242.00	13.85
	-0.85	10.04	-11.15	16.20	0.0176	206.00	14.36
X2	19.17	10.03	-1.29	21.10	0.0331	95.00	14.23
	18.46	10.03	-2.00	18.79	0.0164	481.00	14.42
	17.97	10.03	-2.49	18.80	0.0102	243.00	15.61
	15.77	10.03	-4.68	14.56	0.0125	1277.00	13.18
	13.37	10.03	-7.09	17.39	0.0110	176.00	14.23
	11.46	10.03	-9.00	17.87	0.0156	76.00	15.29
	9.06	10.03	-11.40	18.38	0.0176	104.00	16.48
	7.36	10.03	-13.10	19.56	0.0284	97.00	16.88
	5.17	10.03	-15.29	16.92	0.0284	130.00	14.73
	2.97	10.03	-17.48	20.52	0.0257	129.00	15.29
	0.71	10.03	-19.74	19.07	0.0240	108.00	15.53
-1.34	10.03	-21.79	19.53	0.0219	168.00	15.26	
X3	29.15	10.04	-1.23	20.71	0.0203	409.00	14.80
	28.52	10.04	-1.87	20.15	0.0139	213.00	13.43
	27.74	10.04	-2.64	18.82	0.0126	765.00	13.12
	25.62	10.04	-4.76	16.41	0.0161	577.00	12.35
	23.43	10.04	-6.96	14.96	0.0217	831.00	12.40
	21.31	10.04	-9.08	14.80	0.0124	445.00	13.22
	19.25	10.04	-11.13	15.68	0.0167	139.00	14.46
	17.13	10.04	-13.25	14.30	0.0208	89.00	14.57
	15.15	10.04	-15.23	15.37	0.0172	143.00	13.70
	12.96	10.04	-17.42	15.96	0.0127	106.00	15.01
	10.84	10.04	-19.54	16.22	0.0136	135.00	15.94
	8.51	10.04	-21.88	17.26	0.0168	232.00	16.47
	6.60	10.04	-23.79	17.35	0.0221	100.00	16.98
	4.33	10.04	-26.05	17.49	0.0183	115.00	17.03
2.21	10.04	-28.17	18.31	0.0135	119.00	16.53	
0.09	10.04	-30.29	17.42	0.0135	176.00	16.76	
Y1	8.93	5.08	-1.30	16.71	0.0150	335.00	12.93
	7.87	5.08	-2.36	16.62	0.0194	777.00	12.98
	7.30	5.08	-2.93	16.69	0.0234	468.00	12.44
	5.54	5.08	-4.69	16.37	0.0200	521.00	11.65
	3.20	5.08	-7.03	18.82	0.0430	637.00	12.63
	1.58	5.08	-8.65	15.96	0.0323	294.00	13.45
-0.90	5.08	-11.13	15.65	0.0201	190.00	14.41	

**Table 2. Published\* Laboratory Estimates of Matrix Porosity, van Genuchten Alpha, Matrix Klinkenberg Coefficient, and Water Content from the Apache Leap Research Site. Spatial Locations are Based on a Local Coordinate System Using the Lower Lip of the Z3 Borehole Casing as the Origin and Oriented 8° West of North.**

[Note that 1.0 m = 3.28 ft, and 1.0 kPa = 0.14504 psi] (continued)

Borehole	x (m)	y (m)	z (m)	Porosity (cm <sup>3</sup> /cm <sup>3</sup> , percent)	van Genuchten alpha (kPa <sup>-1</sup> )	Klinkenberg coefficient (kPa)	Water content (cm <sup>3</sup> /cm <sup>3</sup> , percent)
Y2	18.76	5.20	-1.58	23.40	0.0394	325.00	16.06
	17.70	5.20	-2.64	19.16	0.0153	808.00	15.55
	17.14	5.20	-3.21	18.61	0.0412	708.00	15.63
	15.65	5.20	-4.69	16.87	0.0184	904.00	13.01
	13.46	5.20	-6.88	17.21	0.0205	234.00	14.26
	11.34	5.20	-9.00	20.64	0.0238	114.00	15.02
	9.22	5.20	-11.12	18.18	0.0333	204.00	15.73
	6.95	5.20	-13.39	20.82	0.0329	67.00	17.51
	4.97	5.20	-15.37	16.90	0.0263	123.00	16.15
	2.71	5.20	-17.63	17.59	0.0215	105.00	16.98
	0.73	5.20	-19.61	17.63	0.0184	130.00	17.20
-1.39	5.20	-21.73	18.67	0.0186	137.00	17.06	
Y3	28.65	5.35	-1.68	20.48	0.0256	439.00	13.69
	27.88	5.35	-2.46	21.97	0.0256	865.00	13.34
	27.17	5.35	-3.17	22.43	0.0314	538.00	13.47
	25.68	5.35	-4.65	18.86	0.0643	250.00	12.70
	23.49	5.35	-6.84	14.33	0.0126	757.00	13.34
	21.30	5.35	-9.03	27.51	0.0297	160.00	14.67
	18.75	5.35	-11.58	17.79	0.0218	257.00	15.56
	17.20	5.35	-13.14	14.55	0.0196	109.00	13.65
	14.94	5.35	-15.40	14.49	0.0161	35.00	12.75
	12.96	5.35	-17.38	14.70	0.0120	170.00	13.89
	10.69	5.35	-19.64	16.15	0.0158	109.00	14.41
	8.64	5.35	-21.69	17.61	0.0205	162.00	15.33
	6.59	5.35	-23.74	16.43	0.0246	202.00	15.00
	4.26	5.35	-26.08	18.17	0.0195	185.00	16.21
2.28	5.35	-28.06	17.16	0.0195	130.00	15.60	
0.30	5.35	-30.04	16.94	0.0130	199.00	15.93	
Z1	20.79	0.00	-1.60	18.31	0.0234	497.00	16.98
	21.64	0.00	-2.45	17.94	0.0234	541.00	16.75
	22.35	0.00	-3.16	22.56	0.0220	290.00	15.67
	23.69	0.00	-4.50	15.49	0.0173	1260.00	14.16
	26.02	0.00	-6.83	15.29	0.0182	382.00	12.36
	28.29	0.00	-9.10	17.23	0.0297	434.00	13.59
	30.34	0.00	-11.15	15.74	0.0193	1047.00	13.10
Z2	11.21	0.03	-1.61	17.57	0.0257	584.00	13.01
	11.92	0.03	-2.32	16.58	0.0177	356.00	12.91
	12.63	0.03	-3.02	16.87	0.0179	255.00	12.89
	14.40	0.03	-4.79	16.93	0.0192	142.00	13.58
	16.38	0.03	-6.77	20.84	0.0216	108.00	14.48
	18.57	0.03	-8.96	25.77	0.0311	174.00	16.86
	20.62	0.03	-11.01	17.44	0.0182	967.00	13.75

**Table 2. Published\* Laboratory Estimates of Matrix Porosity, van Genuchten Alpha, Matrix Klinkenberg Coefficient, and Water Content from the Apache Leap Research Site. Spatial Locations are Based on a Local Coordinate System Using the Lower Lip of the Z3 Borehole Casing as the Origin and Oriented 8° West of North.**

[Note that 1.0 m = 3.28 ft, and 1.0 kPa = 0.14504 psi] (continued)

Borehole	x (m)	y (m)	z (m)	Porosity (cm <sup>3</sup> /cm <sup>3</sup> , percent)	van Genuchten alpha (kPa <sup>-1</sup> )	Klinkenberg coefficient (kPa)	Water content (cm <sup>3</sup> /cm <sup>3</sup> , percent)
	23.02	0.03	-13.42	16.11	0.0258	242.00	13.68
	24.86	0.03	-15.26	14.55	0.0198	282.00	12.93
	27.12	0.03	-17.52	14.77	0.0171	232.00	12.53
	29.17	0.03	-19.57	14.98	0.0200	210.00	13.69
	31.37	0.03	-21.76	17.54	0.0200	236.00	15.11
Z3	1.41	0.00	-1.41	16.12	0.0212	774.00	12.44
	2.12	0.00	-2.12	16.80	0.0316	262.00	10.93
	2.69	0.00	-2.69	18.82	0.0514	99.00	10.54
	4.67	0.00	-4.67	17.41	0.0431	98.00	10.14
	6.93	0.00	-6.93	16.53	0.0279	281.00	11.18
	8.98	0.00	-8.98	19.40	0.0325	101.00	12.60
	11.17	0.00	-11.17	19.41	0.0312	213.00	13.94
	13.29	0.00	-13.29	14.98	0.0205	199.00	13.65
	15.27	0.00	-15.27	14.94	0.0244	161.00	12.30
	17.47	0.00	-17.47	15.71	0.0238	90.00	13.72
	19.59	0.00	-19.59	15.31	0.0205	136.00	14.65
	21.71	0.00	-21.71	14.82	0.0146	177.00	14.92
	23.83	0.00	-23.83	17.45	0.0232	335.00	14.82
	26.02	0.00	-26.02	16.47	0.0233	168.00	15.04
	28.07	0.00	-28.07	16.90	0.0182	237.00	14.64
	30.33	0.00	-30.33	16.53	0.0202	217.00	14.39

\*Rasmussen, T.C., D.D. Evans, P.J. Sheets, and J.H. Blanford. NUREG/CR-5596, "Unsaturated Fractured Rock Characterization Methods and Data Sets at the Apache Leap Tuff Site." Washington, DC: NRC. August 1990.

**Table 3. Published\* Laboratory Estimates of Dry Thermal Conductivity, Saturated Thermal Conductivity, and Dry Rock Specific Heat from the Apache Leap Research Site. Spatial Locations are Based on a Local Coordinate System Using the Lower Lip of the Z3 Borehole Casing as the Origin and Oriented 8° West of North. [Note that 1.0 m = 3.28 ft, 1.0 J/(kg·K) = 2.39 × 10<sup>-4</sup> Btu/(lb·°F), and 1.0 J/(m·s·K) = 0.57782 Btu/(h·ft·°F)]**

Borehole	x (m)	y (m)	z (m)	Dry thermal conductivity (J/(m·s·K))	Saturated thermal conductivity (J/(m·s·K))	Dry rock specific heat (J/(kg·K))
X1	8.84	10.04	-1.46	1.20	1.88	595.09
	8.20	10.04	-2.10	1.49	1.62	822.37
	7.64	10.04	-2.67	1.39	1.99	692.02
	5.44	10.04	-4.86	1.49	2.14	604.79
	3.25	10.04	-7.05	1.60	1.94	795.11
	1.34	10.04	-8.96	1.35	2.08	680.09
	-0.85	10.04	-11.15	1.47	1.99	637.67
X2	19.17	10.03	-1.29	1.06	1.85	1168.30
	18.46	10.03	-2.00	1.20	1.92	1125.20
	17.97	10.03	-2.49	1.43	2.17	748.75
	15.77	10.03	-4.68	1.34	1.71	770.39
	13.37	10.03	-7.09	1.28	1.89	498.71
	11.46	10.03	-9.00	1.32	2.02	748.78
	9.06	10.03	-11.40	1.33	1.64	915.32
	7.36	10.03	-13.10	1.19	2.03	837.35
	5.17	10.03	-15.29	1.20	2.02	694.59
	2.97	10.03	-17.48	1.27	1.90	511.14
	0.71	10.03	-19.74	1.40	1.66	756.31
	-1.34	10.03	-21.79	0.99	1.60	468.52
X3	29.15	10.04	-1.23	1.09	1.84	447.99
	28.52	10.04	-1.87	1.22	1.98	583.80
	27.74	10.04	-2.64	1.15	1.90	578.51
	25.62	10.04	-4.76	1.31	1.84	512.15
	23.43	10.04	-6.96	1.33	1.91	626.39
	21.31	10.04	-9.08	1.34	1.91	345.18
	19.25	10.04	-11.13	1.44	2.24	726.25
	17.13	10.04	-13.25	1.28	2.20	976.70
	15.15	10.04	-15.23	1.29	1.88	482.28
	12.96	10.04	-17.42	1.13	1.77	548.81
	10.84	10.04	-19.54	1.21	1.75	726.72
	8.51	10.04	-21.88	1.11	1.85	580.79
	6.60	10.04	-23.79	1.14	1.77	724.15
	4.33	10.04	-26.05	1.34	1.62	668.97
	2.21	10.04	-28.17	1.23	1.76	683.57
0.09	10.04	-30.29	1.97	1.83	517.48	
Y1	8.93	5.08	-1.30	1.16	1.84	447.65
	7.87	5.08	-2.36	1.29	1.82	556.68
	7.30	5.08	-2.93	1.15	1.61	463.63
	5.54	5.08	-4.69	1.43	1.81	698.21
	3.20	5.08	-7.03	1.11	2.49	920.67
	1.58	5.08	-8.65	1.26	1.87	831.53
-0.90	5.08	-11.13	1.55	1.95	757.09	

**Table 3. Published\* Laboratory Estimates of Dry Thermal Conductivity, Saturated Thermal Conductivity, and Dry Rock Specific Heat from the Apache Leap Research Site. Spatial Locations are Based on a Local Coordinate System Using the Lower Lip of the Z3 Borehole Casing as the Origin and Oriented 8° West of North. [Note that 1.0 m = 3.28 ft, 1.0 J/(kg·K) = 2.39 × 10<sup>-4</sup> Btu/(lb·°F), and 1.0 J/(m·s·K) = 0.57782 Btu/(h·ft·°F)] (continued)**

Borehole	x (m)	y (m)	z (m)	Dry thermal conductivity (J/(m·s·K))	Saturated thermal conductivity (J/(m·s·K))	Dry rock specific heat (J/(kg·K))
Y2	18.76	5.20	-1.58	0.92	1.87	832.36
	17.70	5.20	-2.64	1.19	1.80	703.04
	17.14	5.20	-3.21	1.18	1.94	762.28
	15.65	5.20	-4.69	1.29	1.94	732.48
	13.46	5.20	-6.88	1.23	2.01	927.96
	11.34	5.20	-9.00	1.04	1.97	874.61
	9.22	5.20	-11.12	1.28	1.70	807.99
	6.95	5.20	-13.39	1.31	1.77	463.54
	4.97	5.20	-15.37	1.43	1.86	583.58
	2.71	5.20	-17.63	1.31	1.31	511.87
	0.73	5.20	-19.61	1.43	1.44	814.70
	-1.39	5.20	-21.73	1.28	1.67	676.75
Y3	28.65	5.35	-1.68	1.36	1.85	710.29
	27.88	5.35	-2.46	1.02	1.67	632.48
	27.17	5.35	-3.17	1.12	1.81	881.11
	25.68	5.35	-4.65	1.08	1.77	603.27
	23.49	5.35	-6.84	1.29	1.70	587.53
	21.30	5.35	-9.03	1.11	1.55	609.91
	18.75	5.35	-11.58	1.28	1.92	680.03
	17.20	5.35	-13.14	1.45	2.24	812.99
	14.94	5.35	-15.40	1.31	1.81	755.20
	12.96	5.35	-17.38	1.24	1.98	708.60
	10.69	5.35	-19.64	1.19	1.64	587.56
	8.64	5.35	-21.69	1.32	1.50	663.59
	6.59	5.35	-23.74	1.23	2.04	764.81
	4.26	5.35	-26.08	1.33	1.76	635.28
2.28	5.35	-28.06	1.32	1.61	616.55	
0.30	5.35	-30.04	1.28	1.90	783.01	
Z1	20.79	0.00	-1.60	1.37	1.93	813.14
	21.64	0.00	-2.45	1.20	1.84	962.41
	22.35	0.00	-3.16	1.16	1.78	893.94
	23.69	0.00	-4.50	1.32	1.90	797.72
	26.02	0.00	-6.83	1.30	1.86	1043.50
	28.29	0.00	-9.10	1.13	1.60	1037.70
	30.34	0.00	-11.15	1.06	1.77	728.54
Z2	11.21	0.03	-1.61	1.31	1.82	832.19
	11.92	0.03	-2.32	1.36	1.93	588.45
	12.63	0.03	-3.02	1.34	2.03	683.39
	14.40	0.03	-4.79	1.21	1.82	793.15
	16.38	0.03	-6.77	1.15	1.96	713.16
	18.57	0.03	-8.96	0.83	1.29	600.20
20.62	0.03	-11.01	1.15	1.66	501.12	

**Table 3. Published\* Laboratory Estimates of Dry Thermal Conductivity, Saturated Thermal Conductivity, and Dry Rock Specific Heat from the Apache Leap Research Site. Spatial Locations are Based on a Local Coordinate System Using the Lower Lip of the Z3 Borehole Casing as the Origin and Oriented 8° West of North. [Note that 1.0 m = 3.28 ft, 1.0 J/(kg·K) = 2.39 × 10<sup>-4</sup> Btu/(lb·°F), and 1.0 J/(m·s·K) = 0.57782 Btu/(h·ft·°F)] (continued)**

Borehole	x (m)	y (m)	z (m)	Dry thermal conductivity (J/(m·s·K))	Saturated thermal conductivity (J/(m·s·K))	Dry rock specific heat (J/(kg·K))
	23.02	0.03	-13.42	1.26	1.76	903.52
	24.86	0.03	-15.26	1.33	1.99	511.48
	27.12	0.03	-17.52	1.39	1.89	946.67
	29.17	0.03	-19.57	1.25	1.84	820.72
	31.37	0.03	-21.76	1.18	1.60	757.07
Z3	1.41	0.00	-1.41	1.45	1.55	684.52
	2.12	0.00	-2.12	1.28	1.89	714.16
	2.69	0.00	-2.69	1.39	1.54	437.31
	4.67	0.00	-4.67	1.24	1.85	662.24
	6.93	0.00	-6.93	1.19	1.93	851.96
	8.98	0.00	-8.98	1.17	1.58	538.89
	11.17	0.00	-11.17	1.10	1.60	469.63
	13.29	0.00	-13.29	1.33	1.78	917.89
	15.27	0.00	-15.27	1.30	2.01	921.40
	17.47	0.00	-17.47	1.30	1.94	619.63
	19.59	0.00	-19.59	1.40	1.62	535.86
	21.71	0.00	-21.71	1.35	1.61	823.33
	23.83	0.00	-23.83	1.17	1.36	531.63
	26.02	0.00	-26.02	1.19	1.57	529.64
	28.07	0.00	-28.07	1.22	1.74	853.37
	30.33	0.00	-30.33	1.29	1.90	500.82

\*Rasmussen, T.C., D.D. Evans, P.J. Sheets, and J.H. Blanford. NUREG/CR-5596, "Unsaturated Fractured Rock Characterization Methods and Data Sets at the Apache Leap Tuff Site." Washington, DC: NRC. August 1990.

**Table 4. Fracture Orientation Data for Each Borehole at Apache Leap Research Site.\***  
**Inferred Dip Direction Confirmed for Boreholes X1, X2, and X3 Using Figure 1.17 of**  
**Rasmussen.† Terzaghi Factors Calculated using Eq. (2-1) of This Report and Borehole**  
**Orientations. All Boreholes Dip 45°; Boreholes X1, X2, X3, Y1, Y2, and Y3 Dip 8**  
**Approximately Westward (8° South of West) and Boreholes Z1, Z2, and Z3 Dip**  
**Approximately Eastward (8° North of East). [1.0 m = 3.28 ft]**

Borehole Name	Fracture Location Along Borehole, m	Strike Orientation, Degrees	Dip Angle, Degrees	Inferred Dip Direction	Terzaghi Factor
X1	1.77	345	75	West	2.11
X1	4.14	352	85	West	1.56
X1	4.33	215	12	East	1.25
X1	4.36	346	73	West	2.22
X1	4.62	329	76	West	2.58
X1	4.79	336	84	West	1.83
X1	5.73	326	82	West	2.25
X1	6.92	359	75	West	1.92
X1	7.13	358	69	West	2.33
X1	8.92	31	48	West	4.00
X1	9.79	35	64	West	3.48
X2	1.77	359	82	West	1.72
X2	2.32	300	56	West	4.00
X2	2.47	359	85	West	1.60
X2	4.85	191	17	East	1.12
X2	5.18	354	84	West	1.67
X2	9.45	347	78	West	2.05
X2	13.38	331	75	West	2.84
X2	13.56	342	59	West	4.00
X2	15.59	20	17	West	2.06
X2	15.51	20	17	West	2.06
X2	18.68	32	47	West	4.00
X2	19.95	327	89	-	1.95
X2	21.03	334	67	West	4.00
X2	21.67	16	30	West	3.62
X2	22.49	347	79	West	1.99
X2	24.78	339	76	West	2.39
X2	28.47	303	60	West	4.00
X2	28.65	44	63	West	4.00
X2	29.23	318	78	West	3.46
X2	29.52	3	72	West	2.28
X3	4.14	356	74	West	2.18
X3	4.67	338	14	West	1.82
X3	7.01	19	6	West	1.56
X3	8.82	5	79	West	1.83
X3	9.02	337	76	West	2.46
X3	10.13	20	73	West	2.25

**Table 4. Fracture Orientation Data for Each Borehole at Apache Leap Research Site.\***  
**Inferred Dip Direction Confirmed for Boreholes X1, X2, and X3 Using Figure 1.17 of**  
**Rasmussen.† Terzaghi Factors Calculated using Eq. (2-1) of This Report and Borehole**  
**Orientations. All Boreholes Dip 45°; Boreholes X1, X2, X3, Y1, Y2, and Y3 Dip 8**  
**Approximately Westward (8° South of West) and Boreholes Z1, Z2, and Z3 Dip**  
**Approximately Eastward (8° North of East). [1.0 m = 3.28 ft] (continued)**

Borehole Name	Fracture Location Along Borehole, m	Strike Orientation, Degrees	Dip Angle, Degrees	Inferred Dip Direction	Terzaghi Factor
X3	12.45	332	83	West	2.12
X3	13.32	343	76	West	2.27
X3	15.85	336	66	West	4.00
X3	18.63	11	67	West	2.76
X3	18.89	6	71	West	2.34
X3	21.03	334	71	West	3.19
X3	25.6	10	67	West	2.76
X3	25.72	336	66	West	4.00
X3	28.68	8	74	West	2.11
X3	29.66	329	72	West	3.41
X3	29.81	11	66	West	2.89
X3	30.55	312	87	West	2.85
X3	30.6	336	78	West	2.33
X3	31.08	328	66	West	4.00
X3	31.58	336	64	West	4.00
X3	32.95	332	85	West	2.00
X3	33.64	337	82	West	2.03
X3	34.46	339	87	West	1.75
X3	34.61	342	72	West	2.67
X3	35.13	324	81	West	2.61
X3	35.23	323	80	West	2.77
X3	35.96	316	36	West	3.05
X3	42.26	52	55	West	4.00
X3	42.64	309	86	West	3.26
Y1	3.27	119	17	-	1.30
Y1	3.73	169	89	-	1.52
Y1	5.94	12	81	-	1.78
Y1	10.20	316	34	-	2.68
Y1	10.42	13	88	-	1.52
Y1	11.77	291	1	-	1.38
Y1	12.87	11	59	-	4.00
Y1	14.79	21	72	-	2.44
Y2	2.26	336	69	-	3.47
Y2	3.96	4	77	-	1.96
Y2	5.42	344	77	-	2.21
Y2	5.85	345	69	-	2.98
Y2	7.62	3	65	-	3.12
Y2	8.29	264	76	-	2.94

**Table 4. Fracture Orientation Data for Each Borehole at Apache Leap Research Site.\*  
 Inferred Dip Direction Confirmed for Boreholes X1, X2, and X3 Using Figure 1.17 of  
 Rasmussen.† Terzaghi Factors Calculated using Eq. (2-1) of This Report and Borehole  
 Orientations. All Boreholes Dip 45°; Boreholes X1, X2, X3, Y1, Y2, and Y3 Dip 8  
 Approximately Westward (8° South of West) and Boreholes Z1, Z2, and Z3 Dip  
 Approximately Eastward (8° North of East). [1.0 m = 3.28 ft] (continued)**

Borehole Name	Fracture Location Along Borehole, m	Strike Orientation, Degrees	Dip Angle, Degrees	Inferred Dip Direction	Terzaghi Factor
Y2	9.04	251	44	-	1.35
Y2	16.43	15	6	-	1.55
Y2	19.33	102	40	-	1.72
Y2	19.77	237	26	-	1.18
Y2	19.87	293	17	-	1.57
Y2	22.4	25	56	-	4.00
Y2	28.62	214	87	-	1.51
Y3	4.48	294	22	-	1.70
Y3	5.09	21	67	-	2.84
Y3	5.25	298	4	-	1.44
Y3	6.51	311	45	-	4.00
Y3	9.57	26	74	-	2.24
Y3	13.73	4	77	-	1.92
Y3	15.92	345	84	-	1.76
Y3	17.21	160	89	-	1.58
Y3	17.37	348	88	-	1.58
Y3	19.43	26	76	-	2.10
Y3	19.77	17	73	-	2.20
Y3	20.21	164	82	-	1.36
Y3	20.31	4	67	-	2.73
Y3	23.33	24	65	-	3.22
Y3	23.76	350	80	-	1.87
Y3	23.8	341	89	-	1.63
Y3	24.39	340	77	-	2.26
Y3	24.4	336	87	-	1.80
Y3	24.49	343	66	-	3.44
Y3	26.32	353	81	-	1.79
Y3	29.98	23	74	-	2.19
Y3	44.6	216	86	-	1.50
Z1	3.95	10	18	-	1.11
Z1	4.57	303	47	-	1.40
Z1	5.16	143	79	-	2.94
Z1	6.21	248	84	-	3.85
Z1	6.26	220	89	-	1.77
Z1	6.35	312	78	-	1.89
Z1	6.38	188	77	-	1.99

**Table 4. Fracture Orientation Data for Each Borehole at Apache Leap Research Site.\* Inferred Dip Direction Confirmed for Boreholes X1, X2, and X3 Using Figure 1.17 of Rasmussen.† Terzaghi Factors Calculated using Eq. (2-1) of This Report and Borehole Orientations. All Boreholes Dip 45°; Boreholes X1, X2, X3, Y1, Y2, and Y3 Dip 8° Approximately Westward (8° South of West) and Boreholes Z1, Z2, and Z3 Dip Approximately Eastward (8° North of East). [1.0 m = 3.28 ft] (continued)**

Borehole Name	Fracture		Dip Angle, Degrees	Inferred Dip Direction	Terzaghi Factor
	Location Along Borehole, m	Strike Orientation, Degrees			
Z1	9.39	210	57	—	4.00
Z1	9.49	190	81	—	1.78
Z1	10.49	280	25	—	1.49
Z1	10.59	337	63	—	1.17
Z1	11.06	164	85	—	1.78
Z1	11.29	20	19	—	1.10
Z1	11.78	70	20	—	1.26
Z1	12.01	341	75	—	1.28
Z1	12.45	174	87	—	1.60
Z1	12.74	317	65	—	1.42
Z1	13.85	340	85	—	1.50
Z1	14.38	310	83	—	2.21
Z1	14.67	4	22	—	1.07
Z1	15.1	109	10	—	1.44
Z1	16.5	112	89	—	4.00
Z2	2.9	339	87	—	1.57
Z2	3.65	42	8	—	1.25
Z2	4.51	275	42	—	1.92
Z2	5.19	259	32	—	1.99
Z2	5.74	73	30	—	1.29
Z2	7.64	181	24	—	2.55
Z2	7.76	222	32	—	3.13
Z2	8.3	181	85	—	1.63
Z2	11.75	140	87	—	2.39
Z2	12.02	204	77	—	2.11
Z2	12.73	127	36	—	2.53
Z2	13.18	227	73	—	3.41
Z2	13.8	140	18	—	1.81
Z2	13.89	112	14	—	1.50
Z2	14.38	41	35	—	1.08
Z2	14.47	336	73	—	1.30
Z2	14.59	335	83	—	1.52
Z2	14.78	327	75	—	1.45
Z2	14.79	339	80	—	1.40
Z2	14.92	304	85	—	2.75

**Table 4. Fracture Orientation Data for Each Borehole at Apache Leap Research Site.\* Inferred Dip Direction Confirmed for Boreholes X1, X2, and X3 Using Figure 1.17 of Rasmussen.† Terzaghi Factors Calculated using Eq. (2-1) of This Report and Borehole Orientations. All Boreholes Dip 45°; Boreholes X1, X2, X3, Y1, Y2, and Y3 Dip 8° Approximately Westward (8° South of West) and Boreholes Z1, Z2, and Z3 Dip Approximately Eastward (8° North of East). [1.0 m = 3.28 ft] (continued)**

Borehole Name	Fracture Location Along Borehole, m	Strike Orientation, Degrees	Dip Angle, Degrees	Inferred Dip Direction	Terzaghi Factor
Z2	15.63	184	80	—	1.84
Z2	15.8	223	73	—	3.12
Z2	15.83	232	88	—	2.15
Z2	16.01	342	68	—	1.19
Z2	16.02	296	61	—	1.85
Z2	16.08	321	65	—	1.37
Z2	16.28	297	68	—	2.08
Z2	18.53	174	68	—	2.93
Z2	19.12	179	58	—	4.00
Z2	19.37	304	76	—	2.14
Z2	19.99	298	84	—	3.23
Z2	22.49	156	23	—	2.24
Z2	22.73	320	89	—	2.13
Z2	22.98	309	87	—	2.56
Z2	23.01	300	87	—	3.39
Z2	23.04	310	86	—	2.42
Z2	23.55	148	89	—	1.96
Z2	24.41	142	16	—	1.75
Z2	26.46	131	23	—	1.90
Z2	27.1	80	55	—	1.69
Z2	27.85	207	2	—	1.41
Z2	27.97	36	7	—	1.25
Z2	28.1	211	77	—	2.23
Z2	28.35	93	62	—	2.54
Z2	28.5	170	34	—	4.00
Z2	28.85	256	16	—	1.58
Z2	28.98	94	74	—	4.00
Z2	29.13	166	84	—	1.81
Z2	29.88	183	65	—	3.25
Z2	30.02	309	74	—	1.85
Z3	8.26	339	89	—	1.60
Z3	9.69	350	73	—	1.18
Z3	11.19	193	84	—	1.61
Z3	11.84	145	83	—	2.36
Z3	11.85	263	60	—	4.00
Z3	12.06	262	72	—	4.00

**Table 4. Fracture Orientation Data for Each Borehole at Apache Leap Research Site.\* Inferred Dip Direction Confirmed for Boreholes X1, X2, and X3 Using Figure 1.17 of Rasmussen.† Terzaghi Factors Calculated using Eq. (2-1) of This Report and Borehole Orientations. All Boreholes Dip 45°; Boreholes X1, X2, X3, Y1, Y2, and Y3 Dip 8° Approximately Westward (8° South of West) and Boreholes Z1, Z2, and Z3 Dip Approximately Eastward (8° North of East). [1.0 m = 3.28 ft] (continued)**

Borehole Name	Fracture Location Along Borehole, m	Strike Orientation, Degrees	Dip Angle, Degrees	Inferred Dip Direction	Terzaghi Factor
Z3	13.19	273	50	—	2.42
Z3	13.31	330	89	—	1.77
Z3	13.63	332	81	—	1.49
Z3	13.72	320	89	—	2.07
Z3	15.3	270	36	—	1.92
Z3	15.9	86	24	—	1.41
Z3	17.21	189	83	—	1.64
Z3	17.32	239	56	—	4.00
Z3	19.62	243	77	—	4.00
Z3	22.16	303	69	—	1.87
Z3	22.17	308	71	—	1.77
Z3	22.32	286	83	—	4.00
Z3	22.94	100	88	—	4.00
Z3	23.49	87	66	—	2.44
Z3	23.57	211	88	—	1.61
Z3	23.63	198	87	—	1.53
Z3	24.32	311	78	—	1.91
Z3	24.89	134	76	—	4.00
Z3	25.57	318	87	—	2.04
Z3	25.75	320	86	—	1.93
Z3	25.81	149	89	—	1.87
Z3	25.88	301	89	—	3.47
Z3	25.94	307	86	—	2.56
Z3	25.98	111	87	—	4.00
Z3	25.98	315	72	—	1.60
Z3	26.26	49	51	—	1.16
Z3	26.45	274	38	—	1.88
Z3	26.7	183	83	—	1.65
Z3	27.8	192	78	—	1.86
Z3	28.41	162	69	—	2.99
Z3	29.44	155	77	—	2.42
Z3	29.51	137	85	—	2.64
Z3	29.87	173	87	—	1.56
Z3	33.02	141	89	—	2.14

**Table 4. Fracture Orientation Data for Each Borehole at Apache Leap Research Site.\* Inferred Dip Direction Confirmed for Boreholes X1, X2, and X3 Using Figure 1.17 of Rasmussen.<sup>†</sup> Terzaghi Factors Calculated using Eq. (2-1) of This Report and Borehole Orientations. All Boreholes Dip 45°; Boreholes X1, X2, X3, Y1, Y2, and Y3 Dip 8° Approximately Westward (8° South of West) and Boreholes Z1, Z2, and Z3 Dip Approximately Eastward (8° North of East). [1.0 m = 3.28 ft] (continued)**

Borehole Name	Fracture Location Along Borehole, m	Strike Orientation, Degrees	Dip Angle, Degrees	Inferred Dip Direction	Terzaghi Factor
Z3	33.45	185	14	—	1.92
Z3	33.6	150	84	—	2.10
Z3	34.83	71	58	—	1.55
Z3	34.89	258	70	—	4.00
Z3	35.2	264	38	—	2.18
Z3	39.23	212	81	—	1.92
Z3	39.81	80	56	—	1.73
Z3	40.66	104	58	—	3.19

\*Rasmussen, T.C., D.D. Evans, P.J. Sheets, and J.H. Blanford. NUREG/CR-5596, "Unsaturated Fractured Rock Characterization Methods and Data Sets at the Apache Leap Tuff Site." Washington, DC: NRC. August 1990.

<sup>†</sup>Rasmussen T.C. and D.D. Evans. NUREG/CR-4655, "Unsaturated Flow and Transport Through Fractured Rock Related to High-Level Waste Repositories, Final Report—Phase II." Washington, DC: NRC. May 1987.